UNIVERSITY OF CALIFORNIA, SAN DIEGO

A Localized *Pseudomonas syringae* Infection Triggers Systemic Clock Responses in *Arabidopsis*

A Dissertation submitted in partial satisfaction of the
requirements for the degree Doctor of Philosophy

in

Biology

by

Zheng Li

Committee in charge:

Professor Jose L. Pruneda-Paz, Chair
Professor Steven Paul Briggs
Professor Susan Stephens Golden
Professor David K. Welsh
Professor Martin F. Yanofsky

2018

The Dissertation of Zheng Li is approved, and it is acceptable in quality and form for publication on microfilm and electronically:

_____

_____

_____

_____

_____

Chair

University of California, San Diego

2018

DEDICATION

This dissertation is dedicated to my family, especially my husband Qingzhi Liu, who supported me with love, patience and encouragement. It is also dedicated to all colleagues and my committee members who contributed to the success of this research.

TABLE OF CONTENTS

LIST OF FIGURES

LIST OF TABLES

LIST OF SUPPLEMENTARY MATERIALS

ACKNOWLEDGMENTS

I would like to acknowledge Professor Jose Pruneda-Paz for his guidance through the whole process of my research, his encouragement and mentorship for me through the difficult times, and his generous support in terms of funding and his precious time.

I would also like to acknowledge my committee members Professor David Welsh, Professor Martin Yanofsky, Professor Steven Briggs and Professor Susan Golden for their advice and support through my graduate research.

I would like to acknowledge Katia as my dear friend and colleague for the days we spent together, the research we performed together and the laughter and tears we shared.

I would like to thank all previous and current colleagues in the Pruneda-Paz lab for their work and help.

Chapter 2, in full, is a reprint of the material as: Zheng Li, Katia Bonaldi, Francisco Uribe, Jose L. Pruneda-Paz. A localized *Pseudomonas syringae* infection triggers systemic clock responses in *Arabidopsis*. Current Biology. 2018 Feb 19; 28(4):630-639. The dissertation author was the primary investigator and author of this paper.

Chapter4, in full, is a reprint of the material as: Katia Bonaldi, Zheng Li, S. Earl Kang, Ghislain Breton, Jose L. Pruneda-Paz. Novel cell surface luciferase reporter for high-throughput yeast one-hybrid screens. Nucleic Acids Res. 2017 Oct 13;45(18):e157. The dissertation author was the co-first investigator and co-first author of this paper.

I would also like to acknowledge Eleni Tente who made great effort to validate protein interaction with tobacco BIFC system (in chapter 5).

VITA

2008	Bachelor of Science, Tsinghua University, Beijing
2011	Master of Science, Tsinghua University, Beijing
2011-2018	Research and Teaching Assistant, University of California, San Diego
2018	Doctor of Philosophy, University of California, San Diego

PUBLICATIONS

Liangsheng Wang*, Zheng Li*, Weiqiang Qian, Wanli Guo, Xiang Gao, Lingling Huang, Han Wang, Huifen Zhu, Jia-Wei Wu, Daowen Wang, Dong Liu. The *Arabidopsis* purple acid phosphatase AtPAP10 is predominantly associated with the root surface and plays an important role in plant tolerance to phosphate limitation. Plant Physiol. 2011 Nov;157(3):1283-99.

Zixing Li, Zheng Li, Xiang Gao, Viswanathan Chinnusamy, Ray Bressan, Zhi-Xin Wang, Jian-Kang Zhu, Jia-Wei Wu, Dong Liu. ROP11 GTPase negatively regulates ABA signaling by protecting ABI1 phosphatase activity from inhibition by the ABA receptor RCAR1/PYL9 in *Arabidopsis*. J Integr Plant Biol. 2012 Mar;54(3):180-8.

Liangsheng Wang, Shan Lu, Ye Zhang, Zheng Li, Xiaoqiu Du, Dong Liu. Comparative genetic analysis of *Arabidopsis* purple acid phosphatases AtPAP10, AtPAP12, and AtPAP26 provides new insights into their roles in plant adaptation to phosphate deprivation. J Integr Plant Biol. 2014 Mar;56(3):299-314.

Katia Bonaldi*, Zheng Li*, S. Earl Kang, Ghislain Breton, Jose L. Pruneda-Paz. Novel cell surface luciferase reporter for high-throughput yeast one-hybrid screens. Nucleic Acids Res. 2017 Oct 13;45(18):e157.

Zheng Li, Katia Bonaldi, Francisco Uribe, Jose L. Pruneda-Paz. A localized *Pseudomonas syringae* infection triggers systemic clock responses in *Arabidopsis*. Current Biology. 2018 Feb 19; 28(4):630-639

*These authors contributed equally

FIELDS OF STUDY

Major Field: Biological Sciences

Studies in Cell and Developmental Biology
Professor Jose L. Pruneda-Paz

ABSTRACT OF THE DISSERTATION

A Localized *Pseudomonas syringae* Infection Triggers Systemic Clock Responses in *Arabidopsis*

by

Zheng Li

Doctor of Philosophy in Biology

University of California, San Diego, 2018

Professor Jose L. Pruneda-Paz, Chair

Many plant physiological and behavioral responses exhibit 24h rhythms that anticipate daily changes in the environment. This key adaptive response is regulated by the circadian clock, which provides an endogenous timekeeping mechanism that coordinates biological activities. Multiple environmental cues, including the infection of biotrophic plant pathogen *Pseudomonas Syringae* and pathogen induced phytohormone

salicylic acid (SA) were shown to affect the clock function. However, the highly dynamic and variable nature of pathogen infection progression and related SA kinetics make it difficult to dissect the clock response to a practical infection. Here, we developed methods to perform local *Pseudomonas Syringae* infection and to apply transient SA treatment. These methods more closely resembled stimuli in a practical infection and allowed us to explore the circadian clock response to these stimuli. Our results indicated that a local infection lengthens the period and reduces the amplitude of circadian rhythms. Transient SA treatment recapitulated the amplitude phenotype and resulted in a phase delay with strongest phase effect at the beginning of the day. Apoplastic ROS production induced by transient SA treatment and *Pseudomonas Syringae* infection was shown to partly mediate these circadian clock responses. Moreover, NPR1, a master regulator of plant defense, counteracted the amplitude decrease by both infection and SA treatment. Furthermore, we discovered that localized *Pseudomonas Syringae* infection predominantly affected the circadian rhythms in the shoot apex and resulted in a delay in plant development. Some TCP transcription factors have been shown to regulate clock function and DNA binding activity of TCPs is regulated by ROS. We therefore characterized TCP transcription factors in order to explore the possible link between defense related ROS production and the regulation of circadian clock function. We performed yeast one hybrid analysis with a newly developed Y1H reporter system on class I TCPs and found that most of them interact with CCA1 promoter. Also, we developed a novel gene-centered Y2H screen system and discovered that class I TCP transcription factors were highly enriched for TCP21 interactors. These results uncovered

the complex nature in which TCP transcription factors interact to regulate circadian clock function.

Chapter 1 Introduction

The circadian clock regulates most aspects of plant growth and development [1]. Clock controlled rhythms have a 24 hour period and allow plants to regulate the onset of biological processes so they are coordinated with convenient conditions in an environment that exhibits daily fluctuations. The clock generates endogenous rhythms that anticipate these environmental changes every day providing an adaptive advantage that results in improved plant growth and survival rates [2,3]. Physiological advantages of such a mechanism require endogenous circadian rhythms and exogenous environmental conditions to oscillate in tight synchrony [4]. In fact, multiple signaling pathways triggered by environmental cues such as light, temperature, nutrients or biotic interactions were shown to regulate the clock function [5-8]. Likely, due to plants sessile nature the clock provides a key mechanism that integrates the timing and nature of environmental cues to coordinate organismal functions and responses accordingly [7,9].

At the molecular level, the circadian clock function relies on multiple overlapped regulatory layers both at the transcriptional and post-transcriptional levels. The main mechanistic feature of the plant clock, which is shared across species, involves several intertwined transcriptional feedback loops that create a vast regulatory circuit with multiple possibilities for regulation [6,10]. In plants, the core transcriptional mechanism is based on the reciprocal regulation between two morning expressed transcription factors, CIRCADIAN CLOCK ASSOCIATED1 (CCA1) and LATE ELONGATED HYPOCOTYL (LHY), which negatively regulate the expression of the evening expressed transcriptional regulator TIMING OF CAB EXPRESSION1 (TOC1). TOC1 closes this feedback loop by

negatively regulating the expression of *CCA1* and *LHY* [3,7,10]. Many additional clock components that integrate with this core feedback loop have been identified [6,10]. While the mechanism is still not fully understood, the pace, amplitude and phase of clock rhythms is set by input pathways that are regulated by cyclic environmental signals such as light and temperature. However, other mechanisms were shown to fine tune the clock function. Nutrient availability, such as nitrogen or iron, regulates the clock function [11-15]. Likewise, abiotic and biotic stress responses also affect the clock function. The phytohormone ABA, which is mediating many responses to salt, osmotic and cold stress is able to regulate clock function by modulating *TOC1* expression [16,17]. In the case of biotic stress responses, *Pseudomonas syringae* infection and salicylic acid treatment are also shown to modulate the clock function [8,18]. These facts indicate that multiple environmental cues can serve as input signals to circadian clock, which renders the clock a highly responsive module and a great hub to integrate signals and correspondingly adjust biological processes at a whole organism level. Furthermore, clock responses to many input signals exhibits a gating feature. For example, the magnitude of the acute induction of *TOC1* promoter activity by ABA treatments differs depending on the time of the day at which the hormone is applied [16]. Similar gating phenomenon is also observed in the clock responses to light and temperature signals [19,20]. In many organisms, phase response curve (PRC) is generated for certain zeitgebers to reveal intrinsic features of the clock and the details of the gating feature for the phase shift [21].

Pseudomonas syringae, a biotrophic plant pathogen, is used extensively together with *Arabidopsis* to explore the mechanisms of plant-pathogen interactions [22]. Upon *Pseudomonas syringae* infection, many immediate and enduring responses are elicited

[23]. The first layer of plant defense is triggered by the recognition of Pathogen-associated Molecular Pattern (PAMP). An important aspect of this response is a burst of reactive oxygen species (ROS) mediated by the NADPH oxidase RBOHD localized at the plasma membrane [24]. RBOHD produces apoplastic ROS in response to multiple kinds of stress signal such as ABA, SA, wounding and pathogen infection [24-28]. Upon pathogen challenge, ROS could serve both as a systemic signal and at the same time a regulator of cell death and survival to contain infection locally [29,30]. Salicylic acid production is also induced by *Pseudomonas syringae* infection and it regulates many aspects of plant defense responses such as transcriptional reprogramming, cell death and survival and initiation of systemic acquired resistance (SAR) [31,32]. Salicylic acid alone is able to induce a burst of ROS, while this change of the oxidative state in the cell causes the translocation of NON-EXPRESSER OF PATHOGEN-RELATED GENES-1 (NPR1), a key regulator of plant defense and SA signaling pathway, from cytoplasm to the nucleus to perform its function. NPR1 interacts with bZIP transcription factors and regulate the expression of SA target genes [33,34].

Both *Pseudomonas syringae* infections and SA treatments were shown to modulated the clock function. However, while whole-plant P. syringae infections shorten the period of clock rhythms, the exogenous treatment with SA results in a transient increase in their amplitude [8,18]. These results reveal the complexity of the clock regulation by defense response. Indeed, depending on the distance to the infection site, and the duration after the infection started, the responses of the plant tissue vary drastically [22,35]. Also, the ROS and SA production induced by *Pseudomonas syringae* infection is highly dynamic. The initial ROS production triggered by the perception of

PAMPs happens in minutes and precedes the production of SA [36,37]. ROS dynamics induced by *Pseudomonas* infection varies with the bacteria. In the case of infection of *Arabidopsis* by the virulent *Pseudomonas syringae* pv. *tomato* DC3000, a rapid burst quickly happens and a later production of ROS lasts at least for days [37-39]. At the same time, SA production is usually peaking within one day after initial infection then decreases from then on [40,41]. To further dissect clock responses to defense signals considering these spatial and temporal complexities, we applied local *P syringae* infection and transient SA treatment to the plant and assessed the clock responses. Our results indicate that a local infection lengthened the period and reduced the amplitude of circadian rhythms. We found that a transient SA treatment recapitulated the amplitude phenotype and also delayed the phase of clock rhythms with the largest phase delay by SA treatment in the morning. Apoplastic ROS production was partially mediating these responses. Finally, we found that NPR1 function provided a safeguard mechanism that pointed to maintain a proper clock function upon SA treatments or *P. syringae* infection. (materials related to this part is included in Chapter 2)

While circadian clock function in plants has long been studied at the whole organism level, emerging evidences are showing that tissue specific patterns of circadian clock-controlled oscillations exist. Vasculature and mesophyll tissues of the leaf have enriched evening and morning expressed genes respectively [42], while the shoot apex of the plant serves as the hierarchical master regulator which is able to synchronize rhythms in other parts of the plant [43]. Our study of local *Pseudomonas* infection is providing a strategy to study how a localized stress can affect the circadian clock function at the whole organism level. Furthermore, we observed that the circadian rhythms from

the shoot apex was preferentially affected by localized leaf *Pseudomonas syringae* infection. This local infection also resulted in a delay of the plant development revealing massive changes in the shoot apex. (materials related to this part is included in Chapter 3)

To find the link from ROS production induced by pathogen challenge or SA treatment to the regulation of the circadian clock function, TCP transcription factors serve as appealing candidates. TCPs are a family of plant-specific transcription factors that contain TCP DNA binding domain [44]. The TCP DNA binding domain is a non-canonical basic helix-loop-helix (bHLH) domain and based on the difference in TCP domain, the TCP transcription factors are classified into two sub families: class I and class II TCP transcription factor [44]. TCPs are reported to be at the crossroad of regulating many aspects of the plant life including development, leaf senescence, circadian clock function, defense response and so on [45-47]. Since the discovery of TCP21 (CHE) function in the clock regulation [46], TCP20 and TCP22 are also reported to play a role in regulating circadian rhythm as activators of CCA1 transcription [48]. Considering the similarity of their binding preference for DNA sequence, more TCPs might participate in clock regulation. At the same time, TCPs could form homo and hetero dimers [49,50], which add another layer of complexity to ultimately solve the puzzle. The DNA binding activity of several TCPs including TCP21 was found to be regulated by the redox status [51], implying potential mechanism how multiple sources of stress could input into redox state as a hub of signal and regulate outcome responses including circadian clock function through TCPs. To start unraveling the complicated possible regulations of circadian clock function by TCPs, we tested the interaction between class I TCPs and CCA1 promoter

with yeast one hybrid technique exploiting novel yeast cell surface reporter. We found that most class I TCPs could bind CCA1 promoter through TCP binding site (TBS). (materials related to this part is included in chapter 4). Furthermore, we developed a high throughput yeast two hybrid screen system and identified 68 novel interactors of TCP21, and class I TCPs were highly enriched for TCP21 interactors. We also validated the interaction between TCP21 and the top interactor TCP19 with BiFC assay (materials related to this part is included in chapter 5). Although these findings are far from resolving the whole picture about the regulation of clock function by TCPs, they provide starting information to find the path.

References

1. Covington, M.F., Maloof, J.N., Straume, M., Kay, S.A., and Harmer, S.L. (2008). Global transcriptome analysis reveals circadian regulation of key pathways in plant growth and development. Genome Biol. *9*, r130.

2. Harmer, S.L. (2009). The Circadian System in Higher Plants. Annu. Rev. Plant Biol. *60*, 357–377.

3. McClung, C.R. (2006). Plant Circadian Rhythms. Plant Cell *18*, 792–803.

4. Dodd, A.N., Salathia, N., Hall, A., Kevei, E., Toth, R., Nagy, F., Hibberd, J.M., Millar, A.J., and Webb, A.A. (2005). Plant Circadian Clocks Increase Photosynthesis, Growth, Survival, and Competitive Advantage. Science (80-.). *309*, 630–633.

5. Greenham, K., and McClung, C.R. (2015). Integrating circadian dynamics with physiological processes in plants. Nat. Rev. Genet. *16*, 598–610.

6. Hsu, P.Y., and Harmer, S.L. (2014). Wheels within wheels: The plant circadian system. Trends Plant Sci. *19*, 240–249.

7. Pruneda-Paz, J.L., and Kay, S.A. (2010). An expanding universe of circadian networks in higher plants. Trends Plant Sci. *15*, 259–265.

8. Zhang, C., Xie, Q., Anderson, R.G., Ng, G., Seitz, N.C., Peterson, T., McClung, C.R., McDowell, J.M., Kong, D., Kwak, J.M., and Lu, H. (2013). Crosstalk between the Circadian Clock and Innate Immunity in *Arabidopsis*. PLoS Pathog. *9*, e1003370.

9. Sanchez, S.E., and Kay, S.A. (2016). The Plant Circadian Clock: From a Simple Timekeeper to a Complex Developmental Manager. Cold Spring Harb. Perspect. Biol. *8*, a027748.

10. Nagel, D.H., and Kay, S.A. (2013). Complexity in the wiring and regulation of plant circadian networks. Curr. Biol. *23*, 95–96.

11. Yuan, S., Zhang, Z.-W., Zheng, C., Zhao, Z.-Y., Wang, Y., Feng, L.-Y., Niu, G., Wang, C.-Q., Wang, J.-H., Feng, H., Xu, F., Bao, F., Hu, Y., Cao, Y., Ma, L., Wang, H., Kong, D.-D., Xiao, W., Lin, H.-H., and He, Y. (2016). *Arabidopsis* cryptochrome 1 functions in nitrogen regulation of flowering. Proc. Natl. Acad. Sci. *113*, 7661–7666.

12. Gutierrez, R.A., Stokes, T.L., Thum, K., Xu, X., Obertello, M., Katari, M.S., Tanurdzic, M., Dean, A., Nero, D.C., McClung, C.R., and Goruzzi, G.M. (2008). Systems approach identifies an organic nitrogen-responsive gene network that is regulated by the master clock control gene CCA1. Proc. Natl. Acad. Sci. *105*, 4939–4944.

13. Chen, Y.-Y., Wang, Y., Shin, L.-J., Wu, J.-F., Shanmugam, V., Tsednee, M., Lo, J.-C., Chen, C.-C., Wu, S.-H., and Yeh, K.-C. (2013). Iron Is Involved in the Maintenance of Circadian Period Length in *Arabidopsis*. Plant Physiol. *161*, 1409–1420.

14. Salomé, P.A., Oliva, M., Weigel, D., and Krämer, U. (2013). Circadian clock adjustment to plant iron status depends on chloroplast and phytochrome function. EMBO J. *32*, 511–523.

15. Hong, S., Kim, S.A., Guerinot, M.L., and McClung, C.R. (2013). Reciprocal Interaction of the Circadian Clock with the Iron Homeostasis Network in *Arabidopsis*. Plant Physiol. *161*, 893–903.

16. Legnaioli, T., Cuevas, J., and Mas, P. (2009). TOC1 functions as a molecular switch connecting the circadian clock with plant responses to drought. EMBO J. *28*, 3745–3757.

17. Lee, H.G., Mas, P., and Seo, P.J. (2016). MYB96 shapes the circadian gating of ABA signaling in *Arabidopsis*. Sci. Rep. *6*, 1–11.

18. Zhou, M., Wang, W., Karapetyan, S., Mwimba, M., Marqués, J., Buchler, N.E., and Dong, X. (2015). Redox rhythm reinforces the circadian clock to gate immune response. Nature *523*, 472–476.

19. Michael, T.P., Salome, P.A., and McClung, C.R. (2003). Two *Arabidopsis* circadian oscillators can be distinguished by differential temperature sensitivity. Proc. Natl. Acad. Sci. *100*, 6878–6883.

20. Covington, M.F., Panda, S., Liu, X.L., Strayer, C. a, Wagner, D.R., and Kay, S. a (2001). ELF3 modulates resetting of the circadian clock in *Arabidopsis*. Plant Cell *13*, 1305–1315.

21. Johnson, C.H. (1992). Phase Response Curves: What can they tell us about circadian clocks. In Circadian Clocks from Cell to Human, pp. 209–246.

22. Katagiri, F., Thilmony, R., and He, S.Y. (2002). The *Arabidopsis* Thaliana-Pseudomonas Syringae Interaction. In *Arabidopsis* Book, p. 39.

23. Xin, X.F., and He, S.Y. (2013). Pseudomonas syringae pv. tomato DC3000: A Model Pathogen for Probing Disease Susceptibility and Hormone Signaling in Plants. Annu. Rev. Phytopathol. *51*, 473–498.

24. Kadota, Y., Shirasu, K., and Zipfel, C. (2015). Regulation of the NADPH Oxidase RBOHD during Plant Immunity. Plant Cell Physiol. *56*, 1472–1480.

25. Kwak, J.M., Mori, I.C., Pei, Z.M., Leonhardt, N., Angel Torres, M., Dangl, J.L., Bloom, R.E., Bodde, S., Jones, J.D.G., and Schroeder, J.I. (2003). NADPH oxidase *AtrbohD* and *AtrbohF* genes function in ROS-dependent ABA signaling in Arabidopsis. EMBO J. *22*, 2623–2633.

26. Torres, M.A., and Dangl, J.L. (2005). Functions of the respiratory burst oxidase in biotic interactions, abiotic stress and development. Curr. Opin. Plant Biol. *8*, 397–403.

27. Miller, G., Schlauch, K., Tam, R., Cortes, D., Torres, M.A., Shulaev, V., Dangl, J.L., and Mittler, R. (2009). The plant NADPH oxidase RBOHD mediates rapid systemic signaling in response to diverse stimuli. Sci. Signal. *2*, 1–11.

28. Kalachova, T., Iakovenko, O., Kretinin, S., and Kravets, V. (2013). Involvement of phospholipase D and NADPH-oxidase in salicylic acid signaling cascade. Plant Physiol. Biochem. PPB *66*, 127–133.

29. Alvarez, M.E., Pennell, R.I., Meijer, P.J., Ishikawa, A., Dixon, R.A., and Lamb, C. (1998). Reactive oxygen intermediates mediate a systemic signal network in the establishment of plant immunity. Cell *92*, 773–784.

30. Torres, M.A., Jones, J.D.G., and Dangl, J.L. (2006). Reactive oxygen species signaling in response to pathogens. Plant Physiol. *141*, 373–378.

31. Vlot, A.C., Dempsey, D.A., and Klessig, D.F. (2009). Salicylic Acid, a Multifaceted Hormone to Combat Disease. Annu. Rev. Phytopathol. *47*, 177–206.

32. Fu, Z.Q., and Dong, X. (2013). Systemic acquired resistance: turning local infection into global defense. Annu. Rev. Plant Biol. *64*, 839–863.

33. Wang, D., Amornsiripanitch, N., and Dong, X. (2006). A genomic approach to identify regulatory nodes in the transcriptional network of systemic acquired resistance in plants. PLoS Pathog. *2*, 1042–1050.

34. Mou, Z., Fan, W., and Dong, X. (2003). Inducers of plant systemic acquired resistance Regulate NPR1 function through redox changes. Cell *113*, 935–944.

35. Fu, Z.Q., Yan, S., Saleh, A., Wang, W., Ruble, J., Oka, N., Mohan, R., Spoel, S.H., Tada, Y., Zheng, N., and Dong, X. (2012). NPR3 and NPR4 are receptors for the immune signal salicylic acid in plants. Nature *486*, 228–232.

36. Spanu, P.D. (2015). Salicylic acid and reactive oxygen species interplay in the transcriptional control of defense genes expression. Front. Plant Sci. *6*, 171.

37. Smith, J.M., and Heese, A. (2014). Rapid bioassay to measure early reactive oxygen species production in *Arabidopsis* leave tissue in response to living Pseudomonas syringae. Plant Methods *10*, 6.

38. Ravichandran, S., Stone, S.L., Benkel, B., and Prithiviraj, B. (2013). Purple Acid Phosphatase5 is required for maintaining basal resistance against Pseudomonas syringae in *Arabidopsis*. BMC Plant Biol. *13*, 107.

39. Lou, Y., Bor, M., Yan, J., Preuss, A.S., Jander, G., Thompson, B., and L, N.Y.Y. (2016). *Arabidopsis* NATA1 Acetylates Putrescine and Decreases Defense-Related Hydrogen Peroxide Accumulation 1. Plant Physiol. *171*, 1443–1455.

40. Ederli, L., Madeo, L., Calderini, O., Gehring, C., Moretti, C., Buonaurio, R., Paolocci, F., and Pasqualini, S. (2011). The *Arabidopsis thaliana* cysteine-rich receptor-like kinase CRK20 modulates host responses to Pseudomonas syringae pv . tomato DC3000 infection. J. Plant Physiol. *168*, 1784–1794.

41. Ding, Y., Dommel, M., and Mou, Z. (2016). Abscisic acid promotes proteasome-mediated degradation of the transcription coactivator NPR1 in *Arabidopsis* thaliana. Plant J. *86*, 20–34.

42. Endo, M., Shimizu, H., Nohales, M. a., Araki, T., and Kay, S. A. (2014). Tissue-specific clocks in *Arabidopsis* show asymmetric coupling. Nature *515*, 419–422.

43. Takahashi, N., Hirata, Y., Takahashi, N., Hirata, Y., Aihara, K., and Mas, P. (2015). Article A Hierarchical Multi-oscillator Network Orchestrates the *Arabidopsis* Circadian System Article A Hierarchical Multi-oscillator Network Orchestrates the *Arabidopsis* Circadian System. Cell *163*, 148–159.

44. Li, S. (2015). The *Arabidopsis* thaliana TCP transcription factors : A broadening

horizon beyond development. Plant Signal. Behav. *10(7)*, e1044192.

45. Cubas, P., and Martı, M. (2009). TCP genes : a family snapshot ten years later. Trends Plant Sci. *15*, 31–9.

46. Jose L. Pruneda-Paz, Ghislain Breton, Alessia Para, S.A.K. (2009). A Functional Genomics Approach Reveals CHE as a Component of the *Arabidopsis* Circadian Clock. Science. *323*, 1481–1485.

47. Danisman, S. (2016). TCP Transcription Factors at the Interface between Environmental Challenges and the Plant ' s Growth Responses. Front. Plant Sci. *7*, 1930.

48. Wu, J., Tsai, H., Joanito, I., Wu, Y., Chang, C., and Li, Y. (2016). LWD-TCP complex activates the morning gene CCA1 in *Arabidopsis*. Nat. Commun. *7*, 1–10.

49. Aggarwal, P., Gupta, M. Das, Joseph, A.P., Chatterjee, N., Srinivasan, N., and Nath, U. (2010). Identification of Specific DNA Binding Residues in the TCP Family of Transcription Factors in *Arabidopsis*. Plant Cell *22*, 1174–1189.

50. Kosugi, S., and Ohashi, Y. (2002). DNA binding and dimerization specificity and potential targets for the TCP protein family. plant J. *30*, 337–348.

51. Viola, I.L., Güttlein, L.N., and Gonzalez, D.H. (2013). Redox Modulation of Plant Developmental Regulators from the Class I TCP Transcription Factor Family 1. Plant Physiol. *162*, 1434–1447.

Chapter 2 A localized *Pseudomonas syringae* infection triggers systemic clock responses in *Arabidopsis*

AUTHORS/AFFILIATIONS

Zheng Li[1], Katia Bonaldi[1], Francisco Uribe[1] and Jose L. Pruneda-Paz[1,2,*]

[1]Division of Biological Sciences, University of California San Diego, La Jolla, CA 92093, USA.

[2]Center for Chronobiology, University of California San Diego, La Jolla, CA 92093, USA.

*Correspondence: jprunedapaz@ucsd.edu (J.L.P-P.)

Summary

The circadian clock drives daily rhythms of many plant physiological responses providing a competitive advantage that improves plant fitness and survival rates [1-5]. Whereas multiple environmental cues are predicted to regulate the plant clock function, most studies focused on understanding the effects of light and temperature [5-8]. Increasing evidence indicates a significant role of plant-pathogen interactions on clock regulation [9, 10], but the underlying mechanisms remain elusive. In *Arabidopsis*, the clock function largely relies on a transcriptional feedback loop between morning (*CCA1* and *LHY*)- and evening (*TOC1*)- expressed transcription factors [6-8]. Here, we focused on these core components to investigate the *Arabidopsis* clock regulation using a unique biotic stress approach. We found that a single leaf *Pseudomonas syringae* infection systemically lengthened the period and reduced the amplitude of circadian rhythms in distal uninfected tissues. Remarkably, the low amplitude phenotype observed upon infection was recapitulated by a transient treatment with the defense related phytohormone salicylic acid (SA), which also triggered a significant clock phase delay. Strikingly, despite SA modulated circadian rhythms, we revealed that the master regulator of SA signaling, NPR1 [11, 12], antagonized clock responses triggered by both SA-treatment and *P. syringae*. In contrast, we uncovered that the NADPH oxidase RBOHD [13] largely mediated the aforementioned clock responses after either SA treatment or the bacterial infection. Altogether, we demonstrated novel and unexpected roles for SA, NPR1 and redox signaling in clock regulation by *P. syringae* and revealed a previously unrecognized layer of systemic clock regulation by locally perceived environmental cues.

KEYWORDS

Arabidopsis, Circadian clock, *P. syringae*, salicylic acid (SA), reactive oxygen species (ROS), *CCA1*, *LHY*, *TOC1*, *NPR1*, *RBOHD*.

Results

Localized *P. syringae* infection triggered a systemic clock amplitude reduction and period lengthening

To study plant clock responses to a localized pathogen challenge we used the *Arabidopsis-Pseudomonas syringae* pathosystem following a leaf-restricted infection. *Arabidopsis* seedlings carrying a luciferase reporter gene (*LUC+*) expressed under the control of the *CIRCADIAN CLOCK ASSOCIATED 1* (*CCA1)* promoter *(CCA1::LUC+)* were used to analyze the clock function after a single leaf *P. syringae* pv. *tomato* DC3000 (*Pst* DC3000) or mock treatments (performed at zeitgeber time [ZT]24) (Supplemental Figure 2.1A). Analysis of the whole plant luciferase activity after treatment indicated that *Pst* DC3000 infection results in low amplitude and long period clock rhythms (Supplemental Figure 2.1B and data not shown). However, *CCA1::LUC+* activity in the infected leaf rapidly decayed and became arrhythmic, suggesting that the observed phenotypes reflected the clock status in untreated tissues (Figure 2.1A-C). We reasoned that the amplitude reduction found after whole plant bioluminescence analysis was likely overestimated due to the inclusion of the infected leaf and the reduction of plant size after single leaf infection (Supplemental Figure 2.1C). Thus, we reanalyzed bioluminescence results considering only untreated tissues (of *Pst* DC3000 and mock treated plants) and normalizing bioluminescence counts to the estimated plant area at each time point (Supplemental Figure 2.1D). This analysis indicated that *Pst* DC3000 infection resulted

in systemic clock rhythms of significantly lower amplitude (Figure 2.1D-F) and ~0.5h longer period (Figure 2.1D and G). In addition, the period-normalized phase of *CCA1::LUC+* rhythms was slightly, albeit not significantly, advanced by the infection (Figure 2.1H and Supplemental Figure 2.1E). To confirm these results we performed the same experiment using *Arabidopsis* reporter lines carrying either the *LATE ELONGATED HYPOCOTYL* (*LHY) or TIMING OF CAB EXPRESSION 1* (*TOC1)* promoter driving the expression of the *LUC+* gene *(LHY::LUC+ or TOC1::LUC+)*. Notably, as we observed for the *CCA1* promoter activity, both new reporters exhibited a significant decay in the luminescence emitted by the infected leaf as soon as 24h post infection (Supplemental Figure 2.1F). When clock rhythms were analyzed in untreated tissues of single leaf *Pst* DC3000 versus mock treated plants we observed a significant amplitude and robustness reduction, and ~0.7h longer period upon infection (Figure 2.1E-G, I and J). In addition, *LHY* (but not *TOC1*) promoter-driven oscillations exhibited a phase advance upon infection (Figure 2.1H and Supplemental Figure 2.1G). To further evaluate the reduced amplitude phenotype, we quantified *CCA1*, *LHY* and *TOC1* mRNA levels in untreated tissues of single leaf *Pst* DC3000 and mock treated plants. As shown in Supplemental Figure 2.1H, we observed significantly reduced *CCA1* and *LHY* mRNA levels in infected plants supporting the results obtained via bioluminescence assays. Altogether, these findings revealed that a localized *Pst* DC3000 infection triggered a systemic signal that reduced the amplitude, lengthened the period, and minimally advanced the phase (for morning expressed reporters) of clock rhythms in untreated tissues.

Figure 2.1 Localized *P. syringae* infection triggers systemic clock responses.
(A) Representative time course pseudocolored bioluminescence images of soil grown *CCA1::LUC+* plants upon single leaf *Pst* DC3000 infection or mock treatment (hpi: hours post infection). Triangles (*Pst* DC3000: orange, mock: green) point to the treated leaf. (B) Luciferase activity from treated leaf or untreated tissues of soil grown *Arabidopsis CCA1::LUC+* plants upon single leaf *Pst* DC3000 infection (orange) or mock treatment (black). Treatments were performed at ZT24 (denoted by the black arrow) (see also Supplemental Figure 2.1A). Results indicate mean values [± SD, n=6] and are representative of 5 independent experiments. (C) Mean amplitude (left panel) and relative amplitude error (RAE) (right panel) values [± SEM] of *CCA1::LUC+* rhythms in treated leaf or untreated tissues upon single leaf *Pst* DC3000 infection (orange) or mock treatment (black) for experiments indicated in (B) (n=30). (D) Luciferase activity (normalized by plant size) from untreated tissues of soil grown *Arabidopsis CCA1::LUC+* plants upon single leaf *Pst* DC3000 infection (orange) or mock treatment (black). Results indicate mean values [± SD, n=6] and are representative of 5 independent experiments. (E-H) Mean amplitude (E), relative amplitude error (RAE) (F), period (G) and phase shift values (H) [± SEM] of *CCA1::LUC+* (n=30), *LHY::LUC+* (n=15) and *TOC1::LUC+* (n=15) normalized luciferase activity rhythms upon single leaf *Pst* DC3000 infection (orange) or mock treatment (gray) for experiments indicated in (D, I and J). (I-J) Luciferase activity (normalized by plant size) from untreated tissues of soil grown *Arabidopsis LHY::LUC+* and *TOC1::LUC+* plants upon single leaf *Pst* DC3000 infection (orange) or mock treatment (black). Results indicate mean values [± SD, n=9] and are representative of 2 independent experiments. Statistical analyses between mock and infected plants were performed using the *t* test (C, E, F, G and H). Stars indicate the level of significance (*$p<0.01$, **$p<0.001$, ***$p<0.0001$).

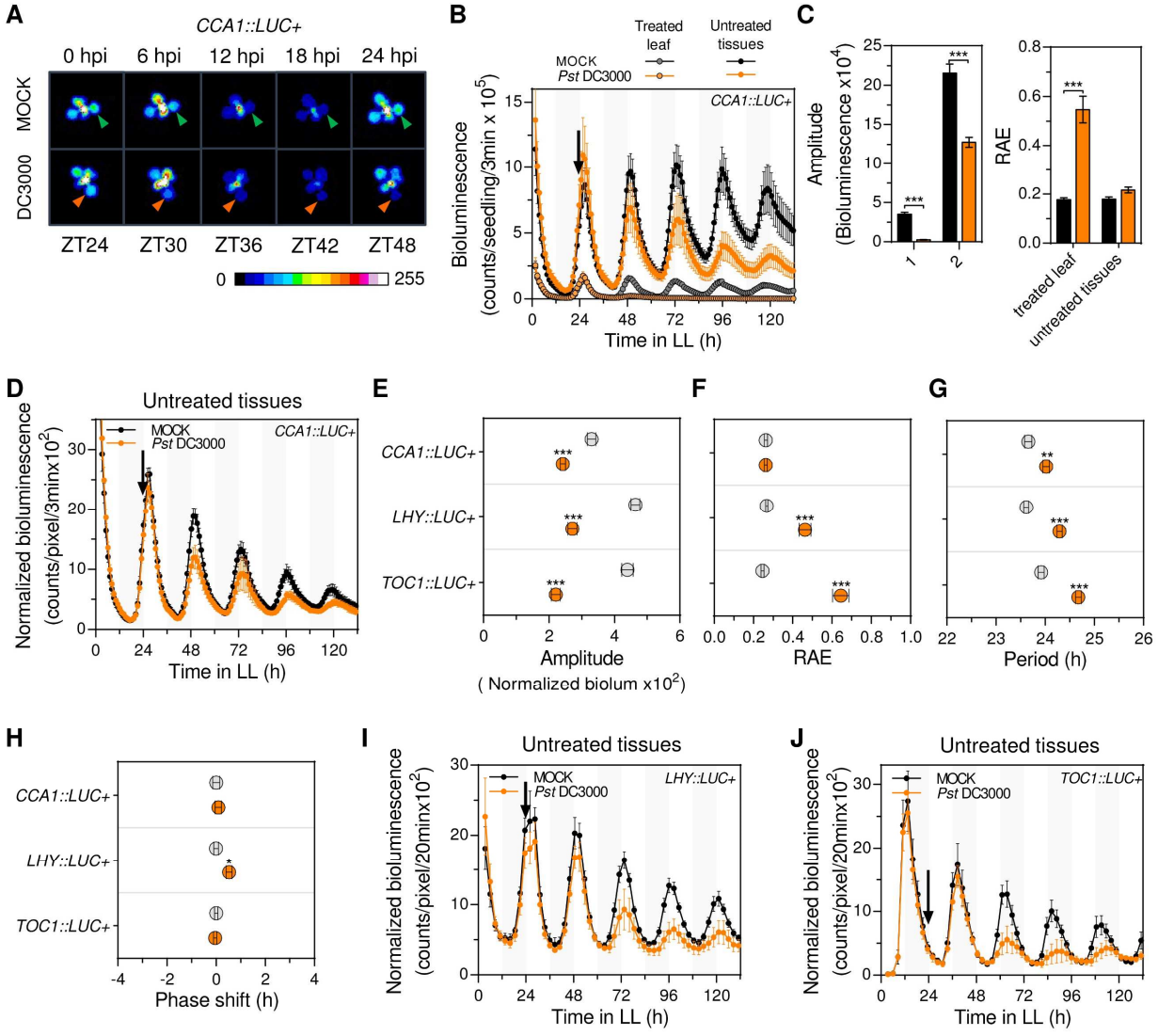
A
CCA1::LUC+
0 hpi
6 hpi
12 hpi
18 hpi
24 hpi
MOCK
DC3000
ZT24
ZT30
ZT36
ZT42
ZT48
0
255
B
Treated leaf
Untreated tissues
MOCK
Pst DC3000
CCA1::LUC+
Bioluminescence (counts/seedling/3min x 10^5)
Time in LL (h)
C
Amplitude (Bioluminescence x10^4)
RAE
treated leaf
untreated tissues
D
Untreated tissues
MOCK
Pst DC3000
CCA1::LUC+
Normalized bioluminescence (counts/pixel/3minx10^2)
Time in LL (h)
E
CCA1::LUC+
LHY::LUC+
TOC1::LUC+
Amplitude
(Normalized biolum x10^2)
F
RAE
G
Period (h)
H
Phase shift (h)
I
Untreated tissues
LHY::LUC+
Normalized bioluminescence (counts/pixel/20minx10^2)
Time in LL (h)
J
Untreated tissues
TOC1::LUC+
Normalized bioluminescence (counts/pixel/20minx10^2)
Time in LL (h)

Transient SA treatment phenocopied *P. syringae* triggered amplitude reduction and delayed the phase of clock rhythms

The phytohormone salicylic acid (SA), produced in response to plant infections, regulates many aspects of plant immunity in distal non-infected tissues [12, 14, 15]. While this critical role anticipated that SA could mediate the observed clock phenotypes upon infection, it was previously shown that SA increased (rather than reduced) the amplitude of clock rhythms [10]. Given that this previous finding likely indicated a clock response to long-term plant exposure to SA and that SA is transiently induced after a bacterial pathogen challenge [16], we analyzed *Arabidopsis* clock responses to a short-term SA treatment (performed at ZT24) using *CCA1::LUC+* seedlings (Supplemental Figure 2.2A). Similar to *Pst* DC3000 infection, a transient SA treatment resulted in low amplitude rhythms (Figure 2.2A- B) although without affecting their robustness (Figure 2.2C). This amplitude reduction was not influenced by plant size, as plant biomass was not affected by the transient SA treatment (Supplemental Figure 2.2B), or by SA effects over luciferase activity, as plants that constitutively express the *LUC+* reporter gene displayed same overall bioluminescence levels after SA or mock treatment (Supplemental Figure 2.2C). In contrast to the infection context, however, the period of *CCA1* promoter driven oscillations was not changed by the SA treatment (Figure 2.2D) and instead a significant phase delay was observed (Figure 2.2E and F). To evaluate if these clock responses depended on the time at which SA was applied, the experiment outlined above was performed initiating the treatment at different times of the day (ZT24, 28, 32, 36, 40, 44). Interestingly, while the period length remained unaltered in all experiments, we observed a greater phase shift when SA treatment was started close to the subjective dawn (Figure

2.2G and H). In contrast, the amplitude was overall reduced to a similar extent regardless of SA treatment start time (Figure 2.2I).

To validate *CCA1::LUC+* results, we next evaluated the clock function upon SA treatment in *LHY::LUC+* and *TOC1::LUC+* reporter lines. Indeed, we observed that a short-term SA treatment caused the same amplitude reduction and phase delay phenotypes in both *LHY::LUC+* and *TOC1::LUC+* rhythms (Figure 2.2B and F, Supplemental Figure 2.2D and E). To further evaluate these clock phenotypes we quantified *CCA1*, *LHY* and *TOC1* mRNA levels in SA and mock treated plants. In agreement with bioluminescence experiments, we observed a significant phase delay for all transcripts upon SA treatment (Supplemental Figure 2.2F and G). Furthermore, although we expected that (due to its limit of sensitivity) real time quantitative PCR would not detect the small amplitude differences found in bioluminescence assays, we did observe a tendency towards a reduced amplitude of mRNA oscillations (for *LHY* and *TOC1* transcripts) (Supplemental Figure 2.2F and G). Altogether, our results indicated that a pulse of SA significantly affected the phase and amplitude of clock rhythms, indicating a general role for SA in the regulation of *Arabidopsis* clock function. Furthermore, a SA pulse phenocopied the amplitude reduction that we observed after localized *Pst* DC3000 inoculation, suggesting that SA was one of the systemic signals that mediated the amplitude phenotype upon infection.

Figure 2.2 Transient SA treatment phenocopies *P. syringae*-triggered amplitude reduction and delays the phase of clock rhythms.
(A) Luciferase activity from *CCA1::LUC+* seedlings after transient SA treatment. Seedlings were treated with medium alone (mock) or supplemented with SA (0.2mM and 1 mM) at ZT24 for 4h (denoted by the orange shadowed area) (see also Supplemental Figure 2.2A). Results indicate mean values [± SEM, n=12] and are representative of 7 independent experiments. (B-D) Mean amplitude (B), relative amplitude error (RAE) (C) and period (D) values [± SEM] of *CCA1::LUC+* (n=110), *LHY::LUC+* (n=60) and *TOC1::LUC+* (n=60) rhythms after mock (grey), 0.2mM SA (blue) or 1mM SA (red) transient treatments for experiments indicated in (A) and Supplemental Figure 2.2D. (E) Normalized phase and RAE values of *CCA1::LUC+* rhythms after transient SA treatment for experiments indicated in (A) (mock: black, 0.2mM SA: blue and 1mM SA: red) (each dot represents one individual). The angular position of dots and arrows indicates the normalized phase value (0-24h) and the radial position indicates the RAE value (RAE=0 at the outmost radial position and RAE=1 at the center). The arrow points to the mean normalized phase and the arrow length indicates the mean RAE. (F) Mean phase shift values [± SEM] of *CCA1::LUC+* (n=110), *LHY::LUC+* (n=60) and *TOC1::LUC+* (n=60) rhythms after mock (grey), 0.2mM SA (blue) or 1mM SA (red) transient treatments indicated in (A) and Supplemental Figure 2.2D. (G-I) Period (G), phase shift (H) and normalized amplitude (ratio over mean mock) (I) values of *CCA1::LUC+* rhythms after mock (black) or 1mM SA (red) transient treatments performed at different times of the day. Plants were grown as indicated in (A) and treatments were started at 6 different times during the second day in LL (ZT24, ZT28, ZT32, ZT36, ZT40, ZT44). Results represent mean values [± SEM, n=48] of 4 independent experiments. Statistical analyses between mock and SA treated plants were performed using the *t* test (B, C, D and F) and Watson-Williams test (E). Stars indicate the level of significance (*$p<0.01$, **$p<0.001$, ***$p<0.0001$).

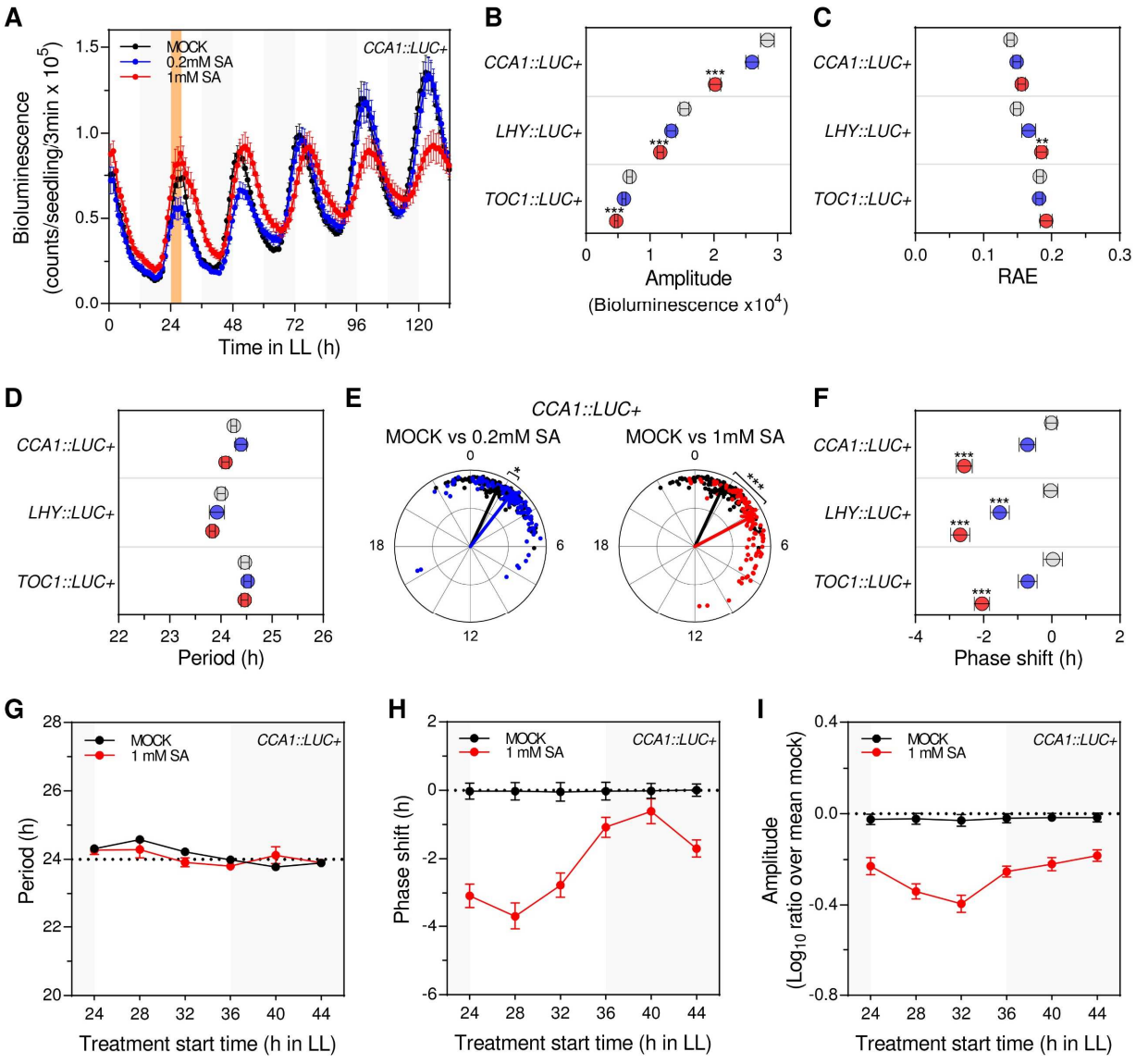
A
MOCK
0.2mM SA
1mM SA
CCA1::LUC+
Bioluminescence (counts/seedling/3min x 10^5)
Time in LL (h)
B
CCA1::LUC+
LHY::LUC+
TOC1::LUC+
Amplitude (Bioluminescence x10^4)
C
RAE
D
Period (h)
E
CCA1::LUC+
MOCK vs 0.2mM SA
MOCK vs 1mM SA
F
Phase shift (h)
G
MOCK
1 mM SA
Period (h)
Treatment start time (h in LL)
H
Phase shift (h)
I
Amplitude (Log10 ratio over mean mock)

SA effects on the clock function were antagonized by *NPR1*

Given that most SA responses are dependent on the transcription cofactor NONEXPRESSER OF PR GENES 1 (NPR1) [12], we next investigated whether clock effects triggered by a transient SA treatment were mediated by NPR1. For that, we introduced the loss-of-function *npr1-1* allele into the *CCA1::LUC+* and *LHY::LUC+* reporter backgrounds and treated the resulting lines with SA at ZT24 (as described above, Supplemental Figure 2.2A). As expected, we observed that a transient SA treatment caused a significant amplitude reduction in WT plants for both reporter lines (Figure 2.3A and B). Strikingly, in *npr1-1* plants the amplitude was reduced to a significantly greater extent in both *CCA1::LUC+* and *LHY::LUC+* reporter backgrounds (Figure 2.3A-C and Supplemental Figure 2.3A). Consistent with these results, *CCA1* and *LHY* promoter driven oscillations exhibited a decreased robustness when the SA treatment was applied to *npr1-1* compared to WT plants (Supplemental Figure 2.3B). It should be noted that the amplitude reduction was not influenced by a change in plant size, as same biomass was observed between mock and SA treated *npr1-1* plants (Supplemental Figure 2.3C). We next determined *CCA1*, *LHY* and *TOC1* mRNA levels in SA and mock treated *npr1-1* plants and observed that indeed transcript levels for these genes oscillated with a significantly reduced amplitude upon exposure to SA (Supplemental Figure 2.3D and E). To further validate these findings, we analyzed the clock function after a transient SA treatment in *CCA1::LUC+* and *LHY::LUC+* reporter lines that overexpressed *NPR1* (*NPR1-OX*, Supplemental Figure 2.3F). We found that, unlike in WT plants, SA did not reduce the clock amplitude in *NPR1-OX* plants (Figure 2.3A, B, E and Supplemental Figure 2.3A).

On the other hand, the period of clock oscillations remained mostly unchanged in all backgrounds and treatment conditions (Supplemental Figure 2.3G). Importantly, similar to the aforementioned amplitude phenotypes, analysis of period-normalized phase shifts for *CCA1::LUC+* and *LHY::LUC+* rhythms indicated that SA treatment resulted in greater or milder phase delay in *npr1-1* or *NPR1-OX* backgrounds, respectively, when compared to WT plants (Figure 2.3D, Supplemental Figure 2.3H and I). Altogether, these observations revealed that *NPR1* loss of function and overexpression respectively enhanced and reduced the impact of SA on amplitude and phase phenotypes, revealing an unexpected role for NPR1, which functioned as an antagonist of transient SA effects on the circadian clock.

P. syringae*-triggered amplitude reduction of clock rhythms was antagonized by *NPR1

Given the antagonistic effect of NPR1 on the regulation of circadian rhythms by SA, and that both *Pst* DC3000 infections and SA treatment decreased amplitude of clock rhythms, we next hypothesized that NPR1 may also counteract the amplitude phenotype that we observed after infection. To evaluate this possibility, we performed single leaf *Pst* DC3000 infections in WT, *npr1-1* and *NPR1-OX* plants carrying the *CCA1::LUC+* reporter. Analysis of the luciferase activity in untreated tissues showed that the amplitude of clock controlled rhythms in uninfected tissues was more significantly reduced by the infection in *npr1-1* compared to WT plants, albeit a similar amplitude reduction was observed in *NPR1-OX* versus WT backgrounds (Figure 2.3F, G and Supplemental Figure 2.4A). Consistent with the lower amplitude, a greater decrease in the robustness of clock

rhythms was observed after infection in *npr1-1* versus WT plants (Supplemental Figure 2.4B). Likewise, the period of *CCA1::LUC+* rhythms was lengthened to a significantly greater extent after infection in *npr1-1* versus WT and *NPR1-OX* plants (Figure 2.3H and I). Of note, as described above for WT plants (Figure 2.1H), the period-normalized phase of *CCA1::LUC+* rhythms was only minimally changed after infection in both *NPR1* genetic backgrounds (Figure 2.3J and Supplemental Figure 2.4C). These results indicated that (as described for a transient SA treatment) *NPR1* antagonized the systemic amplitude reduction, while additionally counteracting period lengthening, of clock rhythms observed after single leaf *Pst* DC3000 infection.

Figure 2.3 NPR1 antagonizes clock responses triggered by transient SA treatment or single leaf *P. syringae* infection.
(A, C and E) CCA1::LUC+ activity in wild type (WT) (A), npr1-1 (C) and NPR1-OX (E) seedlings after transient SA treatment. Seedlings were treated with medium alone (mock) or supplemented with SA (0.2mM and 1 mM) at ZT24 for 4h (denoted by the orange shadowed area) (see also Supplemental Figure 2.2A). Results indicate mean values [± SEM, n=12] and are representative of 4 independent experiments. (B and D) Mean normalized amplitude (ratio over mean mock) (B) and phase shift (D) values [± SEM] of *CCA1::LUC+* (left panel) (n=72) and *LHY::LUC+* (right panel) (n≥58) rhythms in WT, *npr1-1 and NPR1-OX* seedlings after 0.2mM (blue) and 1mM (red) transient SA treatment of 4 independent experiments indicated in (A, C and E) (see also Supplemental Figure 2.3A, H and I). (F) *CCA1::LUC+* activity (normalized by plant size) from untreated tissues of soil grown WT and *npr1-1* plants upon a single leaf *Pst* DC3000 infection (orange) or mock treatment (black). Treatments were performed at ZT24 (denoted by the black arrow) (see also Supplemental Figure 2.1A). Results indicate mean values [± SD, n=6] and are representative of 5 independent experiments. (G, I, J) Mean normalized amplitude (ratio over mean mock) (G), period length change (∆period) (I), and phase shift (J) values [± SEM, n=30] of *CCA1::LUC+* rhythms (normalized by plant size) in WT, *npr1-1 and NPR1-OX* plants after a single leaf *Pst* DC3000 infection for experiments indicated in (F) (see also Supplemental Figure 2.4 A and C). (H) Mean period estimates [± SEM, n=30] of *CCA1::LUC+* rhythms (normalized by plant size) in WT, *npr1-1 and NPR1-OX* plants upon single leaf *Pst* DC3000 infection (orange) or mock treatment (gray) for experiments indicated in (F). Statistical analyses compared to WT plants (B, D, G, I and J), or compared mock treated plants (H) were performed using the *t* test. Stars indicate the level of significance (*p<0.01, **p<0.001, ***p<0.0001).

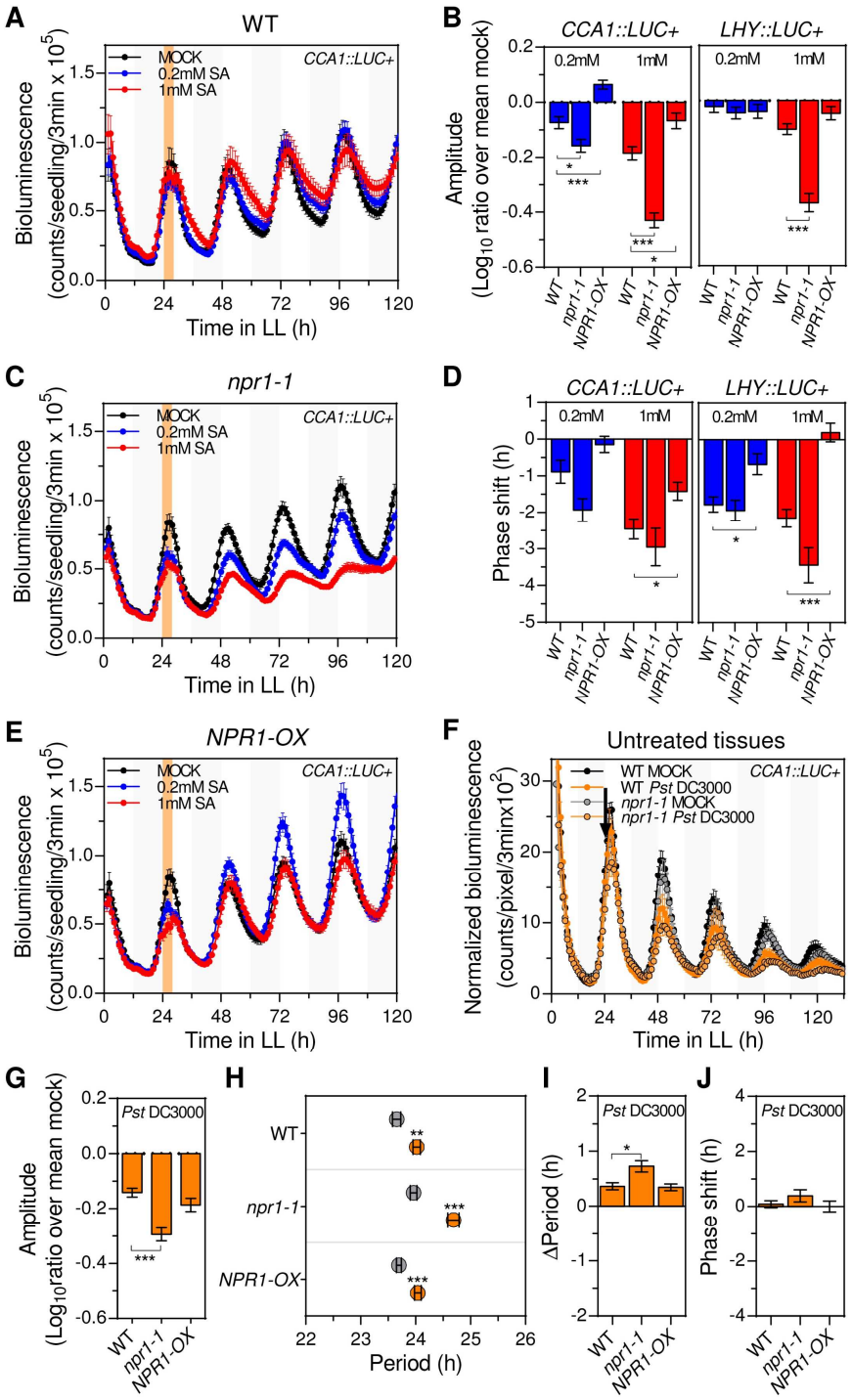
A
WT
MOCK
0.2mM SA
1mM SA
CCA1::LUC+
Bioluminescence (counts/seedling/3min x 10^5)
Time in LL (h)
B
CCA1::LUC+
LHY::LUC+
0.2mM
1mM
Amplitude (Log10 ratio over mean mock)
WT
npr1-1
NPR1-OX
C
npr1-1
D
Phase shift (h)
E
NPR1-OX
F
Untreated tissues
WT MOCK
WT Pst DC3000
npr1-1 MOCK
npr1-1 Pst DC3000
Normalized bioluminescence (counts/pixel/3minx10^2)
G
Pst DC3000
H
Period (h)
I
ΔPeriod (h)
J

SA effects on the circadian clock were phenocopied by H_2O_2 treatment and partly mediated by *RBOHD*

Considering that SA responses are partly mediated by a rapid increase of reactive oxygen species (ROS) [15, 17], we next hypothesized that ROS may mediate the clock phenotypes observed after transient SA treatment. To test this possibility, we first analyzed the effect of a transient H_2O_2 treatment on *CCA1::LUC+* rhythms (Supplemental Figure 2.2A). Remarkably, we found that (as observed for SA, Figure 2.2 and Supplemental Figure 2.2) a transient H_2O_2 treatment did not affect the robustness and period of circadian rhythms but did cause a profound amplitude reduction and phase delay (Figure 2.4A-E). Given that SA could induce apoplastic H_2O_2 production through the nicotinamide adenine dinucleotide phosphate (NADPH)-oxidase RESPIRATORY BURST OXIDASE HOMOLOGUE D (RBOHD) [13, 18], we next tested the possibility that *RBOHD* may mediate SA effects on the clock function. For that, we analyzed *CCA1::LUC+* rhythms after a transient SA treatment in *rbohd* mutant plants (Supplemental Figure 2.2A). Strikingly, when bioluminescence was analyzed in mock treated plants (without SA or H_2O_2 treatment), amplitude reduction and phase advance phenotypes were observed in *rbohd* mutant compared to WT plants (Figure 2.4F, Supplemental Figure 2.4D and E). Upon SA treatment, however, the degree of amplitude reduction was similar in *rbohd* versus WT plants (Figure 2.4F, G and Supplemental Figure 2.4D), whereas the robustness and period continued being mostly unchanged in both genetic backgrounds (Supplemental Figure 2.4F and G). In sharp contrast, whereas SA treatment continued to delay the clock phase in WT plants, we did not observe any SA-induced phase change in the *rbohd* mutant background (Figure 2.4H and Supplemental

Figure 2.4E). Altogether, these results revealed that SA effects on the clock were fully mimicked by the H_2O_2 treatment, suggesting that ROS likely mediated SA-induced clock regulation. Furthermore, the absence of SA-induced phase, but not amplitude, phenotype in *rbohd* mutant plants suggested that clock regulation by SA relied on RBOHD-dependent (i.e. apoplastic ROS) and RBOHD-independent ROS sources.

P. syringae **infection effects on the circadian clock were partly mediated by** ***RBOHD***

Given that SA-effects on clock regulation were partly mediated by *RBOHD* and that pathogen recognition rapidly triggers RBOHD-dependent ROS production [19, 20], we next investigated a putative role for RBOHD on the regulation of systemic clock phenotypes induced by a localized *Pst* DC3000 infection. For that, we performed single leaf infection experiments in WT and *rbohd* mutant plants carrying the *CCA1::LUC+* reporter (Supplemental Figure 2.1A). As described above for the SA amplitude effect in *rbohd* mutant plants (Figure 2.4G), we observed that the amplitude and robustness of *CCA1* promoter driven rhythms were equally affected by the infection in both WT and *rbohd* plants (Figure 2.4I, J, Supplemental Figure 2.4H and I). Remarkably, we found that both the slight phase advance and the significant period lengthening that we observed in WT plants upon infection were no longer detected in the *rbohd* mutant background (Figure 2.4K-M and Supplemental Figure 2.4J). These results supported the notion that while RBOHD-dependent ROS did not mediate the infection-induced amplitude reduction, it did trigger the systemic clock period and phase phenotypes observed after a localized *Pst* DC3000 infection.

Figure 2.4 Apoplastic ROS partly mediates clock responses triggered by transient SA treatment or single leaf *P. syringae* infection.
(A) Luciferase activity of *CCA1::LUC+* seedlings after transient H_2O_2 treatment. Seedlings were treated with medium alone (mock) (n=24) or supplemented with 50mM (n=12) or 200mM (n=12) H_2O_2 at ZT24 for 4h (denoted by the orange shadowed area) (see also Supplemental Figure 2.2A). Results indicate mean values [± SEM] and are representative of 2 independent experiments. (B-E) Mean amplitude (B), relative amplitude error (RAE) (C), period (D) and phase shift (E) values [± SEM] of *CCA1::LUC+* rhythms after mock (black bars) (n=49), 50mM H_2O_2 (gray bars) (n=33) or 200mM H_2O_2 (striped bars) (n=30) transient treatments for experiments indicated in (A). (F) *CCA1::LUC+* activity in wild type (WT) (n=24) and *rbohd* (n=12) seedlings after transient 1mM SA treatment as indicated in Supplemental Figure 2.2A. Results indicate mean values [± SEM] and are representative of 4 independent experiments. (G and H) Mean normalized amplitude (ratio over mean mock) (G) and phase shift (H) values [± SEM] of *CCA1::LUC+* rhythms in WT (n=80) and *rbohd* (n=64) seedlings after 0.2mM (blue) and 1mM (red) transient SA treatment for experiments indicated in (F) (see also Supplemental Figure 2.4D-E). (I) *CCA1::LUC+* activity (normalized by plant size) from untreated tissues of soil grown WT and *rbohd* plants upon single leaf *Pst* DC3000 infection (orange) or mock treatment (black). Treatments were performed at ZT24 (denoted by the black arrow) (see also Supplemental Figure 2.1A). Results indicate mean values [± SD, n=6] and are representative of 3 independent experiments. (J, L, M) Mean normalized amplitude (ratio over mean mock) (J), period length change (∆period) (L), and phase shift (M) [± SEM, n=18] for *CCA1::LUC+* rhythms in WT and *rbohd* after single leaf *Pst* DC3000 infection for experiments indicated in (I) (see also Supplemental Figure 2.4H and J). (K) Mean period estimates [± SEM, n=18] for *CCA1::LUC+* rhythms in WT and *rbohd* plants upon single leaf *Pst* DC3000 infection (orange) or mock treatment (gray) for experiments indicated in (I). Statistical analyses compared to mock treated plants (B-E and K), or compared to WT plants (G, H, J, L and M) were performed using the *t* test. Stars indicate the level of significance (*$p<0.01$, **$p<0.001$, ***$p<0.0001$).

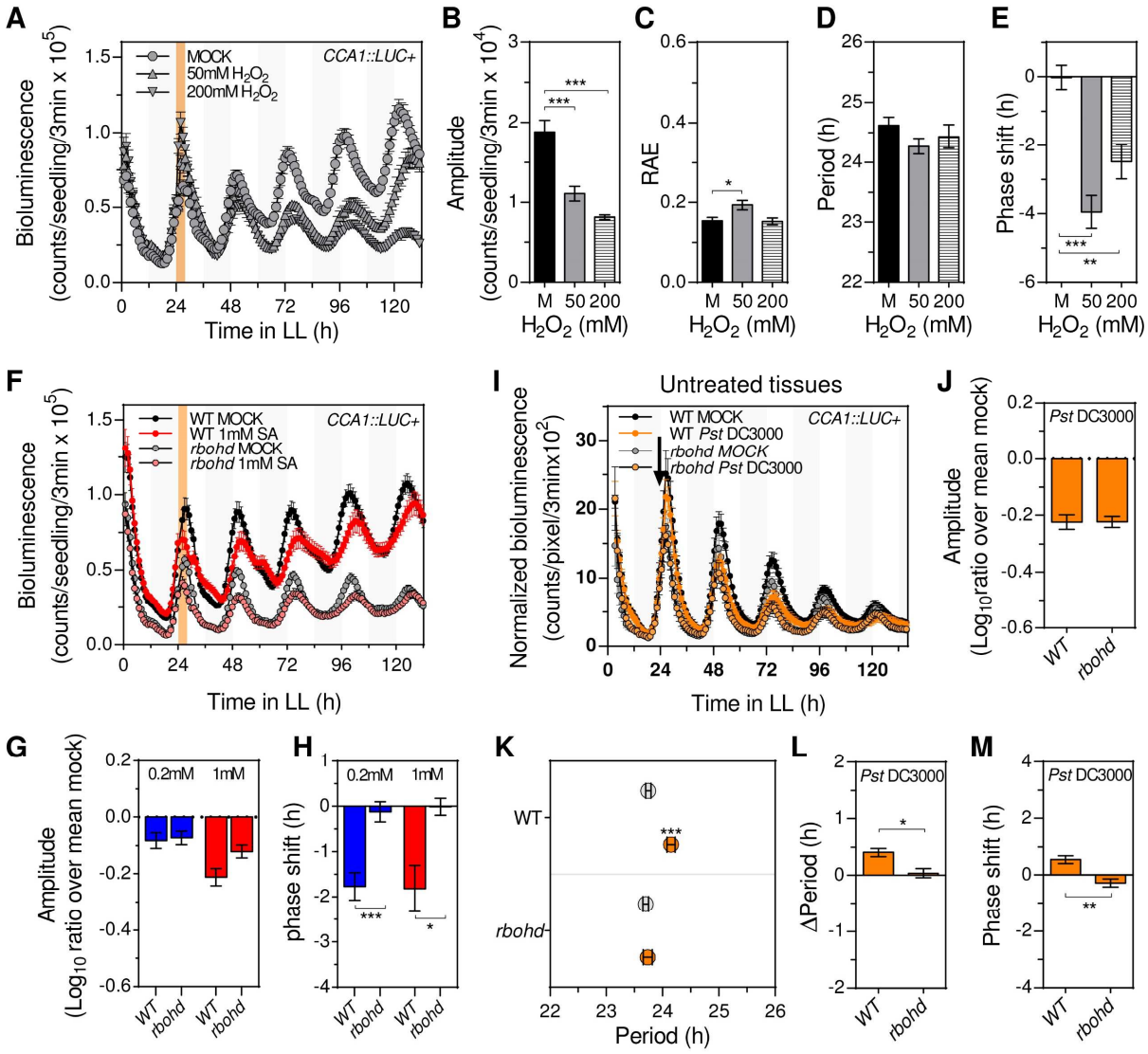
A
Bioluminescence (counts/seedling/3min x 10^5)
MOCK
50mM H2O2
200mM H2O2
CCA1::LUC+
Time in LL (h)
B
Amplitude (counts/seedling/3min x 10^4)
H2O2 (mM)
C
RAE
D
Period (h)
E
Phase shift (h)
F
WT MOCK
WT 1mM SA
rbohd MOCK
rbohd 1mM SA
I
Untreated tissues
Normalized bioluminescence (counts/pixel/3minx10^2)
WT Pst DC3000
rbohd Pst DC3000
J
Pst DC3000
Amplitude (Log10ratio over mean mock)
G
0.2mM
1mM
H
phase shift (h)
K
WT
rbohd
Period (h)
L
ΔPeriod (h)
M

Discussion

The circadian clock is an endogenous timekeeping mechanism that orchestrates daily rhythms in most plant biological processes [1, 4, 7]. This function, critical for sessile plants, requires daily adjustments by multiple environmental cues predicted to signal into the core clock mechanism through a network of heavily integrated circuits [5, 8]. While plants are exposed to a wide range of abiotic and biotic environmental signals, there was a gap in knowledge on how biotic interactions affect plant circadian rhythms and what are the pathways involved in these responses. Our work provided solid evidence indicating that a single leaf *Pst* DC3000 infection (despite being localized) significantly modulated the clock function at the whole plant level and identified the mechanisms involved, revealing novel roles for SA, NPR1 and redox signaling in the regulation of circadian rhythms (see model in Supplemental Figure 2.4K).

We found that the clock function was systemically affected in response to a local *Pst* DC3000 infection, displaying low amplitude and long period phenotypes (Figure 2.1 D, E, G, I, J and Supplemental Figure 2.1H). These findings were unexpected as a previous study using *P. syringae* pv*. maculicola* ES4326 (*Pma*DG3) reported a short (rather than long) period phenotype after infection [9]. It should be noted that (in contrast to the local leaf infection and soil grown conditions that we used) in the last-mentioned study whole *Arabidopsis* seedlings were fully soaked into a bacterial cell suspension and plants were subsequently grown in sucrose supplemented tissue culture medium [9]. Given that a pathogen challenge (i.e. *P. syringae* inoculation) reduces the photosynthetic capacity in the infected tissues [21, 22] and that sucrose treatment influences the clock function in plants with reduced photosynthesis [23], it is possible that the differences in

infection protocols and sucrose availability may have accounted for the disparate results. Furthermore, it has been reported that *Pma*DG3 and *Pst* DC3000 infections trigger distinct transcriptional responses in *Arabidopsis* [24], which could have also contributed to the contrasting observations. Nonetheless, together with the study published by Zhang et al., our work raises the possibility that multiple variables such as the affected tissues, the energy status of the plant and the pathogen strain may influence the outcome of clock regulation by a bacterial infection.

One of the most valuable contributions from our study was to expose an unrecognized regulatory layer within the plant circadian system in which the overall clock function is modulated by environmental cues that locally affect specific plant tissues (Figure 2.1 and Supplemental Figure 2.1). This is an exciting observation since a recent report indicated that the plant circadian system has a hierarchical organization with a master oscillator located at the shoot apical meristem (SAM) and peripheral subordinate clocks in other tissues [25]. Thus, our findings suggest that a systemic signal originated at the infected leaf may regulate the SAM clock and therefore affect the clock function at the whole plant level. Alternatively, it is possible that a systemic signal triggered after the localized infection directly modulates peripheral clocks.

Importantly, our studies support the view that SA, which is produced transiently upon infections [16], was one of the aforementioned systemic signals that regulated the circadian clock in non-infected tissues (Figure 2.2A, B and Supplemental Figure 2.2D). It should be noted that previous work by Zhou et al. found that SA increases (rather than decreases) the amplitude of clock rhythms [10]. While this result is in sharp contrast with the sustained amplitude reduction that we observed after both *Pst* DC3000 infection and

transient SA treatment (Figure 2.1D, E, I, J, Supplemental Figure 2.1H, Supplemental Figure 2.2A, B and D), it is possible that these discrepancies reflect the overall dynamic nature of SA responses. For example, it was suggested that spatiotemporal changes in SA concentrations could lead to opposite responses [26] and that SA responses are diminished as plants age [27]. Thus, different hormone concentrations, longer exposure time, and/or slightly older plants used by Zhou et al. may have accounted for the disparate results. Remarkably, our results also showed for the first time that a transient SA treatment impinged a profound phase delay on clock oscillations (Figure 2.2E, F, H and Supplemental Figure 2.2E-G). Notably, such phase delay phenotype was not detected in *Pst* DC3000 infected plants, which instead exhibited a slight phase advance (Figure 2.1H, Supplemental Figure 2.1E and G), raising the possibility that SA-independent pathways neutralized and/or overruled the SA induced phase delay during infection. Likewise, only *Pst* DC3000, but not SA, lengthened the clock period (Figure 2.1G and Figure 2.2D), further suggesting SA-independent pathways that also modulated the clock period upon infection. Given that we observed the same amplitude reduction and phase delay phenotypes even after a longer (12h) transient SA treatment (data not shown), altogether our results suggested that SA-dependent and -independent pathways are integrated to determine the ultimate clock phenotypes in infected plants (depicted in Supplemental Figure 2.4K and further discussed below). However, we cannot completely rule out the possibility that (in the context of *Pst* DC3000 infection) SA might regulate the clock in a manner that was not fully recapitulated by the transient SA treatment used in our study.

Our work also revealed an unexpected antagonistic role for NPR1 in the regulation of circadian rhythms by both SA and *P. syringae* infection. While NPR1 mediates most

SA-induced transcriptional responses [12], we counterintuitively found that NPR1 prevented the amplitude reduction and phase delay triggered by a transient SA treatment (Figure 2.3A-E, Supplemental Figure 2.3A, D and E). Importantly, the amplitude reduction induced by *Pst* DC3000 infection was also enhanced in *npr1-1* mutant plants (Figure 2.3F-G and Supplemental Figure 2.4A), supporting the biological significance of the aforementioned antagonistic NPR1 effect on clock regulation by SA (modeled in Supplemental Figure 2.4K). These results are in line with previous work suggesting that NPR1 not only mediates SA responses but also provides a safeguard mechanism to counteract SA signaling. For example, it was reported that NPR1 negatively regulates SA synthesis [28] and that NPR1 proteasome-mediated degradation plays dual roles in plant immunity (required for both inactivation and activation of target genes) [29].

Finally, our study uncovered a previously unrecognized role for RBOHD (and thus apoplastic ROS) in clock regulation both before and after infection. We first found that *rbohd* mutant plants exhibited a reduced amplitude and advanced phase in basal conditions (Figure 2.4F, Supplemental Figure 2.4D and E), revealing a previously unrecognized and pivotal role for apoplastic ROS in maintaining the overall function of the *Arabidopsis* clock function under steady state conditions. In addition, consistently with enhanced ROS signaling upon SA treatment or pathogen recognition [15, 17], we observed that clock responses to SA were phenocopied by a transient H_2O_2 treatment (Figure 2.4A-E). These results were consistent with a previous study indicating that spraying seedlings with H_2O_2 or ROS-inducing-chemicals (likely resulting in a prolonged ROS treatment) induces phase delayed clock rhythms [30]. Importantly, despite multiple ROS sources [15, 17], our results indicated that SA-induced phase delay was mediated

by apoplastic ROS as it was reverted when apoplastic ROS production was compromised (*rbohd* mutant plants) (Figure 2.4H and Supplemental Figure 2.4E). In contrast, we found that the amplitude phenotype likely involved other ROS sources since SA and *Pst* DC3000 equally reduced the clock amplitude in wild-type and *rbohd* mutant plants (Figure 2.4G and J). Finally, although we could not observe any period phenotype after (transient) H_2O_2 treatment (Figure 2.4D), the aforementioned study by Lai et al. showed that (likely sustained) ROS treatments did lengthened the clock period [30] and we observed that the long period phenotype detected after *Pst* DC3000 infection depended on RBOHD (Figure 2.4K-L). Thus, together with the result by Lai et al., our work supported a model in which persistently elevated aplopastic ROS levels lengthened the clock period after infection, which is consistent with the continued ROS accumulation [31, 32] and enhanced RBOHD activity in infected plants [19, 20]. Given that the period phenotype was not observed after SA treatment (Figure 2.2D), these results suggested that the putative SA-independent pathways that regulated the clock function after infection were, at least partly, mediated by apoplastic ROS. Consistently, our results suggested that SA-independent apoplastic ROS also promoted the slight phase advance observed after infection (Figure 2.4M). Thus, we propose that RBOHD-dependent ROS production is a key signal that largely mediated the aforementioned SA-dependent and -independent pathways that fine-tuned the overall plant clock after a leaf-restricted infection (Supplemental Figure 2.4K). This is in line with previous studies indicating that RBOHD propagates a systemic long distance ROS wave triggered by a localized stress [33, 34]. It remains unclear, however, how apoplastic ROS (or RBOHD) delayed the clock phase downstream SA (i.e. upon sole SA treatment) while having the opposite effect in the

infection context (i.e. a net advancing phase effect after infection). Possible explanations include different levels, duration and/or distribution of SA-independent versus SA-dependent apoplastic ROS, in addition to contextual regulation induced by specific signals in infected plants.

In conclusion, our work used a unique approach to investigate the *Arabidopsis* clock, characterizing for the first time how a virulent pathogen infection modulated circadian rhythms in soil grown plants. Remarkably, we revealed a new layer of regulation within the plant circadian system in which the overall clock function is modulated by locally perceived environmental cues. Period and phase changes predict that upon infection plant endogenous rhythms would be desynchronized from external environmental cycles, anticipating a suboptimal photosynthetic capacity [2]. It is possible that this mechanism may have evolved to prevent ROS hyper accumulation and its negative consequences after infection. In addition, amplitude reduction indicates a weakened clock function upon infection, which may be necessary to allow continuous immunity to contain the infectious bacteria and prevent re-infection. Importantly, we identified critical signaling pathways (SA and ROS) and key components of these pathways (NPR1 and RBOHD) that regulated clock responses after infection. Most saliently, we revealed an unexpected antagonistic role for NPR1 in SA-triggered clock responses, and a novel role for apoplastic ROS as a regulator of circadian rhythms, not only upon biotic stress but also in basal conditions. Given that ROS signaling is found at the crossroad of most plant biotic or abiotic stress signaling pathways [34, 35] our findings may also illuminate how plant circadian rhythms are adjusted by multiple stress responses. Thus, our study disentangles the highly complex regulation of circadian rhythms after infection and paves

the way for future studies aiming at potentially tweaking the clock to enhance plant performance in general, and specifically after pathogen encounter.

AUTHOR CONTRIBUTIONS

Conceptualization, J.L.P.; Methodology, Z.L. and J.L.P.; Validation, Z.L. and J.L.P.; Formal Analysis, Z.L.; Investigation, Z.L., K.B. and F.U.; Writing-Original Draft, Z.L. and J.L.P.; Writing-Review & Editing, Z.L. and J.L.P.; Funding Acquisition, J.L.P.; Resources, Z.L. and J.L.P.; Supervision, J.L.P.

CONFLICT OF INTEREST

The authors declare no competing conflicts of interest.

Star Methods

CONTACT FOR REAGENT AND RESOURCE SHARING

Further information and requests for resources and reagents should be directed to and will be fulfilled by the Lead Contact, Jose L. Pruneda-Paz (jprunedapaz@ucsd.edu).

EXPERIMENTAL MODEL AND SUBJECT DETAILS

Plant materials

Arabidopsis thaliana (*Arabidopsis*) seedlings used in this work were from the Columbia ecotype (Col-0). *CCA1::LUC+* [37], *LHY::LUC+* [38], *TOC1::LUC+* [39] reporter lines, and *npr1-1* [44] and *rbohd* (SALK_070610) [18] loss-of function lines were previously described.

To generate *NPR1* overexpression lines, *NPR1* protein coding sequence was PCR amplified (primer sequences are indicated in Supplementary Table 2.1) and cloned into the pENTR/D-TOPO vector (Life technologies). The resulting pENTR/D-NPR1 vector was used to transfer *NPR1* coding sequence into the pMDC32 binary vector [40] using LR Clonase II (Life Technologies). Finally, pMDC32-NPR1 was transferred into the *Arabidopsis CCA1::LUC+* or *LHY::LUC+* backgrounds by *Agrobacterium*-mediated transformation [45]. For that, Agrobacterium GV3101 cells carrying the pMDC32-NPR1 plasmid were grown overnight in liquid Luria-Bertani medium supplemented with kanamycin (50mg/L) and gentamycin (30mg/L). Cells were harvested by centrifugation (3220 x *g* for 10min at room temperature) and resuspended in 5% sucrose solution containing 0.02% Silwet L-77 (Lehle seeds). Developing *Arabidopsis* inflorescences for the aforementioned reporter lines were dipped into the agrobacterium cell suspension for 30sec, and dipped plants were wrapped with a plastic film and incubated horizontally in a growth chamber for 16-24 h. Finally, the plastic film was removed, and plants were returned to the normal growth position and incubated in a growth chamber until seed collection (~1.5 months). To generate *35S::LUC+* lines, the multiple cloning site (MCS) from pBluescript KS(-) was PCR amplified (primer sequences are indicated in Supplementary Table 2.1) and cloned into pENTR/D-TOPO. The resulting pENTR/D-MCS vector was used to transfer MCS sequence into the pMDCLUC+ vector [42] using LR Clonase II. Finally, pMDC-MCSLUC+ was transferred into the *Arabidopsis* Col-0 background by *Agrobacterium*-mediated transformation [45], as described above.

The *rbohd(CCA1::LUC+), npr1-1(CCA1::LUC+)* and *npr1-1(LHY::LUC+)* lines were generated by genetic cross and mutations were confirmed by PCR.

Plant growth conditions

For *Pseudomonas syringae* infection assays, stratified sterile seeds were grown in autoclaved soil (Sunshine professional mix, Sungro) under 12h light (~100 $\mu mol.m^{-2}.s^{-1}$) / 12h dark cycles (LD) for 14 days at 22°C. At the beginning of day 15, plants were transferred to constant light (60 $\mu mol.m^{-2}.s^{-1}$, 22°C) (LL) for bioluminescence imaging or RNA time course tissue collection. Single leaf infections were performed at the beginning of the second day in LL (ZT24).

For transient SA or H_2O_2 treatments, *Arabidopsis* seeds were placed on 60mm plates (12 seeds/plate) containing 1x Murashige & Skoog basal salts (MS) medium (Caisson Labs) supplemented with 3% sucrose overlaid with a nylon mesh (50 micron square opening, white) (Small parts) and stratified for 2-3 days at 4ºC. Plates were incubated for 10 days under 12 hour light (100 $\mu mol.m^{-2}.s^{-1}$)/12 hour dark cycles (LD) at 22ºC. At the beginning of the 11^{th} day, plants were transferred to constant light (60 $\mu mol.m^{-2}.s^{-1}$, 22°C) (LL) for bioluminescence imaging or RNA time course tissue collection. Transient SA or H_2O_2 treatments were performed during the second day in LL.

To determine *NPR1* expression level in NPR1 overexpression lines, seedlings were grown in petri dishes containing 1x MS - 3% sucrose medium for 10 days under LD cycles at 22ºC.

Pseudomonas syringae culture conditions

Pseudomonas syringae pv. *tomato* DC3000 *(Pst* DC3000*)* [36] liquid cultures (King's B medium: 2% Proteose peptone No.3, 1% Glycerol, 8.6mM K_2HPO_4 and 6mM $MgSO_4$) were grown in the dark at 28ºC (shaking at 175rpm) until OD600 between 0.6

and 0.7 was reached (several dilutions were started to assure that a suitable culture was available at the time of treatment).

Accession numbers

Gene models in this article can be found in The *Arabidopsis* Information Resource (TAIR) (www.arabidopsis.org) with the following accession numbers: *CCA1*, AT2G46830; *LHY*, AT1G01060; *TOC1*, AT5G61380; *RBOHD*, AT5G47910; *NPR1*, AT1G64280; *IPP2*, AT3G02780; *PP2A*, AT1G13320.

METHOD DETAILS

Single leaf Pseudomonas syringae infection

To prepare *Pst* DC3000 cell suspension inoculum, bacteria from a liquid culture (OD600 between 0.6 and 0.7) were harvested by centrifugation at 3220 x *g* for 2min, resuspended in sterile water (LabChem), and harvested by centrifugation at 3220 x *g* for 3min. The bacterial pellet was resuspended in water (LabChem) adjusting OD600 to 0.2 (~1x10^8 cfu), and Silwet L77 (Lehle seeds) was added to a final concentration of 0.025%. About half of a single leaf was dipped into this *Pst* DC3000 cell suspension or a mock solution (0.025% Silwet L77) for 1min. After treatment, excess inoculum was blot-dried from the leaf surface using a sterile filter paper strip and plants were returned to LL for bioluminescence imaging (Supplemental Figure 2.1A) or for RNA time course tissue collection.

Transient SA and H2O2 treatment

Nylon meshes with seedlings were transferred from growth plates (1x MS - 3% sucrose) to treatment plates (1x MS - 3% sucrose containing 0.2mM SA, 1mM SA, 50mM

H_2O_2, or 200mM H_2O_2), or mock plates (MS without SA or H_2O_2). Treatment and mock plates were incubated in LL for 4 hours. After incubation, nylon meshes with seedlings were briefly blotted on a sterile filter paper, and then placed back to the original MS plate and incubated in LL for bioluminescence imaging (Supplemental Figure 2.2A) or for RNA time course tissue collection.

Bioluminescence detection

One day before the imaging period started, plants were sprayed with 5mM of D-lucifernin potassium salt (in 0.01% triton X-100 solution). For soil grown plants, 5mM D-lucifernin potassium salt (in water solution) was also added to the soil at the same time (3ml per plant). Bioluminescence was quantified every 1h (for *CCA1::LUC+* soil or MS grown seedlings), every 2h (for *LHY::LUC+* and *TOC1::LUC+* MS grown seedlings) or every 2.5h (for *LHY::LUC+* and *TOC1::LUC+* soil grown seedlings) using a Pixis 1024 CCD camera (Princeton Instruments).

Bioluminescence data analysis

Bioluminescence images were processed using the MetaMorph image analysis software (Molecular Devices) to determine bioluminescence counts (for plate and soil grown plants) and number of bioluminescent pixels (for soil grown plants) per plant or for a specific tissue section. To estimate plant size across an entire time course experiment, a third-order polynomial curve was regressed from the experimental pixel count data using GraphPad Prism version 6 (GraphPad Software, www.graphpad.com) (curve fitting was used to minimize pixel count bias due to plant movement and unequal signal bleeding due to rhythmic bioluminescence levels). Bioluminescence counts (for plate grown seedlings) and plant size normalized bioluminescence values (for soil grown plants or

tissue sections) for each experiment were analyzed by Fast Fourier Transform-Non Linear Least Squares (FFT-NLLS) [46] using the interface provided by the Biological Rhythms Analysis Software System (BRASS) [42]. Amplitude changes within each experiment were calculated as the ratio between the amplitude value obtained for each individual (both for mock and treated plants) and the mean amplitude obtained for mock treated plants (amplitude change = individual amplitude / mean amplitude mock) (log_{10} transformed ratios were used for statistical analysis). Normalized phase values were calculated as [24*(t-24)/p], where p is the period of the corresponding individual plant calculated by BRASS and t is the fitted acrophase time closest to the second subjective morning (ZT24) extrapolated using BRASS. Normalized phase mean values were calculated using an R circular statistics package [47]. Phase shifts were calculated by subtracting the normalized phase of each individual from the mean normalized phase of mock treated plants (phase shift = mean phase mock – individual phase) (phase advance or delay were indicated by positive or negative values respectively). Normalized phase versus relative amplitude error circular plots were generated using an R “polar.plot” function [43].

Biomass measurement

Tissue collection was performed at the end of single leaf *P. syringae* infection experiments (single plant aerial tissues) (Supplemental Figure 2.1A) or transient SA treatment experiments (pooled whole seedlings from each treatment plate) (Supplemental Figure 2.2A). Fresh weight was determined immediately after tissue collection and dry weight was determined after 10 days incubation at 37ºC.

mRNA transcript quantification

Pooled tissue samples were collected from MS-grown plants upon mock or SA treatment (12 seedlings per pool), and soil-grown plants upon single leaf mock or *P. syringae* treatment (5 plants without the treated leaf per pool) and snap freezed in liquid nitrogen. Total RNA from these samples was isolated using the RNeasy plant mini kit (Qiagen) and on-column DNAse (Roche) treatment. For cDNA synthesis, 1µg of total RNA was reverse-transcribed using the iScript cDNA synthesis kit (Bio-Rad). Transcript levels in each sample were determined by real time quantitative PCR (qPCR) (Bio-Rad CFX96 Real-time PCR detection system) using the Maxima Sybr green qPCR mix (Life Technologies), and the following PCR conditions: 95°C for 10 minutes, 40 cycles of 95°C for 15 seconds, 60°C for 25 seconds, and 72°C for 25 seconds. qPCR primer sequences are indicated in Supplementary Table 2.1. Gene expression levels were normalized to a reference gene (*IPP2* or *PP2A*) using the comparative Ct method [48] and then to the mean expression of mock samples within each biological replicate. Amplitude values and acrophase times for clock gene expression in mRNA time courses were determined from fitted sine waves of average expression traces by the following formula: Y=Amplitude*sin((2*pi*(t-Acrophase)/period)+pi/2)+baseline (where t is the time in LL and Y is the corresponding gene expression level) using GraphPad Prism version 6.

QUANTIFICATION AND STATISTICAL ANALYSIS

Statistical analyses of circular data (i.e. phase values) were performed using an R circular statistics package [47], and the Watson-Williams test in a matlab circular statistics tool box [49]. All other statistical analyses were performed using GraphPad Prism version

6. Details of statistical tests applied are indicated in figure legends including statistical methods, number of biological replicates, number of individuals, mean and error bar details, and statistical significances.

Table 2.1 Key resources table

REAGENT or RESOURCE	SOURCE	IDENTIFIER
Bacterial and Virus Strains		
Pseudomonas syringae pv. *tomato* DC3000	[36]	N/A
Agrobacterium GV3101	[37]	N/A
Chemicals, Peptides, and Recombinant Proteins		
Salicylic Acid	Sigma-Aldrich	CAS: 69-72-7
Hydrogen Peroxide (H_2O_2), 30% (Certified ACS)	Fisher Scientific	Cat#: H325-100
D-Luciferin Firefly, potassium salt	Gold Biotechnology	Cat#: LUCK-2G
Murashige & Skoog Basal Salts	Caisson labs	Cat#: MSP01-50LT
Water deionized (for *Pst* DC3000 inoculum preparation)	LabChem	Cat#: LC26750-4
Silwet L77	Lehle seeds	Cat#: NC0628903
Critical Commercial Assays		
pENTR™/D-TOPO® Cloning Kit	Life Technologies	Cat#: K2400-20
Gateway™ LR Clonase™ II Enzyme mix	Life Technologies	Cat#: 11791100
RNeasy Plant mini kit	Qiagen	Cat#: 74904
DNase I (RNase-free)	Roche	Cat#: 04-716728001
iScript™ cDNA Synthesis Kit	Bio-Rad	Cat#: 170-8891
Maxima Sybr green qPCR mix	Life Technologies	Cat#: K0253
Experimental Models: Organisms/Strains		
Arabidopsis: Col-0	[37]	N/A
Arabidopsis: npr1-1	ABRC	Stock#: CS3726
Arabidopsis: rbohd	ABRC	Stock#: Salk070610_C
Arabidopsis: CCA1::LUC+	[37]	N/A
Arabidopsis: LHY::LUC+	[38]	N/A
Arabidopsis: TOC1::LUC+	[39]	N/A
Arabidopsis: rbohd (CCA1::LUC+)	This paper	N/A
Arabidopsis: npr1-1 (CCA1::LUC+)	This paper	N/A
Arabidopsis: npr1-1 (LHY::LUC+)	This paper	N/A
Arabidopsis: NPR1-OX (CCA1::LUC+) (line 4)	This paper	N/A
Arabidopsis: NPR1-OX (LHY::LUC+) (line 2)	This paper	N/A
Arabidopsis: 35S::LUC+ (lines19 and 21)	This paper	N/A
Oligonucleotides		
See Supplementary Table 2.1	This paper	N/A
Recombinant DNA		
pENTR/D-NPR1	This paper	N/A
pMDC32 binary vector	[40]	N/A
pMDC32-NPR1	This paper	N/A
pBluescriptKS(-)	Stratagene	N/A
pMDCLUC+	[41]	N/A
pENTR/D-MCS	This paper	N/A
pMDC-MCS LUC+	This paper	N/A

To be continued

Table 2.1 Key resources table (continued)

REAGENT or RESOURCE	SOURCE	IDENTIFIER
Software and Algorithms		
Biological Rhythms Analysis Software System (BRASS)	[42]	N/A
MetaMorph Microscopy Automation and Image Analysis Software	Molecular Devices	Version 7.7.0.0
Matlab (install circular statistics tool box)	Mathworks	https://www.mathworks.com/
R (run with R studio, install circular package)	Rstudio	https://www.rstudio.com/
GraphPad Prism version 6	GraphPad software	https://www.graphpad.com/
R “polar.plot” function	[43]	N/A
Other		
Nylon 6/6 Mesh Sheet (50 microns mesh size)	Small Parts	Cat#: B0013HNZ38
Soil (Sunshine Professional Mix custom blend: 45-50% peat moss, vermiculite, dolomitic, limestone)	Sungro	N/A
Pixis 1024 CCD camera	Princeton Instruments	Model: 7520-0002
Bio-Rad CFX96 Real-time PCR detection system	Bio-Rad	Model: CFX Connect™ Optics Module

Supplemental Information

Supplemental Figure 2.1, related to Figure 2.1. Single leaf Pst DC3000 infection results in systemic down-regulation of *Arabidopsis* clock gene expression.
(A) Graphical outline for the single-leaf *Pst* DC3000 infection procedure. Plants were grown in LD for 14 days and transferred to LL for bioluminescence imaging. On the second subjective morning (ZT24), half of one leaf from each plant was dipped into a mock solution or *Pst* DC3000 cell inoculum for 1min. Excess inoculum on the leaf surface was blot dried using a filter paper and plants were placed back into the imaging system (see materials and methods for details). (B) Luciferase activity of soil grown *Arabidopsis CCA1::LUC+* plants upon single leaf *Pst* DC3000 infection (orange) or mock treatment (black). Treatments were performed at ZT24 (denoted by the black arrow) as outlined in (A). Results indicate mean values [± SD, n=6] and are representative of 5 independent experiments. (C) Aerial tissue fresh and dry weight of single leaf *Pst* DC3000 infected (orange) or mock treated (black) *CCA1::LUC+* plants. Samples were collected 6 days post infection following the protocol outlined in (A). Results indicate mean values [± SEM, n=33] of 5 independent experiments. (D) Fitted polynomial curves of bioluminescent pixels per plant for *CCA1::LUC+* plants upon single leaf *Pst* DC3000 infection (orange) or mock treatment (black) as indicated in (A). Results indicate mean values [± SEM, n=30] of 5 independent experiments. (E and G) Normalized phase and relative amplitude error (RAE) values for *CCA1::LUC+* (E) (n=30)*,LHY::LUC+* (G top panel) (n=15) and *TOC1::LUC+* (G bottom panel) (n=15) rhythms after single leaf *Pst* DC3000 infection (orange) or mock treatment (black) for experiments indicated in Figure 2.1 D, I and J (each dot represents one individual). The angular position of dots and arrows indicates the normalized phase value (0-24h) and the radial position indicates the RAE value (RAE=0 at the outmost radial position and RAE=1 at the center). The arrow points to the mean normalized phase and the arrow length indicates the mean RAE. (F) Representative time course pseudocolored bioluminescence images of *LHY::LUC+* (left panel) and *TOC1::LUC+* (right panel) plants upon single leaf *Pst* DC3000 infection or mock treatment. Triangles (*Pst* DC3000: orange, mock: green) point to the treated leaf. (H) *CCA1*, *LHY* and *TOC1* transcript levels in untreated tissues of WT plants upon single leaf *Pst* DC3000 infection (orange) or mock treatment (black). Samples were collected at the indicated times following the protocol outlined in (A). Results were calculated relative to *PP2A* transcript levels and indicate mean values [± SEM] of 2 independent experiments (statistical significance, determined using the *t* test, is indicated for peak time points). Statistical analyses between mock and *Pst* DC3000 infected plants were performed using the *t* test (C) and Watson Williams test (E and G). Stars indicate the level of significance (*$p<0.01$, ***$p<0.0001$).

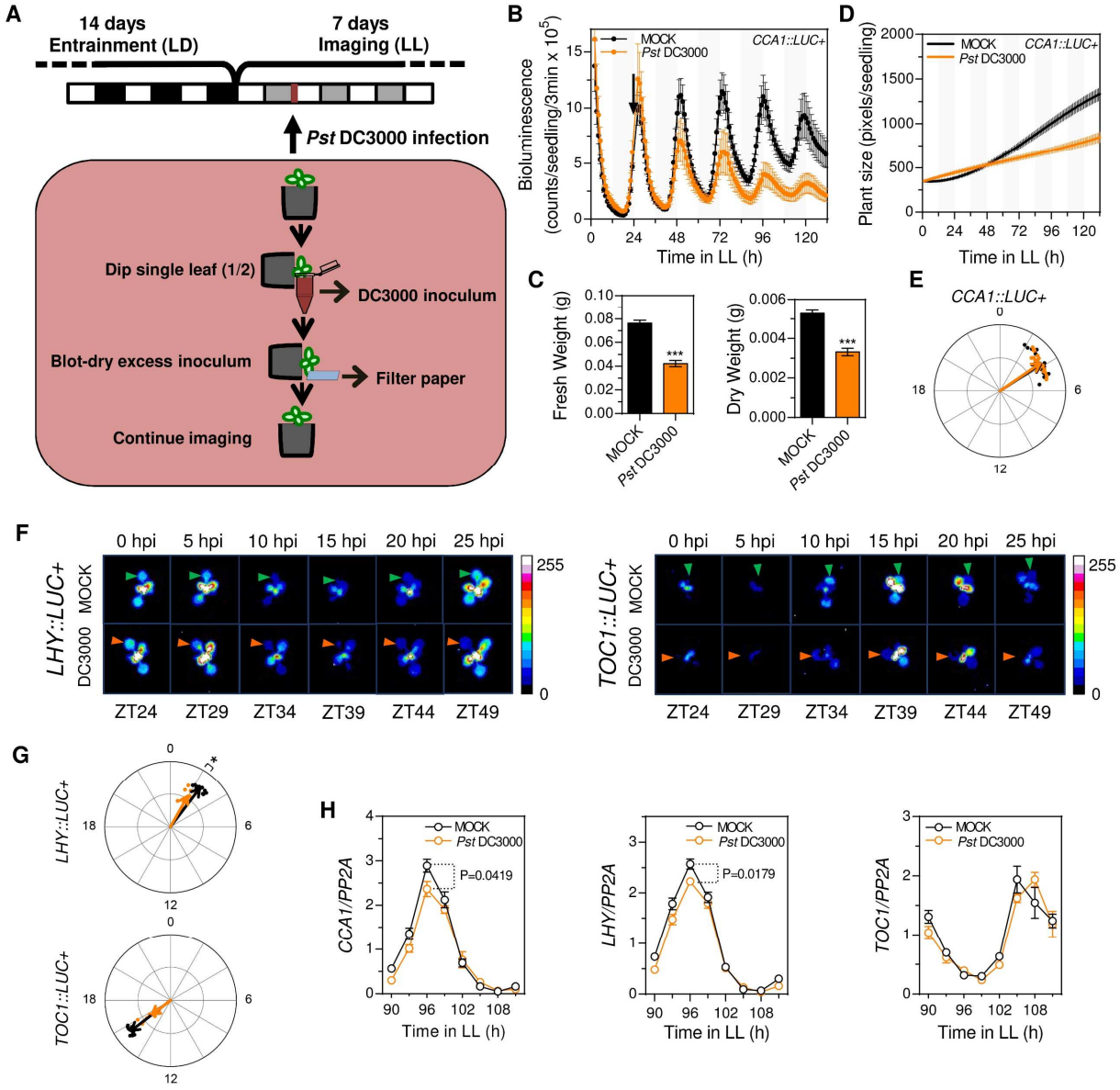
A
14 days
Entrainment (LD)
7 days
Imaging (LL)
Pst DC3000 infection
Dip single leaf (1/2)
DC3000 inoculum
Blot-dry excess inoculum
Filter paper
Continue imaging
B
Bioluminescence (counts/seedling/3min x 10^5)
MOCK
Pst DC3000
CCA1::LUC+
Time in LL (h)
D
Plant size (pixels/seedling)
MOCK
Pst DC3000
CCA1::LUC+
Time in LL (h)
C
Fresh Weight (g)
Dry Weight (g)
***
MOCK
Pst DC3000
E
CCA1::LUC+
F
0 hpi
5 hpi
10 hpi
15 hpi
20 hpi
25 hpi
LHY::LUC+
TOC1::LUC+
MOCK
DC3000
255
0
ZT24
ZT29
ZT34
ZT39
ZT44
ZT49
G
LHY::LUC+
TOC1::LUC+
H
CCA1/PP2A
LHY/PP2A
TOC1/PP2A
MOCK
Pst DC3000
P=0.0419
P=0.0179
Time in LL (h)

Supplemental Figure 2.2, related to Figure 2.2. Transient SA treatment delays the phase of clock gene promoter activity and transcript levels.

(A) Graphical outline of the transient SA or H_2O_2 treatment protocol. Plants were grown in MS plates on top of a nylon mesh under LD cycles for 10 days. Plates were then transferred to LL where luminescence images were acquired at regular intervals for 7 days. On the second day in LL (ZT24), the mesh with seedlings was transferred to MS treatment plates containing SA or H_2O_2 and incubated for 4 h (orange shadowed area). After treatment, the mesh was briefly blot dried and transferred back to the original MS plate. Finally, plates were placed back into the imaging system (see materials and methods for details). (B) Fresh and dry weight of whole wild-type (WT) *CCA1::LUC+* plants after transient mock (black), 0.2mM SA (blue) and 1mM SA (red) treatment. Samples were collected 6 days after treatment following the protocol outlined in (A). Results indicate mean values [± SEM, n=3 pools of 12 seedlings] of 2 independent experiments. (C) Mean luciferase activity from *35S::LUC+* seedlings after transient mock (black), 0.2mM SA (blue) and 1mM SA (red) treatment. Seedlings from two independent transgenic lines were treated according to the protocol outlined in (A) and bioluminescence counts determined every 1h between ZT60-ZT156. Results indicate mean values [± SEM, n=34] of 2 independent experiments. (D) Luciferase activity of *LHY::LUC+* (left panel) and *TOC1::LUC+* (right panel) plants upon transient SA treatment as indicated in (A). Seedlings were treated with medium alone (mock) or supplemented with SA (0.2mM and 1 mM) (denoted by the orange shadowed area). Results indicate mean values [± SEM, n=12] and are representative of 3 independent experiments. (E) Normalized phase and the relative amplitude error (RAE) values of *LHY::LUC+* (top panel) and *TOC1::LUC+* (bottom panel) rhythms after transient SA treatment (mock: black, 0.2mM: blue and 1mM: red) for experiments indicated in (D) (each dot represents one individual). The angular position of dots and arrows indicates the normalized phase value (0-24h) and the radial position indicates the RAE value (RAE=0 at the outmost radial position and RAE=1 at the center). The arrow points to the mean normalized phase and the arrow length indicates the mean RAE. (F) *CCA1*, *LHY* and *TOC1* transcript levels in WT plants upon transient mock (black) or 1mM SA (red) treatments. Samples were collected at the indicated times following the protocol outlined in (A). Results were calculated relative to *PP2A* transcript levels and indicate mean values [± SEM] of 3 independent experiments. Dotted lines denote fitted sine wave for each trace. (G) Amplitude (left panel) and acrophase time (right panel) for *CCA1*, *LHY* and *TOC1* transcript expression patterns shown in (F). Results indicate mean values [± SD] for mock (gray) and 1mM SA (red) treated plants according to fitted sine waves shown in (F). Statistical significance between mock and SA treatment (extra sum-of-squares F test method) is indicated. Statistical analyses between mock and SA treated plants were performed using the t test (B and C) and Watson-Williams test (E). Stars indicate the level of significance (***$p<0.0001$).

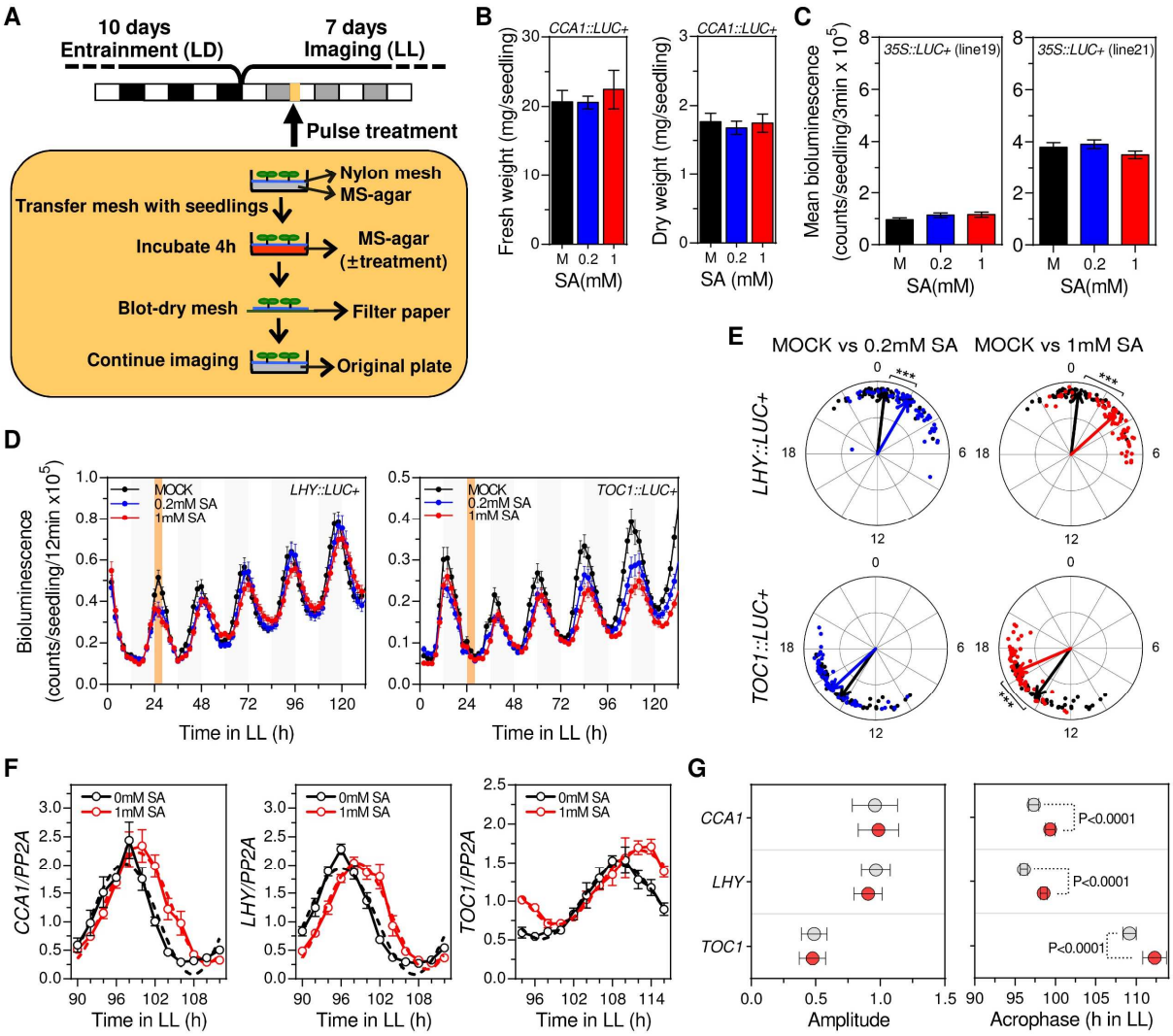
A
10 days
Entrainment (LD)
7 days
Imaging (LL)
Pulse treatment
Nylon mesh
MS-agar
Transfer mesh with seedlings
Incubate 4h
MS-agar
(±treatment)
Blot-dry mesh
Filter paper
Continue imaging
Original plate
B
CCA1::LUC+
Fresh weight (mg/seedling)
Dry weight (mg/seedling)
M 0.2 1
SA(mM)
SA (mM)
C
35S::LUC+ (line19)
35S::LUC+ (line21)
Mean bioluminescence
(counts/seedling/3min x 10^5)
D
Bioluminescence
(counts/seedling/12min x10^5)
MOCK
0.2mM SA
1mM SA
LHY::LUC+
TOC1::LUC+
Time in LL (h)
E
MOCK vs 0.2mM SA
MOCK vs 1mM SA
LHY::LUC+
TOC1::LUC+
***
F
0mM SA
1mM SA
CCA1/PP2A
LHY/PP2A
TOC1/PP2A
Time in LL (h)
G
CCA1
LHY
TOC1
P<0.0001
Amplitude
Acrophase (h in LL)

Supplemental Figure 2.3, related to Figure 2.3. *NPR1* counteracts the reduced amplitude and delayed phase of clock gene expression triggered by transient SA treatment.
(A and B) Mean amplitude (A) and relative amplitude error (RAE) (B) values [± SEM] of *CCA1::LUC+* (left panel) (n=72) and *LHY::LUC+* (right panel) (n≥58) rhythms in wild-type (WT), *npr1-1 and NPR1-OX* seedlings after mock (grey), 0.2mM SA (blue) or 1mM SA (red) transient treatments for experiments indicated in Figure 2.3 B and D. (C) Fresh and dry weight of whole wild-type (WT), *npr1-1* and *NPR1-OX* plants (carrying the *CCA1::LUC+* reporter) after transient mock (black), 0.2mM SA (blue) and 1mM SA (red) treatment. Samples were collected 6 days after treatment following the protocol outlined in Supplemental Figure 2.2A. Results indicate mean values [± SEM, n=3 pools of 12 seedlings] of 2 independent experiments. (D) *CCA1*, *LHY* and *TOC1* transcript levels in *npr1-1* plants upon transient mock (black) or 1mM SA (red) treatments. Samples were collected at the indicated times following the protocol outlined in Supplemental Figure 2.2A. Results were calculated relative to *PP2A* transcript levels and indicate mean values [± SEM] of 3 independent experiments. Dotted lines denote fitted sine wave for each trace. (E) Amplitude (left panel) and acrophase time (right panel) for *CCA1*, *LHY* and *TOC1* transcript expression patterns shown in (D). Results indicate mean values [± SD] for mock (gray) and 1mM SA (red) treated plants according to fitted sine waves shown in (D). Statistical significance between mock and SA treatment (extra sum-of-squares F test method) is indicated. (F) *NPR1* transcript levels in wild-type (WT) and *NPR1* overexpression lines (*NPR1-OX*) in the *CCA1::LUC+* (left panel) and *LHY::LUC+* (right panel) reporter backgrounds. Results were calculated relative to *IPP2* transcript levels and indicate mean values [± SD] of 2 independent experiments. (G) Mean period values [± SEM] of *CCA1::LUC+* (left panel) (n=72) and *LHY::LUC+* (right panel) (n≥58) rhythms in wild-type (WT), *npr1-1 and NPR1-OX* seedlings after mock (grey), 0.2mM SA (blue) or 1mM SA (red) transient treatments for experiments indicated in Figure 2.3 B and D. (H and I) Normalized phase and RAE values of *CCA1::LUC+* (H) and *LHY::LUC+* (I) rhythms in WT, *npr1-1 and NPR1-OX* seedlings after transient SA treatment (mock: black, 0.2mM SA: blue and 1mM SA: red) for experiments indicated in Figure 2.3 B and D (each dot represents one individual). The angular position of dots and arrows indicates the normalized phase value (0-24h) and the radial position the RAE value (RAE=0 at the outmost radial position and RAE=1 at the center). The arrow points to the mean normalized phase and the arrow length indicates the mean RAE. Statistical analyses between mock and SA treated plants were performed using the *t* test (A, B, C and G) and Watson-Williams test (H and I). Statistical analyses between WT and *NPR1-OX* backgrounds were performed using the *t* test (F). Stars indicate the level of significance (*p<0.01, **p<0.001, ***p<0.0001).

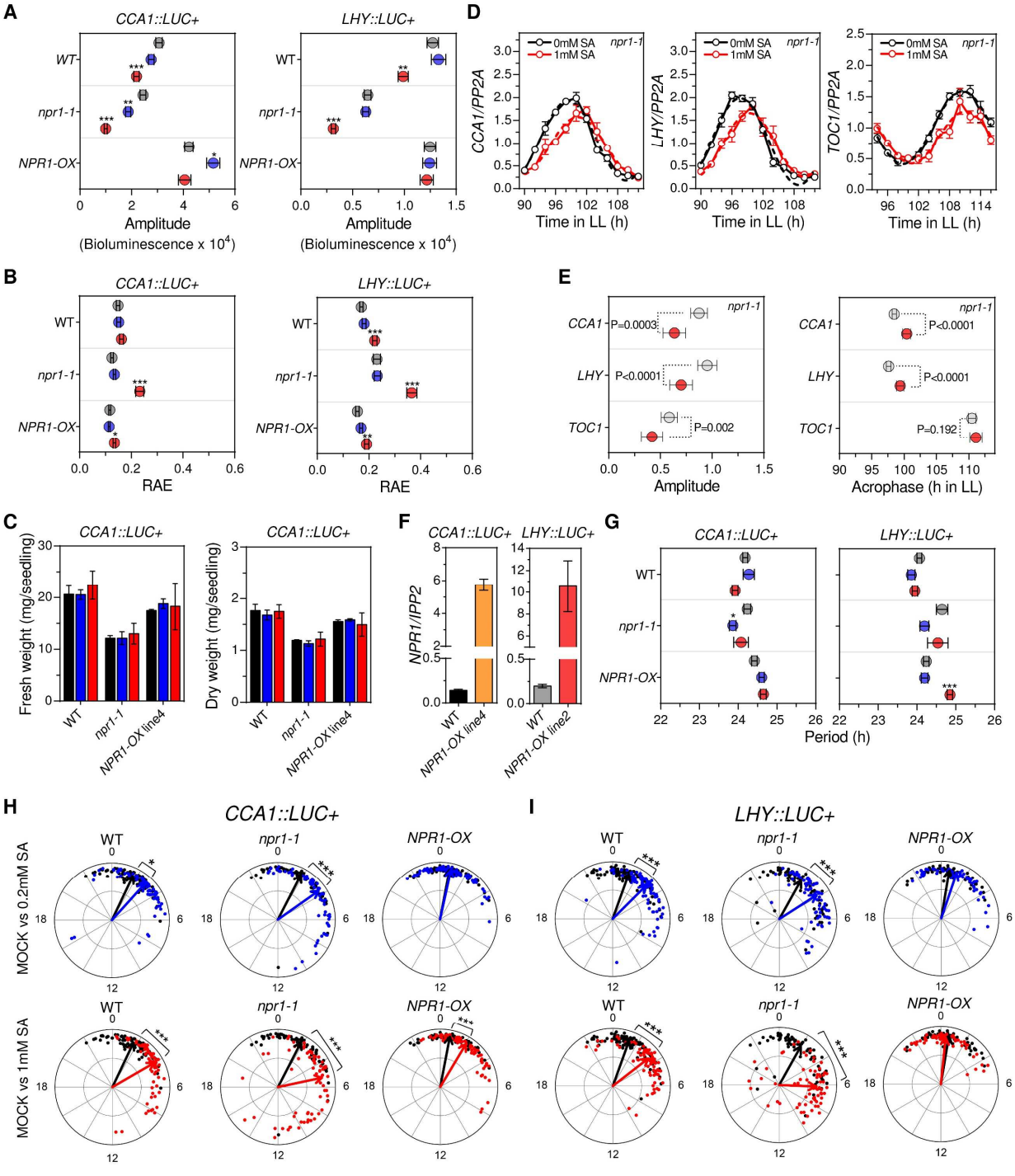
A
CCA1::LUC+
LHY::LUC+
WT
npr1-1
NPR1-OX
Amplitude
(Bioluminescence x 10^4)
B
RAE
C
Fresh weight (mg/seedling)
Dry weight (mg/seedling)
WT
npr1-1
NPR1-OX line4
D
0mM SA
1mM SA
CCA1/PP2A
LHY/PP2A
TOC1/PP2A
Time in LL (h)
E
CCA1
LHY
TOC1
P=0.0003
P<0.0001
P=0.002
P=0.192
Amplitude
Acrophase (h in LL)
F
NPR1/IPP2
NPR1-OX line4
NPR1-OX line2
G
Period (h)
H
I
MOCK vs 0.2mM SA
MOCK vs 1mM SA

Supplemental Figure 2.4, related to Figure 2.3 and Figure 2.4. *NPR1* and *RBOHD* respectively counteract and mediate clock responses to single leaf *P. syringae* infection or transient SA treatment.

(A and B) Mean amplitude (A) and relative amplitude error (RAE) (B) values [± SEM] of *CCA1::LUC+* rhythms in WT, *npr1-1 and NPR1-OX* plants (n=30 per genotype) upon single leaf *Pst* DC3000 infection (orange) or mock treatment (gray) for experiments indicated in Figure 2.3F. (C) Normalized phase and relative amplitude error (RAE) values of *CCA1::LUC+* rhythms in WT, *npr1-1 and NPR1-OX* seedlings after single leaf *Pst* DC3000 infection (orange) or mock treatment (black) for experiments indicated in Figure 2.3F (each dot represents one individual). The angular position of dots and arrows indicates the normalized phase value (0-24h) and the radial position indicates the RAE value (RAE=0 at the outmost radial position and RAE=1 at the center). The arrow points to the mean normalized phase and the arrow length indicates the mean RAE. (D, F and G) Mean amplitude (D), relative amplitude error (RAE) (F) and period (G) values [± SEM] for *CCA1::LUC+* rhythms in wild-type (WT) (n=80) and *rbohd* (n=64) seedlings after mock (grey), 0.2mM SA (blue) or 1mM SA (red) transient treatments for experiments indicated in Figure 2.4F. (E) Normalized phase and relative amplitude error (RAE) values of *CCA1::LUC+* rhythms in WT and *rbohd* seedlings after transient SA treatment (mock: black, 0.2mM SA: blue and 1mM SA: red) for experiments indicated in Figure 2.4F (each dot represents one individual). The angular position of dots and arrows indicates the normalized phase value (0-24h) and the radial position the RAE value (RAE=0 at the outmost radial position and RAE=1 at the center). The arrow points to the mean normalized phase and the arrow length indicates the mean RAE. (H and I) Mean amplitude (H) and relative amplitude error (RAE) (I) values [± SEM] for *CCA1::LUC+* rhythms in WT and *rbohd* plants (n=18 per genotype) upon single leaf *Pst* DC3000 infection (orange) or mock treatment (gray) for experiments indicated in Figure 2.4I. (J) Normalized phase and relative amplitude error (RAE) values of *CCA1::LUC+* rhythms in WT and *rbohd* plants after single leaf *Pst* DC3000 infection (orange) or mock treatment (black) for experiments indicated in Figure 2.4I (each dot represents one individual). The angular position of dots and arrows indicates the normalized phase value (0-24h) and the radial position indicates the RAE value (RAE=0 at the outmost radial position and RAE=1 at the center). The arrow points to the mean normalized phase and the arrow length indicates the mean RAE. (K) Proposed model summarizing clock regulation mechanisms uncovered in this work. *Pst* DC3000 infection triggers both SA-dependent mechanisms (black connectors) that regulate the clock phase and amplitude, and SA-independent mechanisms (orange connectors) that regulate the clock phase and period. The amplitude of clock rhythms is reduced by both *Pst* DC3000 infection and transient SA treatment, and this response is antagonized by NPR1 and independent of RBOHD function. The clock phase is delayed by a transient SA treatment while it is minimally advanced after *Pst* DC3000 infection. Both responses are mediated by RBOHD (thus apoplastic ROS), but the SA-triggered phase delay is antagonized by NPR1. Finally, the clock period is lengthened only after *Pst* DC3000 infection and this response is mediated by RBOHD (thus apoplastic ROS). Pointed and blunt arrows indicate positive and negative regulatory functions respectively. Statistical analyses between mock and SA treated plants (D-G) or mock and infected plants (A-C, H-J) were performed using the *t* test (A-B, D and F-I) and Watson-Williams test (C, E and J). Stars indicate the level of significance (*$p<0.01$, **$p<0.001$, ***$p<0.0001$).

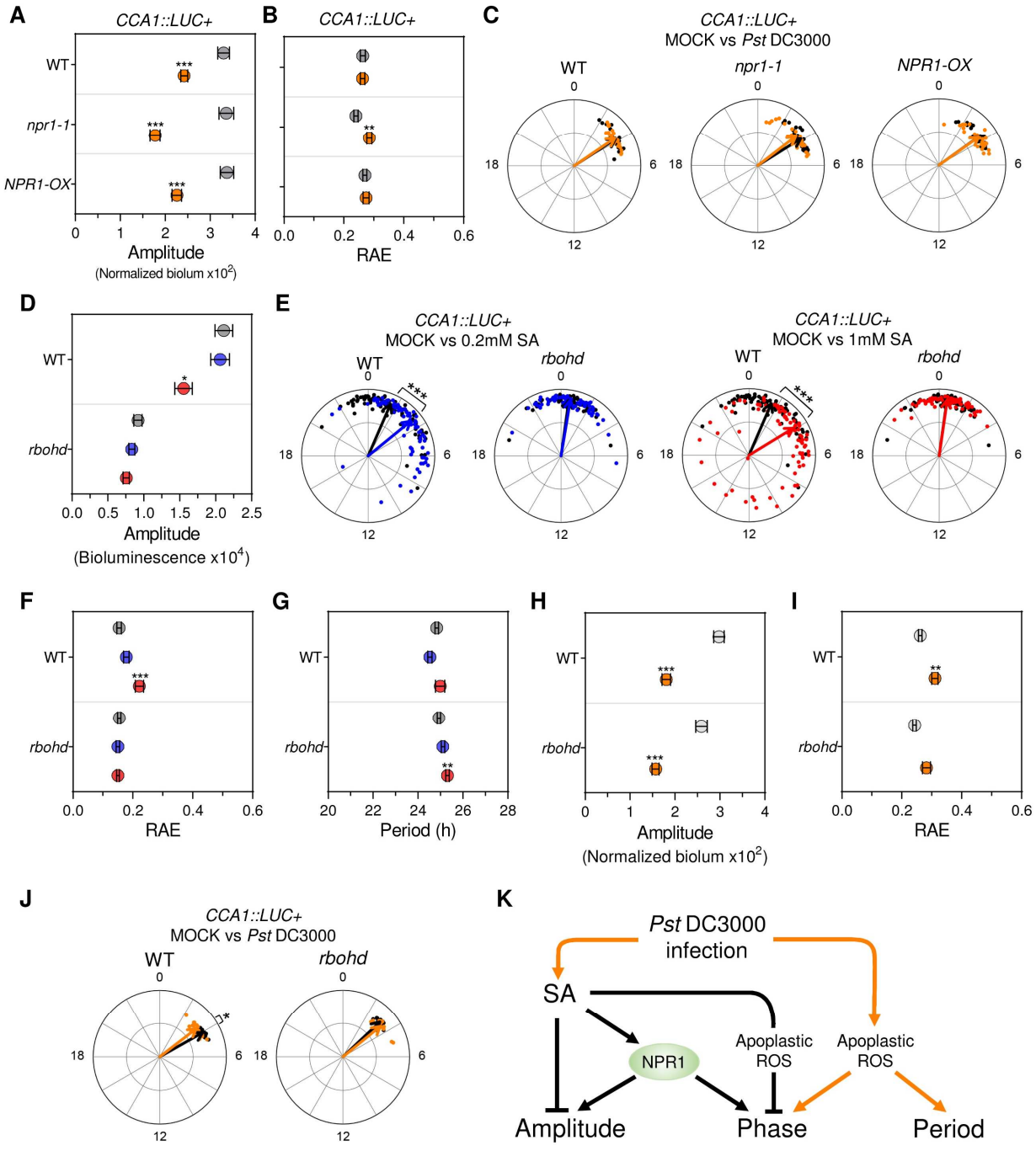
A
CCA1::LUC+
WT
npr1-1
NPR1-OX
Amplitude
(Normalized biolum x10²)
B
CCA1::LUC+
RAE
C
CCA1::LUC+
MOCK vs Pst DC3000
WT
npr1-1
NPR1-OX
D
Amplitude
(Bioluminescence x10⁴)
rbohd
E
CCA1::LUC+
MOCK vs 0.2mM SA
MOCK vs 1mM SA
F
RAE
G
Period (h)
H
Amplitude
(Normalized biolum x10²)
I
RAE
J
CCA1::LUC+
MOCK vs Pst DC3000
K
Pst DC3000
infection
SA
NPR1
Apoplastic
ROS
Amplitude
Phase
Period

Supplemental Table 2.1 List of oligonucleotide primer sequences

Name	Sequence (5' to 3')	Purpose
NPR1 CDS fw	CACCATGGACACCACCATTGATGGA	Cloning NPR1
NPR1 CDS rv	TCACCGACGACGATGAGAGAGT	Cloning NPR1
pENTR MCS fw	CACCATGAGGGAACAAAAGCTGGAGCTCCA	Cloning MCS
pENTR MCS rv	TAGGGCGAATTGGGTACCGGG	Cloning MCS
NPR1 QPCR fw	GGCGGCCGATGAATTGAAGATG	Quantitative PCR
NPR1 QPCR rv	CCGGTGATGTTCTCTTCGTACCAG	Quantitative PCR
IPP2 QPCR fw	GTATGAGTTGCTTCTCCCAGCAAAG	Quantitative PCR
IPP2 QPCR rv	GAGGATGGCTGCAACAAGTGT	Quantitative PCR
CCA1 QPCR fw	CCGCAACTTTCGCCTCAT	Quantitative PCR
CCA1 QPCR rv	GCCAGATTCGGAGGTGAGTTC	Quantitative PCR
LHY QPCR fw	GACTCAAACACTGCCCAGAAGA	Quantitative PCR
LHY QPCR rv	CGTCACTCCCTGAAGGTGTATTT	Quantitative PCR
TOC1 QPCR fw	TCTTCGCAGAATCCCTGTGAT	Quantitative PCR
TOC1 QPCR rv	GCTGCACCTAGCTTCAAGCA	Quantitative PCR
PP2A QPCR fw	TAACGTGGCCAAAATGATGC	Quantitative PCR
PP2A QPCR rv	GTTCTCCACAACCGATTGGT	Quantitative PCR

Acknowledgement

This chapter, in full, is a reprint of the material as: Zheng Li, Katia Bonaldi, Francisco Uribe, Jose L. Pruneda-Paz. A localized *Pseudomonas syringae* infection triggers systemic clock responses in *Arabidopsis*. Current Biology. 2018 Feb 19; 28(4):630-639. The dissertation author was the primary investigator and author of this paper.

We thank Dr. Steve Briggs for providing *Pst* DC3000 strain and sharing infection protocols, and Dr. Frank Harmon for sharing the R script to generate polar plots.

Research reported in this publication was supported by the National Institute of General Medical Sciences of the National Institutes of Health by the National Institutes of Health [R01GM056006 to J.L.P-P (co-investigator)], the Hellman Foundation [to J.L.P-P] and the UCSD Academic Senate [to J.L.P-P].

References

1. Bendix, C., Marshall, C.M., and Harmon, F.G. (2015). Circadian Clock Genes Universally Control Key Agricultural Traits. Molecular plant *8*, 1135-1152.

2. Dodd, A.N., Salathia, N., Hall, A., Kévei, E., Tóth, R., Nagy, F., Hibberd, J.M., Millar, A.J., and Webb, A.A. (2005). Plant circadian clocks increase photosynthesis, growth, survival, and competitive advantage. Science *309*, 630-633.

3. Green, R.M., Tingay, S., Wang, Z.Y., and Tobin, E.M. (2002). Circadian rhythms confer a higher level of fitness to *Arabidopsis* plants. Plant physiology *129*, 576-584.

4. Greenham, K., and McClung, C.R. (2015). Integrating circadian dynamics with physiological processes in plants. Nature reviews. Genetics *16*, 598-610.

5. Sanchez, S.E., and Kay, S.A. (2016). The Plant Circadian Clock: From a Simple Timekeeper to a Complex Developmental Manager. Cold Spring Harbor perspectives in biology *8*.

6. Hsu, P.Y., and Harmer, S.L. (2014). Wheels within wheels: the plant circadian system. Trends in plant science *19*, 240-249.

7. Nohales, M.A., and Kay, S.A. (2016). Molecular mechanisms at the core of the plant circadian oscillator. Nature structural & molecular biology *23*, 1061-1069.

8. Pruneda-Paz, J.L., and Kay, S.A. (2010). An expanding universe of circadian networks in higher plants. Trends in plant science *15*, 259-265.

9. Zhang, C., Xie, Q., Anderson, R.G., Ng, G., Seitz, N.C., Peterson, T., McClung, C.R., McDowell, J.M., Kong, D., Kwak, J.M., and Lu, H. (2013). Crosstalk between the circadian clock and innate immunity in *Arabidopsis*. PLoS pathogens *9*, e1003370.

10. Zhou, M., Wang, W., Karapetyan, S., Mwimba, M., Marqués, J., Buchler, N.E., and Dong, X. (2015). Redox rhythm reinforces the circadian clock to gate immune response. Nature *523*, 472-476.

11. Dong, X. (2004). NPR1, all things considered. Current opinion in plant biology *7*, 547-552.

12. Wang, D., Amornsiripanitch, N., and Dong, X. (2006). A genomic approach to identify regulatory nodes in the transcriptional network of systemic acquired resistance in plants. PLoS pathogens *2*, e123.

13. Kalachova, T., Iakovenko, O., Kretinin, S., and Kravets, V. (2013). Involvement of phospholipase D and NADPH-oxidase in salicylic acid signaling cascade. Plant physiology and biochemistry : PPB *66*, 127-133.

14. Fu, Z.Q., and Dong, X. (2013). Systemic acquired resistance: turning local infection into global defense. Annual review of plant biology *64*, 839-863.

15. Vlot, A.C., Dempsey, D.A., and Klessig, D.F. (2009). Salicylic Acid, a multifaceted hormone to combat disease. Annual review of phytopathology *47*, 177-206.

16. Ederli, L., Madeo, L., Calderini, O., Gehring, C., Moretti, C., Buonaurio, R., Paolocci, F., and Pasqualini, S. (2011). The *Arabidopsis* thaliana cysteine-rich receptor-like kinase CRK20 modulates host responses to Pseudomonas syringae pv. tomato DC3000 infection. Journal of plant physiology *168*, 1784-1794.

17. Herrera-Vásquez, A., Salinas, P., and Holuigue, L. (2015). Salicylic acid and reactive oxygen species interplay in the transcriptional control of defense genes expression. Frontiers in plant science *6*, 171.

18. Pogány, M., von Rad, U., Grün, S., Dongó, A., Pintye, A., Simoneau, P., Bahnweg, G., Kiss, L., Barna, B., and Durner, J. (2009). Dual roles of reactive oxygen species and NADPH oxidase RBOHD in an *Arabidopsis*-Alternaria pathosystem. Plant physiology *151*, 1459-1475.

19. Kadota, Y., Shirasu, K., and Zipfel, C. (2015). Regulation of the NADPH Oxidase RBOHD During Plant Immunity. Plant & cell physiology *56*, 1472-1480.

20. Torres, M.A., and Dangl, J.L. (2005). Functions of the respiratory burst oxidase in biotic interactions, abiotic stress and development. Current opinion in plant biology *8*, 397-403.

21. Bonfig, K.B., Schreiber, U., Gabler, A., Roitsch, T., and Berger, S. (2006). Infection with virulent and avirulent P. syringae strains differentially affects photosynthesis and sink metabolism in *Arabidopsis* leaves. Planta *225*, 1-12.

22. de Torres Zabala, M., Littlejohn, G., Jayaraman, S., Studholme, D., Bailey, T., Lawson, T., Tillich, M., Licht, D., Bölter, B., Delfino, L., Truman, W., Mansfield, J., Smirnoff, N., and Grant, M. (2015). Chloroplasts play a central role in plant defence and are targeted by pathogen effectors. Nature plants *1*, 15074.

23. Haydon, M.J., Mielczarek, O., Robertson, F.C., Hubbard, K.E., and Webb, A.A. (2013). Photosynthetic entrainment of the *Arabidopsis* thaliana circadian clock. Nature *502*, 689-692.

24. Wang, L., Mitra, R.M., Hasselmann, K.D., Sato, M., Lenarz-Wyatt, L., Cohen, J.D., Katagiri, F., and Glazebrook, J. (2008). The genetic network controlling the *Arabidopsis* transcriptional response to Pseudomonas syringae pv. maculicola: roles of major regulators and the phytotoxin coronatine. Molecular plant-microbe interactions : MPMI *21*, 1408-1420.

25. Takahashi, N., Hirata, Y., Aihara, K., and Mas, P. (2015). A hierarchical multi-oscillator network orchestrates the *Arabidopsis* circadian system. Cell *163*, 148-159.

26. Fu, Z.Q., Yan, S., Saleh, A., Wang, W., Ruble, J., Oka, N., Mohan, R., Spoel, S.H., Tada, Y., Zheng, N., and Dong, X. (2012). NPR3 and NPR4 are receptors for the immune signal salicylic acid in plants. Nature *486*, 228-232.

27. Carella, P., Wilson, D.C., and Cameron, R.K. (2014). Some things get better with age: differences in salicylic acid accumulation and defense signaling in young and mature *Arabidopsis*. Frontiers in plant science *5*, 775.

28. Delaney, T.P., Friedrich, L., and Ryals, J.A. (1995). *Arabidopsis* signal transduction mutant defective in chemically and biologically induced disease resistance. Proceedings of the National Academy of Sciences of the United States of America *92*, 6602-6606.

29. Spoel, S.H., Mou, Z., Tada, Y., Spivey, N.W., Genschik, P., and Dong, X. (2009). Proteasome-mediated turnover of the transcription coactivator NPR1 plays dual roles in regulating plant immunity. Cell *137*, 860-872.

30. Lai, A.G., Doherty, C.J., Mueller-Roeber, B., Kay, S.A., Schippers, J.H., and Dijkwel, P.P. (2012). CIRCADIAN CLOCK-ASSOCIATED 1 regulates ROS homeostasis and oxidative stress responses. Proceedings of the National Academy of Sciences of the United States of America *109*, 17129-17134.

31. Lou, Y.R., Bor, M., Yan, J., Preuss, A.S., and Jander, G. (2016). *Arabidopsis* NATA1 Acetylates Putrescine and Decreases Defense-Related Hydrogen Peroxide Accumulation. Plant physiology *171*, 1443-1455.

32. Ravichandran, S., Stone, S.L., Benkel, B., and Prithiviraj, B. (2013). Purple Acid Phosphatase5 is required for maintaining basal resistance against Pseudomonas syringae in *Arabidopsis*. BMC plant biology *13*, 107.

33. Miller, G., Schlauch, K., Tam, R., Cortes, D., Torres, M.A., Shulaev, V., Dangl, J.L., and Mittler, R. (2009). The plant NADPH oxidase RBOHD mediates rapid systemic signaling in response to diverse stimuli. Science signaling *2*, ra45.

34. Mittler, R., Vanderauwera, S., Suzuki, N., Miller, G., Tognetti, V.B., Vandepoele, K., Gollery, M., Shulaev, V., and Van Breusegem, F. (2011). ROS signaling: the new wave? Trends in plant science *16*, 300-309.

35. Sewelam, N., Kazan, K., and Schenk, P.M. (2016). Global Plant Stress Signaling: Reactive Oxygen Species at the Cross-Road. Frontiers in plant science *7*, 187.

36. Whalen, M.C., Innes, R.W., Bent, A.F., and Staskawicz, B.J. (1991). Identification of Pseudomonas syringae pathogens of *Arabidopsis* and a bacterial locus determining avirulence on both *Arabidopsis* and soybean. The Plant cell *3*, 49-59.

37. Pruneda-Paz, J.L., Breton, G., Para, A., and Kay, S.A. (2009). A functional genomics approach reveals CHE as a component of the *Arabidopsis* circadian clock. Science *323*, 1481-1485.

38. Baudry, A., Ito, S., Song, Y.H., Strait, A.A., Kiba, T., Lu, S., Henriques, R., Pruneda-Paz, J.L., Chua, N.H., Tobin, E.M., Kay, S.A., and Imaizumi, T. (2010). F-box proteins FKF1 and LKP2 act in concert with ZEITLUPE to control *Arabidopsis* clock progression. The Plant cell *22*, 606-622.

39. Alabadi, D., Oyama, T., Yanovsky, M.J., Harmon, F.G., Más, P., and Kay, S.A. (2001). Reciprocal regulation between TOC1 and LHY/CCA1 within the *Arabidopsis* circadian clock. Science *293*, 880-883.

40. Curtis, M.D., and Grossniklaus, U. (2003). A gateway cloning vector set for high-throughput functional analysis of genes in planta. Plant physiology *133*, 462-469.

41. Farré, E.M., and Kay, S.A. (2007). PRR7 protein levels are regulated by light and the circadian clock in *Arabidopsis*. The Plant journal : for cell and molecular biology *52*, 548-560.

42. Southern, M.M., Brown, P.E., and Hall, A. (2006). Luciferases as reporter genes. Methods in molecular biology *323*, 293-305.

43. Marshall, C.M., Tartaglio, V., Duarte, M., and Harmon, F.G. (2016). The *Arabidopsis* sickle Mutant Exhibits Altered Circadian Clock Responses to Cool Temperatures and Temperature-Dependent Alternative Splicing. The Plant cell *28*, 2560-2575.

44. Cao, H., Bowling, S.A., Gordon, A.S., and Dong, X. (1994). Characterization of an *Arabidopsis* Mutant That Is Nonresponsive to Inducers of Systemic Acquired Resistance. The Plant cell *6*, 1583-1592.

45. Zhang, X., Henriques, R., Lin, S.S., Niu, Q.W., and Chua, N.H. (2006). Agrobacterium-mediated transformation of *Arabidopsis* thaliana using the floral dip method. Nature protocols *1*, 641-646.

46. Plautz, J.D., Straume, M., Stanewsky, R., Jamison, C.F., Brandes, C., Dowse, H.B., Hall, J.C., and Kay, S.A. (1997). Quantitative analysis of Drosophila period gene transcription in living animals. Journal of biological rhythms *12*, 204-217.

47. Agostinelli, C., and Lund, U. (2017). R package 'circular': Circular Statistics (version 0.4-93). https://r-forge.r-project.org/projects/circular/.

48. Schmittgen, T.D., and Livak, K.J. (2008). Analyzing real-time PCR data by the comparative C(T) method. Nature protocols *3*, 1101-1108.

49. Berens, P. (2009). CircStat: A MATLAB Toolbox for Circular Statistics. J Stat Softw *31*, 1-21.

Chapter 3 Localized *Pseudomonas syringae* infection delays plant development and affects circadian rhythms predominantly in the shoot apex

Introduction

As an exceptionally active and dynamic part of the plant, the shoot apex is a central driver of plant growth and development as well as the decision maker of transitions in plant life [1–3]. The shoot apex also serves as the hierarchical master regulator of circadian clock which synchronizes oscillation in other parts of the plant [4]. From the studies of shoot apical meristem in the model organism *Arabidopsis*, we have gain a lot of insights about the shoot apical meristem (SAM). There are different phases of SAM, the first phase is vegetative meristem (VM) which generates rosette leaves. Upon floral transition, SAM turns in to inflorescence meristem (IM) which produces flowers and flower shoots. the third phase of the meristem is the floral meristem (FM) which is a determinate meristem which produces the flower [5,6,8,10]. A change in the shoot apical meristem, no matter caused by mutations or external environmental cue (for example, day length) often results in changing the plant developmental program including the morphology and architecture of the plant, flowering time and the final rosette leaf number [1,7,9,11].

Recently, the shoot apex has been reported to act as the hierarchical master regulator in the orchestration of circadian rhythms of the plant [4]. For example, the rhythmicity of the shoot apex determines the oscillation in the root but not vice versa [4] which is further emphasizing the important role of shoot apex in plant life. The circadian clock, as an internal time keeping mechanism, regulates a vast majority of pathways and responses, and positions biological processes to happen at the correct time of day

[12,13]. The *Arabidopsis* circadian clock consists of interlocked feedback loops among which the core loop is formed by three transcription factors, CCA1, LHY and TOC1. CCA1 and LHY function partially redundantly to repress TOC1 transcription in the morning and reciprocally, TOC1 transcription peaks as dusk and represses CCA1 and LHY transcription [14–16]. Circadian clock drives the oscillation of many biological processes by regulating the corresponding output pathways and at the same time, the clock is receiving and integrating multiple input information as a hub [17]. The most potent and routine input signals are light and temperature while more pathways are reported to be able to regulate the clock function including various phytohormones, defense responses, nutrient signals and so on [16,17,19].

We observed that upon a localized *Pseudomonas syringae* infection, at the whole organism level, the clock controlled rhythms (*CCA::LUC+, LHY::LUC+* and *TOC1::LUC+* bioluminescence imaging) exhibited a amplitude reduction and period lengthening phenotype. At the same time, we observed a significant decrease in the plant size and biomass. Since the shoot apical meristem activity is the driving force of plant growth and development [3,18], the decrease of plant size and biomass indicated potential lower meristematic activity. We examined this hypothesis and discovered that in the plant that is locally infected, development of the plant is delayed and shoot apical meristem is less developed. As we reanalyzed the clock-controlled rhythms upon localized infection, we found that the rhythms in the shoot apex was predominantly changed compared to the peripheral leaf tissues. Both of these findings reflected the massive changes that were trigged in the shoot apex upon localized *Pst* DC3000 infection which would have enormous impact on the plant physiology.

Results

The growth and development of *P. syringae* infected plants are delayed

Since we observed an overall reduction of plant size and biomass following localized *P. syringae* infection (Figure 3.1A and Supplemental Figure 2.1C-D), we wanted to explore the possible factors that led to this observation. First, we counted the true leaf number including the infected or mock treated leaf under dissection microscope on 6th day post infection and found that *P. syringae* infected plants exhibited less true leaves compared to mock treated plants (Figure 3.1B). Since primordia of rosette is generated from vegetative meristem, we wonder if earlier floral transition is the reason for less true leaves in the infected plants observed on 6 days post infection. We recorded the flowering time of mock and single leaf infected plants. To our surprise, the infected plants flowered later compared to the mock treated plants (Figure 3.1C).

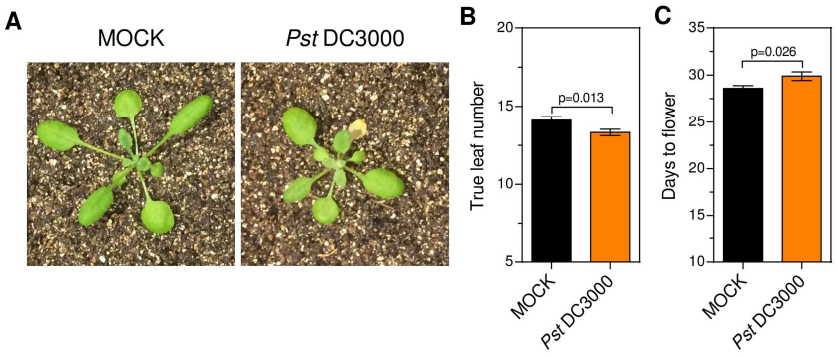

Figure 3.1 *P. syringae* infection results in reduced growth and delayed development of plants.
(A) Representative pictures of mock treated or *Pst* DC3000 infected plants on 6 days post infection. (B) True leaf number (including infected or mock treated leaf) of mock treated or infected plants on 6 days post infection (n=24). (C) Days to flower (from sowing of stratified seeds to observing the emergence of florescence) of mock treated or infected plants. (n=11). Statistical analyses compared to mock treated plants (B and C) were performed using the t test.

This result suggests that the infected plants might go through floral transition later than mock plants and have delay in development. To further test this possibility, we collected aerial tissues from mock treated and *P. syringae* infected plants 3 days after infection and the samples were fixed and further embedded in paraplast to perform longitudinal sections of the shoot apical meristem (SAM). We found that all of the SAMs of mock treated plants and most of the SAMs of infected plants were going through floral transition (Figure 3.2), featured by the SAM enlargement and mounting up, and the elongation of the rib-meristem cells to promoter the elongation of sub-apical pith and stem axis [20–22]. Although the SAMs in both mock treated and infected groups were not developing exactly at the same pace, SAMs from mock treated group were overall more developed and more advanced in the floral transition process (Figure 3.2). Overall, these

results suggest the growth and development of the plant is delayed by localized *P. syringae* infection.

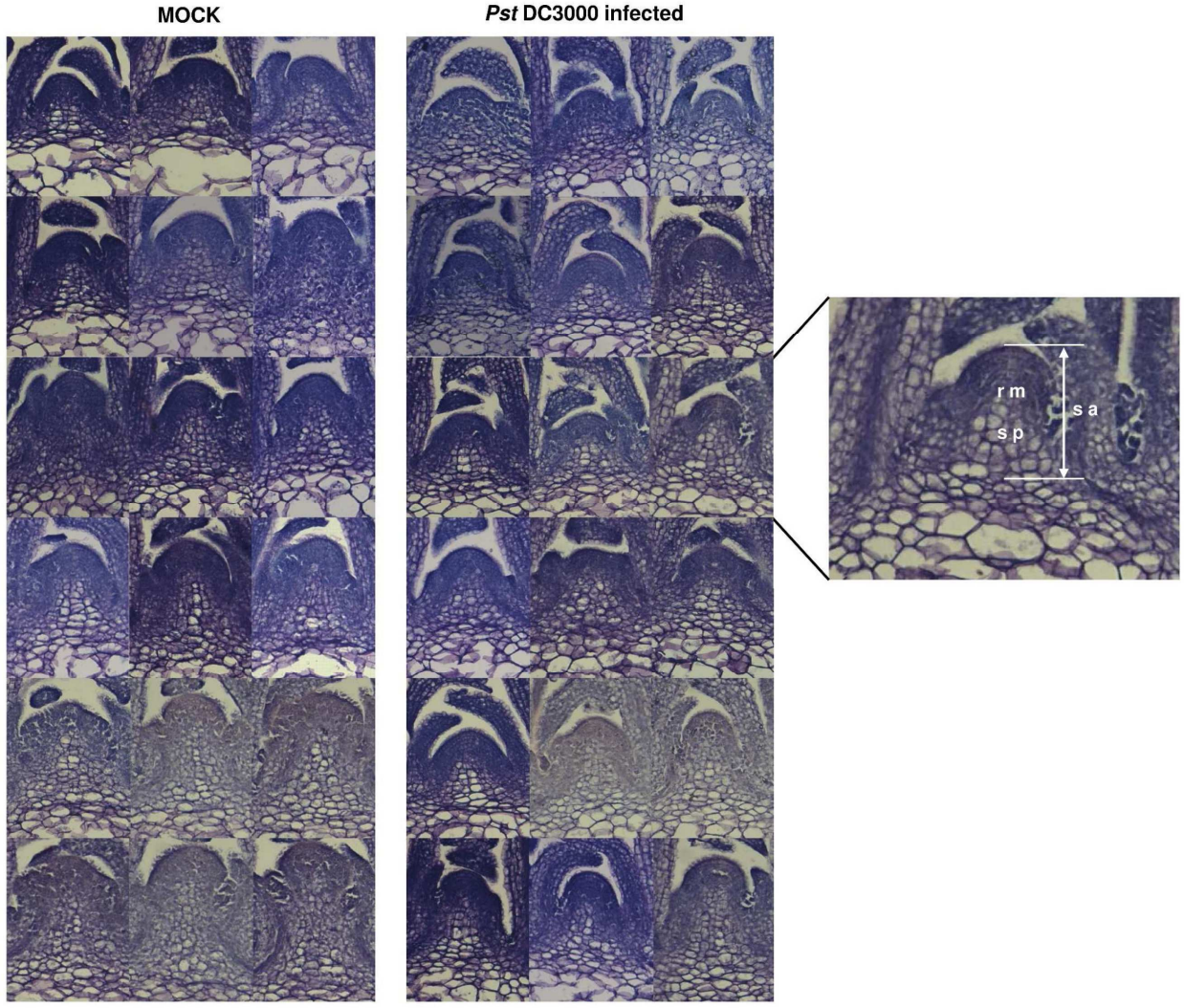

Figure 3.2 *P. syringae* infection delays the development of the shoot apical meristem. The plants were grown in LD (~100µmol.m^{-2}.s^{-1}) for two weeks and transferred to LL (60µmol.m^{-2}.s^{-1}). On the second morning in LL, plants were mock treated or infected with *Pst* DC3000. Tissue samples were harvested 3 dpi (day post infection). The longitudinal section of mock treated (left panel) and infected (right panel) plant apices from two biological repeats were visually aligned from least to most developed and one least and one most developed apices were removed from both groups. r m, rib meristem; s p, sub-apical pith; s a, stem axis. All pictures are taken with the same magnification under microscope.

Localized *Pst* DC3000 infection affects clock-controlled rhythms predominantly in the shoot apex

Considering the developmental delay of the SAM following a localized *Pst* DC3000 infection and the important role of shoot apex as the hierarchical master circadian oscillator, we wonder if the circadian rhythms in the shoot apex would be specifically changed by *Pst* DC3000 infection. We first observed that, as was shown before (Figure 2.1A), the luminescence signal of *CCA1::LUC+* plants from the infected leaf decayed to undetectable level (Figure 3.3). At the same time, the signal from the shoot apex also decreased drastically (Figure 3.3) 3 days after the infection.

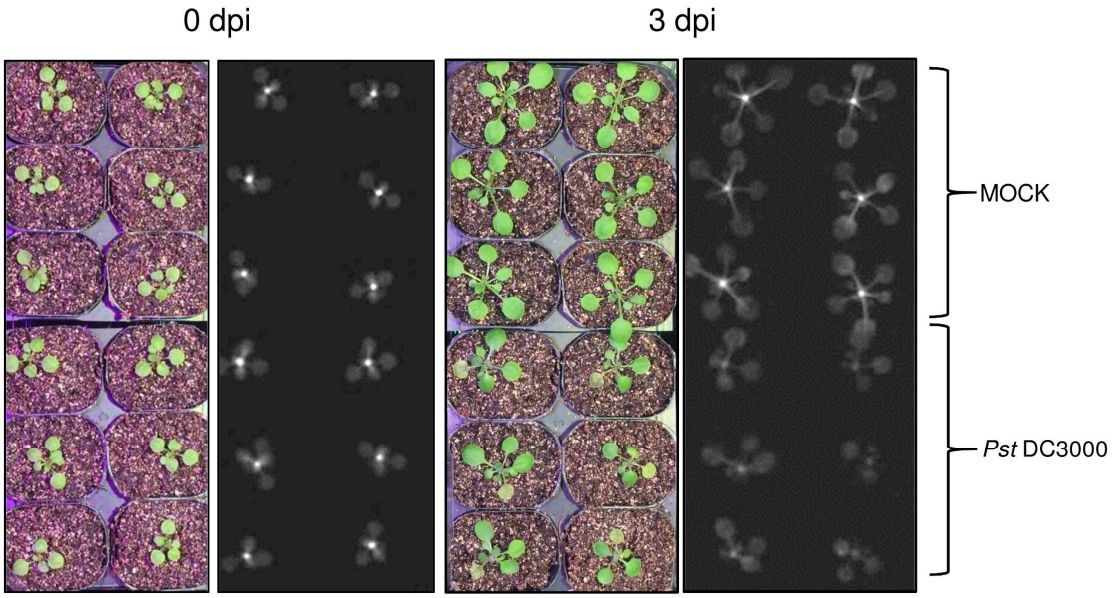

Figure 3.3 *Pst* DC3000 infection decreases the luminescence signal from shoot apex significantly.
CCA1::LUC+ plants were grown and treated as in Supplemental Figure 2.1, bright field images and luminescence images of 0 dpi (days post infection) (left panel) or 3 dpi (right panel) of mock treated or Pst DC3000 infected (in one leaf) plants are shown.

To confirm the decrease of CCA1 promoter activity upon single leaf *Pst* DC3000 infection, we performed single leaf *Pst* DC3000 infection on *CCA1::GUS* plants (3 lines)

as indicated in Supplemental Figure 2.1A. On the third day post infection, aerial tissues of both mock and infected plants were harvested and stained for GUS activity. Different length of GUS staining was performed to avoid masking of difference due to signal oversaturation (Figure 3.4, Supplemental Figure 3.1 and Supplemental Figure 3.2). Compared to plate grown younger seedlings which have *GUS* expressed more universally in the shoot [23], the older soil grown plants displayed more GUS expression in shoot apex and young leaves while older leaves have less GUS expression (Supplemental Figure 3.1). Upon *Pst* DC3000 infection, the *GUS* expression in the shoot apex and young leaves strongly decreased (Figure 3.4, Supplemental Figure 3.1 and Supplemental Figure 3.2). These results further support that the CCA1 promoter transcriptional activity in the shoot apex is strongly decreased upon single leaf *Pst* DC3000 infection.

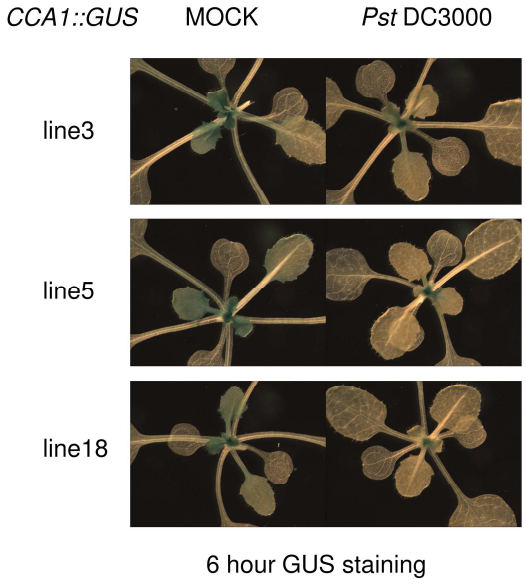

Figure 3.4 Single leaf *Pst* DC3000 infection decreases *CCA1::GUS* expression.
CCA1::GUS plant (3 lines) were grown and infected as indicated in Supplemental Figure 2.1A. 3 days post infection aerial tissues were harvested for GUS staining. Images were taken with the same light and camera setting with the same magnification, more than 4 plants were stained for each line under each condition and one representative image is shown.

To closely evaluate the regulation of circadian rhythms by *Pst* DC3000 infection in the shoot apex, we reanalyzed data in Figure 2.1 by drawing small circular regions to include the signal from the shoot apex and analyzed the circadian rhythms in the shoot apex versus the untreated peripheral tissues. Since there was a reduction of the plant size by *Pst* DC3000 infection, to analyze the rhythms in the untreated peripheral tissues, we normalized bioluminescence counts to the estimated tissue area at each time point. The amplitude was decreased in both shoot apex and peripheral tissues in most cases for the three clock reporters tested, with the exception of *CCA1::LUC+* amplitude not significantly decreased in peripheral tissues (Figure 3.5A-C), and the amplitude changes (ratio of amplitude over mock in log scale) in the shoot apex were more prominent in all three reporters (Figure 3.5D). Similarly, the period lengthening phenotype was more drastic in shoot apex (Figure 3.5A-B and E-F). Stronger effects on relative amplitude error and phase shift are also observed in the shoot apex (Supplemental Figure 3.3).

Figure 3.5 Localized *Pst* DC3000 infection regulates circadian rhythms predominantly in the shoot apex.

(A-B) Luciferase activity from shoot apex and normalized luciferase activity from untreated peripheral tissues of soil grown *Arabidopsis CCA1::LUC+* plants upon single leaf *Pst* DC3000 infection (orange) or mock treatment (black). Treatments were performed at ZT24 (denoted by the black arrow). Results indicate mean values [± SD, n=6] and are representative of 5 independent experiments. (C and E) Mean amplitude (C) and period (E) estimates [± SEM] of *CCA1::LUC+* (n=30), *LHY::LUC+* (n=15) and *TOC1::LUC+* (n=15) apex luciferase activity rhythms and normalized luciferase activity rhythms of untreated peripheral tissues upon single leaf *Pst* DC3000 infection (orange) or mock treatment (gray) for experiments indicated in Figure 2.1. (D and F) amplitude change (ratio over mean mock in log scale) (D) and period change (F) of rhythms in shoot apex (black) and peripheral tissues (gray) upon single leaf *Pst* DC3000 infection.Statistical analyses compared to mock treated plants (C and E), or compared between shoot apex and peripheral tissues (D and F) were performed using the *t* test. Stars indicate the level of significance (*$p<0.01$, **$p<0.001$, ***$p<0.0001$).

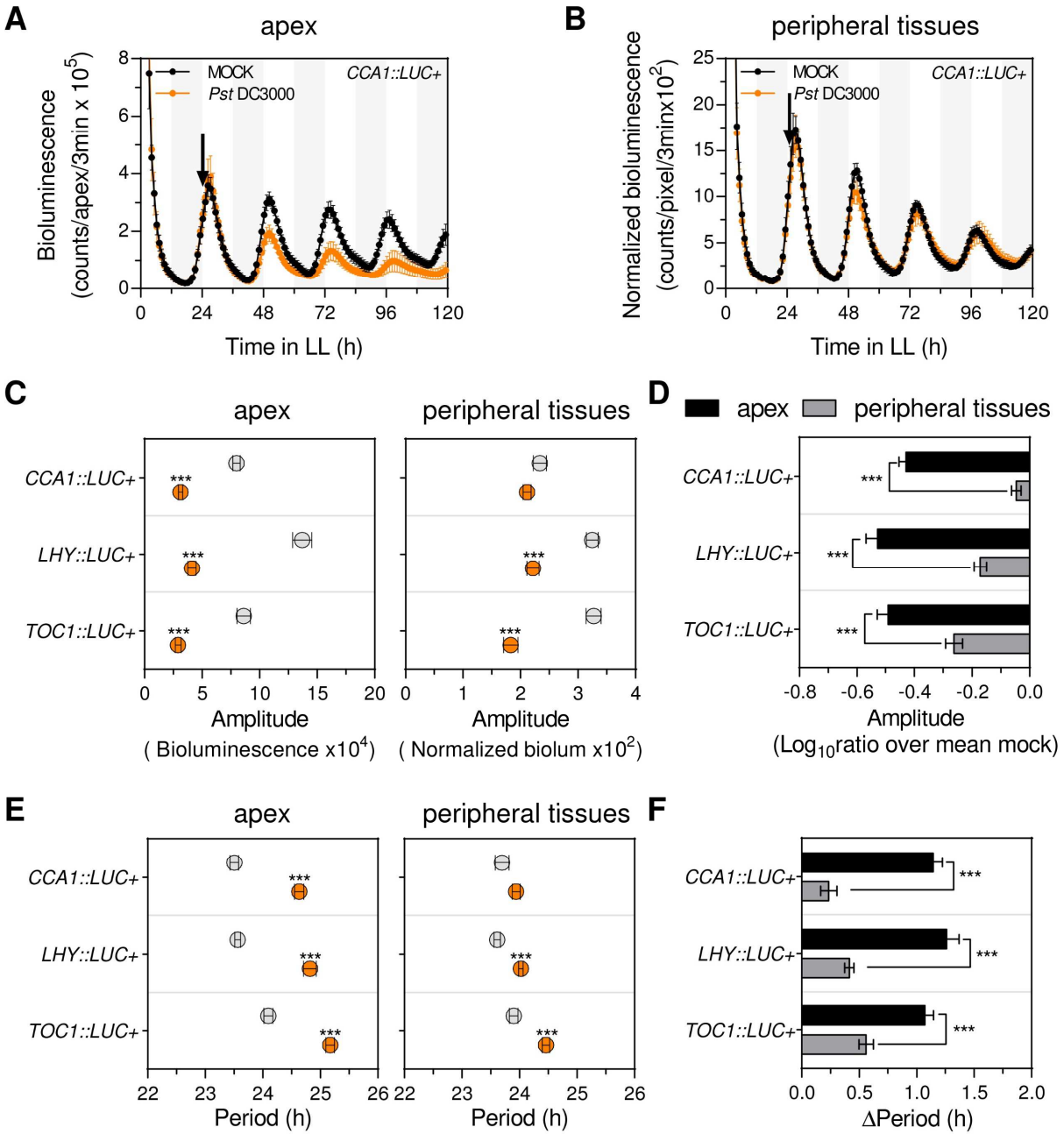
A
apex
Bioluminescence (counts/apex/3min x 10^5)
MOCK
Pst DC3000
CCA1::LUC+
Time in LL (h)
B
peripheral tissues
Normalized bioluminescence (counts/pixel/3minx10^2)
MOCK
Pst DC3000
CCA1::LUC+
Time in LL (h)
C
apex
peripheral tissues
CCA1::LUC+
LHY::LUC+
TOC1::LUC+
Amplitude
(Bioluminescence x10^4)
Amplitude
(Normalized biolum x10^2)
D
apex
peripheral tissues
CCA1::LUC+
LHY::LUC+
TOC1::LUC+
Amplitude
(Log10ratio over mean mock)
E
apex
peripheral tissues
CCA1::LUC+
LHY::LUC+
TOC1::LUC+
Period (h)
Period (h)
F
CCA1::LUC+
LHY::LUC+
TOC1::LUC+
ΔPeriod (h)

Discussion

The relationship between defense and development has been an interesting and complicated question. As from the instinctive understanding, plant under stress condition would try to produce offsprings earlier so as to escape before lethal level of stress happens. However, this is not always true. In the case of abiotic stress, drought could lead to earlier flowering under LD condition while cold and salinity stress delays flowering [24]. Jasmonic acid, the phytohormone mediating plant defense against necrotrophic pathogens, has been reported to promote flowering at low concentration and delay flowering at high concentration [25,26]. Salicylic acid was shown to accelerates flowering [27] and in the case of infection by biotrophic pathogen such as *Pseudomonas syringae*, the outcome depends on the actual context of infection. Korves et al. reported that infection of lower titers leads to faster flowering while as the titer went up, the advancing of flowering time is not as drastic or even revert to the other side [28]. Under our experimental condition, we used relatively high inoculum (OD 0.2) of the virulent pathogen *Pst* DC3000 which will result in a high titer in the infected tissue, and we observed a delay of SAM development and flowering time (Figure 3.1C and Figure 3.2). The detailed mechanism remains to be investigated. We cannot totally exclude the possibility that the loss of leaf tissue due to bacterial infection and the corresponding loss of energy source could contribute to the observed developmental delay, however, removing a leaf is not a great control for less energy source since the cutting procedure will trigger wound related signaling including JA production [29]. We also observed less true leaf number on 6 days post infection at the same time (Figure 3.1B), while on 3 days after infection, we observed that most SAMs of MOCK or infected plants were going through floral transition which

stops the production of rosette leaf primordia. Thus, the observation of less discernable true leaves under dissection microscope of the infected plant could be either (1) the initiation of leaf primordia before floral transition was slowed down upon *Pst* DC3000 infection, or (2) the development and expansion from leaf primordia to discernable leaves was slowed down upon *Pst* DC3000 infection. More morphological characterization of the shoot apices and young leaves before and after the infection need to be done to further dissect the mechanism.

Work by Takahashi et al. demonstrated that shoot apex as the master oscillator of the plant, is able to send clock information to synchronize peripheral clocks (for example, the root clock) [4]. From our study, we found that a localized infection in the peripheral tissue was able to modulate the shoot apex and systemically change the clock function at a whole organism level. This provides an example of reverse modulation of the clock function from the hierarchical organization where peripheral organs could send signals to modulate the master oscillator. Whether the changes of clock-controlled rhythms in uninfected leaves is due to the synchronization effect from the already modulated shoot apex clock, or to the fact that the signals which modulated the shoot apex clock could also travel to the other leaves is still unknow. Of course, it's possible that both of these factors contributed to the final result.

Upon localized *Pseudomonas syringae* infection, the shoot apex was experiencing both developmental delay and alteration of the circadian rhythm. With our current knowledge, we don't know if there was any relationship between these two phenotypes. Altered circadian clock could lead to growth and development phenotype. For example, CCA1 and LHY overexpression plants are very late flowering and several clock related

mutants have abnormal hypocotyl length [14]. At the same time, since shoot apex is very important to the plant clock, it is not surprising to expect that dramatic changes in the morphology and organization of shoot apex might influence clock as well. However, we cannot rule out the possibility that development and clock phenotypes we observed upon infection are not related.

Materials and Methods

Plant material and growth condition

Arabidopsis *thaliana* (Arabidopsis) seedlings used in this work were from the Columbia ecotype (Col-0). *CCA1::LUC+* [23], *LHY::LUC+* [30], *TOC1::LUC+* [31] reporter lines were previously described.

For *Pseudomonas syringae* infection assays, stratified sterile seeds were grown in autoclaved soil (Sunshine professional mix, Sungro) under 12h light (~100 $\mu mol.m^{-2}.s^{-1}$) / 12h dark cycles (LD) for 14 days at 22°C. Plants were watered (with fertilizer) around one week old and slightly watered again on the 14^{th} morning. At the beginning of day 15, plants were transferred to constant light (60 $\mu mol.m^{-2}.s^{-1}$, 22°C) (LL). On the morning of day 16 (ZT0), infection assays were performed.

Pseudomonas syringae culture condition and infection procedure

Pseudomonas syringae pv. *tomato* DC3000 *(Pst* DC3000*)* [43] liquid cultures (King's B medium: 2% Proteose peptone No.3, 1% Glycerol, 8.6mM K_2HPO_4 and 6mM $MgSO_4$) were grown in the dark at 28ºC (shaking at 175rpm) until OD600 between 0.6 and 0.7 was reached (several dilutions were started to assure that a suitable culture was available at the time of treatment).

To prepare *Pst* DC3000 cell suspension inoculum, bacteria from a liquid culture (OD600 between 0.6 and 0.7) were harvested by centrifugation at 3220 x *g* for 2min, resuspended in sterile water (LabChem), and harvested by centrifugation at 3220 x *g* for 3min. The bacterial pellet was resuspended in water (LabChem) adjusting OD600 to 0.2 (~1x10^8 cfu), and Silwet L77 (Lehle seeds) was added to a final concentration of 0.025%. About half of a single leaf was dipped into this *Pst* DC3000 cell suspension or a mock solution (0.025% Silwet L77) for 1min. After treatment, excess inoculum was blot-dried from the leaf surface using a sterile filter paper strip and plants were returned to LL condition.

Leaf counting and flowering time scoring

On 6th day post infection, plants were placed under dissection microscope and true leaf numbers were counted including mock treated or infected leaves. For the small true leaves in the shoot apex, tweezers were used and any leaf that can be lifted and unwrapped by the tweezer was counted. For counting flowering time, plants were kept under LL (60 µmol.m^{-2}.s^{-1}, 22°C). The days from growing stratified seeds on soil to the first visual observation of inflorescence were counted as days to flower.

Meristem longitudinal section and staining

On the morning of day 3 post infection, aerial part of mock treated or single leaf infected plants were harvested and fixed in FAA solution (50% ethanol, 3.7% formaldehyde, 5% acetic acid) with gentle vacuum for twice, 20min each, followed by gentle shaking in fresh FAA for 40min at room temperature (RT) and overnight fixing in FAA at 4°C. Then FAA solution was changed to 70%, 80%, 90% 95% ethanol consecutively shaking at RT, 1 hour each concentration. Another 1h shaking with 95% ethanol and 0.2% EOSIN Y to lightly staining the tissue was performed followed by 1h

95% ethanol shaking to wash away excessive stain. The tissue was embedded in paraplast by the following procedure: three times of 100% ethanol (E) RT shaking 45min, 25% histoclear (H) 75% ethanol (E), 50% H 50% E, 75% H 25% E, 100% H, 100% H, 100%H shaking at RT 45min each. Then 50% histoclear, 50% paraplast overnight at 58°C. Following that, 6 changes of 100% paraplast were performed with samples after each change placed in 58°C for at least 4 hours. More changes of paraplast can be done if the samples still have the smell of histoclear. Then samples were embedded in metal boats, harden at 4°C for more than 20 minutes.

8 µm of longitudinal sectioning was performed and baked onto superfrost slides on slide warmer overnight (42°C). On the next morning, slides were gently shaken in histoclear 10min, 3 times to dewax, then dehydrate in isopropanol 3 times 3 minutes. Air dry for 1h. then dip dried slides into tolouidine blue staining solution (1g tolouidine blue powder and 6g boric acid dissolved in 100ml water, store in dark) for 5-15 secs. Then quickly wash off excessive stain with water 3 times. Dry the slides at room temperature for overnight and mount cover slides with permount.

Imaging analysis

Data sets used were the same data sets as shown in Figure 2.1. To obtain the shoot apex signal, in MetaMorph image analysis software (Molecular Devices), a mall circular region of diameter of 10 pixels was drawn to acquire the shoot apex bioluminescence counts. At each time point, with the bioluminescence counts and number of bioluminescent pixels information already obtained for the whole plant or the treated leaf (mock treated or infected leaf), the bioluminescent counts and bioluminescent pixels were calculated for the untreated peripheral tissues (whole plant subtracting shoot

apex and treated leaf) for each plant. The size of the peripheral tissues was estimated by third order polynomial regression (Graphpad prism 6) and bioluminescent counts were divided by this estimated size. Bioluminescence rhythms of shoot apex and normalized bioluminescence rhythms of peripheral tissues were analyzed with by Fast Fourier Transform-Non Linear Least Squares (FFT-NLLS) [44] using the interface provided by the Biological Rhythms Analysis Software System (BRASS) [45]. Amplitude changes within each experiment were calculated as the ratio between the amplitude value obtained for each individual (both for mock and treated plants) and the mean amplitude obtained for mock treated plants (amplitude change = individual amplitude / mean amplitude mock) (log_{10} transformed ratios were used for statistical analysis). Normalized phase values were calculated as [24*(t-24)/p], where p is the period of the corresponding individual plant calculated by BRASS and t is the fitted acrophase time closest to the second subjective morning (ZT24) extrapolated using BRASS.

Staining of GUS enzymatic activity

On the morning of day 3 after infection, aerial tissues of *CCA1::GUS* plant were collected and incubated in cold 90% acetone for 15-20 minutes. Then acetone was removed and water was added covering the samples and incubated for 5min. After that, water was removed and GUS staining solution was added and incubated with sample at 37°C for desired duration. The content of the GUS staining solution is: 13.42mM Na H_2PO_4, 11.58mM Na_2HPO_4, 5mM Ferrocyanide, 5mM Ferricyanide, 1% Triton X-100, 2.5mM X-Gluc. After the desired duration of incubation, stained samples were fixed with FAA and followed by same ethanol washes as described for the meristem longitudinal

sectioning till the 95% ethanol wash. Samples were preserved and imaged in 95% ethanol wash.

Supplementary Information

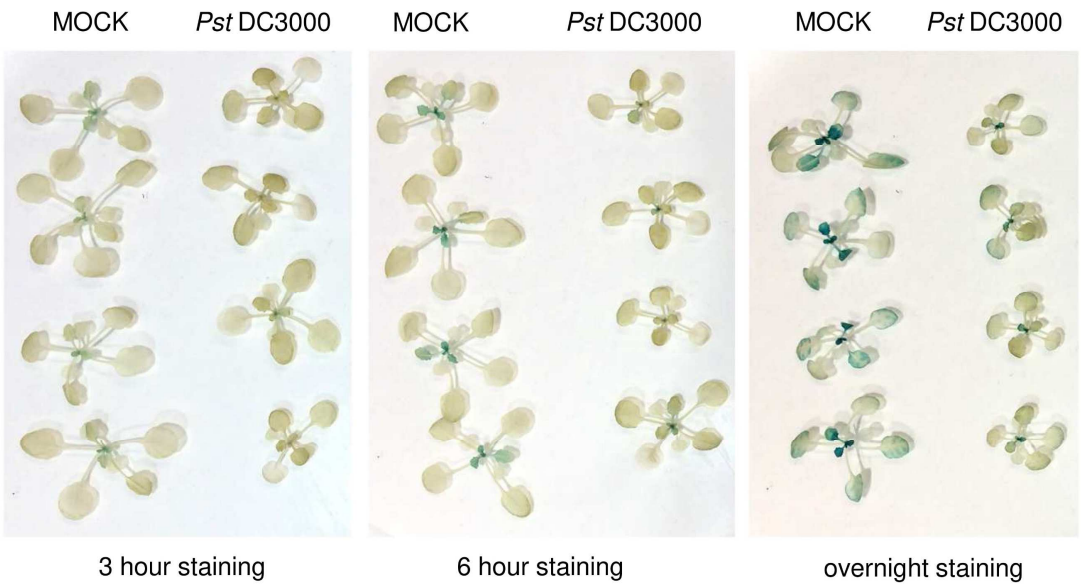

Supplemental Figure 3.1 Single leaf *Pst* DC3000 infection decreases *CCA1::GUS* expression.
CCA1::GUS plant (line 3) were grown and infected as indicated in Supplemental Figure 2.1A. 3 days post infection aerial tissues were harvested for 3 hour, 6 hour or overnight GUS staining.

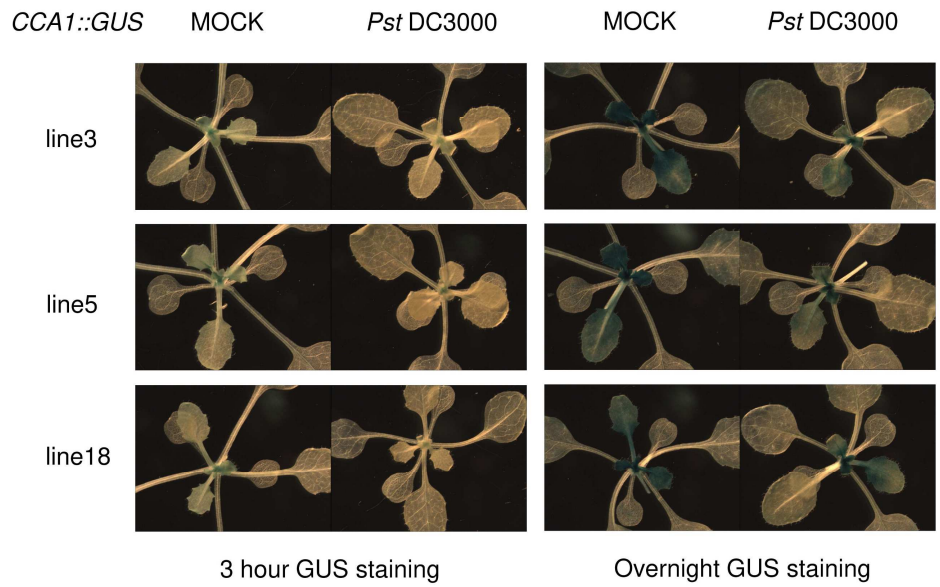

Supplemental Figure 3.2 Single leaf *Pst* DC3000 infection decreases *CCA1::GUS* expression in shoot apex and young leaves.
CCA1::GUS plant (3 lines) were grown and infected as indicated in Supplemental Figure 2.1A. 3 days post infection aerial tissues were harvested for GUS staining. Images were taken with the same light and camera setting with the same magnification, more than 4 plants were staining for each line under each condition and one representative image is shown.

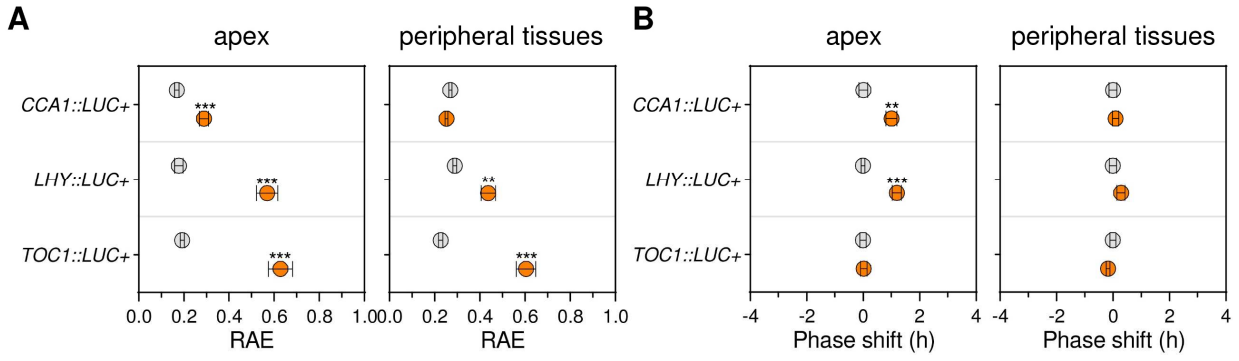

Supplemental Figure 3.3 Single leaf *Pst* DC3000 infection affects clock controlled rhythms more in the shoot apex.
Mean RAE (A) and phase shift (B) estimates [± SEM] of *CCA1::LUC+* (n=30), *LHY::LUC+* (n=15) and *TOC1::LUC+* (n=15) apex luciferase activity rhythms and normalized luciferase activity rhythms of untreated peripheral tissues upon single leaf *Pst* DC3000 infection (orange) or mock treatment (gray) for experiments indicated in Figure 2.1. Statistical analyses compared to mock treated plants were performed using the *t* test. Stars indicate the level of significance (*p<0.01, **p<0.001, ***p<0.0001).

References

1. Barton, M.K. (2010). Twenty years on: the inner workings of the shoot apical meristem, a developmental dynamo. Dev. Biol. *341*, 95–113.

2. Fletcher, J.C. (2002). Shoot and floral meristem maintenance in *Arabidopsis*. Annu. Rev. Plant Biol. *53*, 45–66.

3. Halperin, W. (1978). Organogenesis At the Shoot Apex. Ann. Rev. Plant Physiol *29*, 239–62.

4. Takahashi, N., Hirata, Y., Aihara, K., and Mas, P. (2015). A hierarchical multi-oscillator network orchestrates the *Arabidopsis* circadian system. Cell *163*, 148–159.

5. Huijser, P., and Schmid, M. (2011). The control of developmental phase transitions in plants. Development *138*, 4117–4129.

6. Poethig, R.S. (2003). Phase change and the regulation of developmental timing in plants. Science *301*, 334–336.

7. Song, Y.H., Ito, S., and Imaizumi, T. (2013). Flowering time regulation: photoperiod- and temperature-sensing in leaves. Trends Plant Sci. *18*, 575–583.

8. Jones (1999). An Essay on Juvenility, Phase Change, and Heteroblasty in Seed Plants. Int. J. Plant Sci. *160*, S105–S111.

9. Hyun, Y., Richter, R., and Coupland, G. (2017). Competence to Flower: Age-Controlled Sensitivity to Environmental Cues. Plant Physiol. *173*, 36–46.

10. Conti, L. (2017). Hormonal control of the floral transition: Can one catch them all? Dev. Biol. *430*, 288–301.

11. Pfeiffer, A., Janocha, D., Dong, Y., Medzihradszky, A., Schöne, S., Daum, G., Suzaki, T., Forner, J., Langenecker, T., Rempel, E., Schmid, M. Wirtz, M., Hell, R., and Lohmann, J.U. (2016). Integration of light and metabolic signals for stem cell activation at the shoot apical meristem. Elife *5*.

12. Sanchez, S.E., and Kay, S.A. (2016). The Plant Circadian Clock: From a Simple Timekeeper to a Complex Developmental Manager. Cold Spring Harb. Perspect. Biol. *8*, a027748.

13. Harmer, S.L. (2009). The Circadian System in Higher Plants. Annu. Rev. Plant Biol. *60*, 357–377.

14. Nagel, D.H., and Kay, S.A. (2012). Complexity in the wiring and regulation of plant

circadian networks. Curr. Biol. *22*, R648-57.

15. Hsu, P.Y., and Harmer, S.L. (2014). Wheels within wheels: The plant circadian system. Trends Plant Sci. *19*, 240–249.

16. Pruneda-Paz, J.L., and Kay, S.A. (2010). An expanding universe of circadian networks in higher plants. Trends Plant Sci. *15*, 259–265.

17. Greenham, K., and McClung, C.R. (2015). Integrating circadian dynamics with physiological processes in plants. Nat. Rev. Genet. *16*, 598–610.

18. Kwiatkowska, D. (2008). Flowering and apical meristem growth dynamics. J. Exp. Bot. *59*, 187–201.

19. Chen, Y.-Y., Wang, Y., Shin, L.-J., Wu, J.-F., Shanmugam, V., Tsednee, M., Lo, J.-C., Chen, C.-C., Wu, S.-H., and Yeh, K.-C. (2013). Iron Is Involved in the Maintenance of Circadian Period Length in *Arabidopsis*. Plant Physiol. *161*, 1409–1420.

20. Hempel, F.D., and Feldman, L.J. (1994). Bi-directional inflorescence development in *Arabidopsis thaliana*: Acropetal initiation of flowers and basipetal initiation of paraclades. Planta *192*, 276–286.

21. Vaughan, J.G. (1955). The morphology and growth of the vegetative and reproductive apices of *Arabidopsis* thaliana (L.) Heynh., Capsella bursa-pastoris (L.) Medic. and Anagallis arvensis L. J. Linn. Soc. London, Bot. *55*, 279–301.

22. Jacqmard, A., Gadisseur, I., and Bernier, G. (2003). Cell division and morphological changes in the shoot apex of *Arabidopsis* thaliana during floral transition. Ann. Bot. *91*, 571–576.

23. Pruneda-Paz, J.L., Breton, G., Para, A., and Kay, S.A. (2009). A Functional Genomics Approach Reveals CHE as a Component of the *Arabidopsis* Circadian Clock. Science (80-.). *323*, 1481–1485.

24. Riboni, M., Robustelli Test, A., Galbiati, M., Tonelli, C., and Conti, L. (2014). Environmental stress and flowering time: the photoperiodic connection. Plant Signal. Behav. *9*, e29036.

25. Krajnčič, B., and Nemec, J. (1995). The Effect of Jasmonic Acid on Flowering in Spirodela polyrrhiza (L.) Schleiden. J. Plant Physiol. *146*, 754–756.

26. Zhai, Q., Zhang, X., Wu, F., Feng, H., Deng, L., Xu, L., Zhang, M., Wang, Q., and Li, C. (2015). Transcriptional Mechanism of Jasmonate Receptor COI1-Mediated Delay of Flowering Time in *Arabidopsis*. Plant Cell *27*, 2814–2828.

27. Martinez, C., Pons, E., Prats, G., and Leon, J. (2004). Salicylic acid regulates

flowering time and links defence responses and reproductive development. Plant J. *37*, 209–217.

28. Korves, T.M., and Bergelson, J. (2003). A developmental response to pathogen infection in *Arabidopsis*. Plant Physiol. *133*, 339–347.

29. Koo, A.J.K., and Howe, G.A. (2009). The wound hormone jasmonate. Phytochemistry *70*, 1571–1580.

30. Baudry, A., Ito, S., Song, Y.H., Strait, A.A., Kiba, T., Lu, S., Henriques, R., Pruneda-Paz, J.L., Chua, N.-H., Tobin, E.M., Kay, S.A., and Imaizumi, T. (2010). F-box proteins FKF1 and LKP2 act in concert with ZEITLUPE to control *Arabidopsis* clock progression. Plant Cell *22*, 606–622.

31. Alabadi, D., Oyama, T., Yanovsky, M.J., Harmon, F.G., Mas, P., and Kay, S.A. (2001). Reciprocal regulation between TOC1 and LHY/CCA1 within the *Arabidopsis* circadian clock. Science *293*, 880–883.

Chapter 4 Novel cell surface luciferase reporter for high-throughput yeast one-hybrid screens

Katia Bonaldi [1,2,5], Zheng Li [1,2,5], S. Earl Kang [1,3], Ghislain Breton [1,4], Jose L. Pruneda-Paz [1,2,*]

[1] Division of Biological Sciences, University of California San Diego, La Jolla, CA 92093, USA.

[2] Center for Circadian Biology, University of California San Diego, La Jolla, CA 92093, USA.

[3] Present address: Department of Plant Biology, University of Georgia, Athens, GA 30602, USA.

[4] Present address: Department of Integrative Biology and Pharmacology, McGovern Medical School, Houston, TX 77030, USA.

[5] These authors contributed equally to this work.

*Correspondence: jprunedapaz@ucsd.edu

Abstract

Gene-centered yeast one-hybrid (Y1H) screens provide a powerful and effective strategy to identify transcription factor (TF)-promoter interactions. While genome-wide TF ORFeome clone collections are increasingly available, screening protocols have limitations inherent to the properties of the enzymatic reaction used to identify interactions and to the procedure required to perform the assay in a high-throughput format. Here, we present the development and validation of a streamlined strategy for quantitative and fully automated gene-centered Y1H screens using a novel cell surface Gaussia luciferase reporter.

Introduction

The yeast one-hybrid system (Y1H) provides one of the few straightforward strategies that is commonly used to identify TF-promoter interactions focusing on a single promoter region. The approach requires two main components: a reporter construct (bait) that carries a promoter region driving the expression of a reporter gene (e.g. *lacZ*), typically integrated into the genome of a yeast strain (e.g. YM4271), and an effector construct (prey) that carries a yeast constitutive promoter driving the expression of a TF fused to a transcriptional activation domain (AD) (e.g. Gal4-AD). Following transformation of effector constructs into the reporter strain, TF-promoter interactions are revealed by an increase in the reporter gene activity that depends on the DNA binding affinity and specificity of the TF-AD effector for the promoter bait. As initially designed, the effector constructs for Y1H screens were part of cDNA libraries. However, because TFs are

typically expressed at low levels and often in a specific tissue, developmental stage or physiological condition [1-3], these cDNA libraries only provided a partial and biased pool of potential DNA binding proteins. With the advent of the genomic era, several efforts were made to develop global TF-effector libraries for different species [4-10]. Adapting the Y1H system to these TF ORFeome clone collections provided a remarkable improvement to the approach that enhanced the discovery of functional TF-promoter interactions in an unbiased and comprehensive manner [8,11-15].

Recently, we established a gene-centered high-throughput Y1H (HT-Y1H) screening approach using a clone collection encompassing 80% (1956 clones) of all predicted TFs in the plant model organism *Arabidopsis thaliana* (*Arabidopsis*)(8). This strategy, performed in 384-well plates and entirely in liquid format, evaluated all 1956 potential TF-promoter interactions individually (one interaction per well) using the *lacZ* gene as reporter [8,16]. Importantly, this work indicated that ranking TF-promoter interactions based on the Y1H reporter activity could provide an effective mean for identifying and prioritizing TFs more likely to be involved in biologically meaningful interactions [8]. Although gene-centered Y1H screens already identified a number of novel TF-promoter interactions in *Arabidopsis* [8,14,15,17-22], we found that quantification of the β-galactosidase activity is rapidly saturated when performed in a high-throughput format (i.e. 384-well plates). This issue limits our ability to detect positive interactions when background reporter levels are high [8], and to accurately sort positive interactions to select and prioritize potentially relevant TF candidates for further characterization *in vivo*.

As reported previously the ONPG (2-nitrophenyl-β-D-galactopyranoside)-based method performed in a liquid format provides an accurate quantification of the β-galactosidase activity in yeast cells but often requires of either multiple dilutions of the initial samples or an optimized reaction time for each sample to adjust the colorimetric signal within the linear range [23,24]. While these adjustments are possible when individual samples are handled, they are impracticable in a high-throughput format where several thousand reactions are processed simultaneously [8,16]. For this reason, all enzymatic reactions in HT-Y1H screens performed in a liquid format are stopped at a fixed time regardless of differences among individual reaction kinetics [16], resulting in a short linear range and rapid saturation of the β-galactosidase assay (Supplemental Figure 4.1). Furthermore, because each promoter bait usually drives a different background reporter activity, the progression of the colorimetric reaction has to be continually monitored and the reaction time subjectively determined by an operator in each experiment. This step could be theoretically automated; however, it would require of a sophisticated system to continuously process multiple microplates and determine the optimal incubation time for the enzymatic reaction in each well. Importantly, similar limitations were reported for an alternative HT-Y1H screening method that relies on β-galactosidase-mediated color development in yeast cells spotted on agar plates [25]. While it might be possible to improve either β-galactosidase assay using fluorescent or luminescent reaction products, such reagents would significantly increase the cost of HT-Y1H screens and likely limit its widespread usage [24].

lacZ-based HT-Y1H screens are additionally impacted by technical factors that affect either result analysis or automation efforts. Regarding the former, we found that

incubation of liquid β-galactosidase reactions at 30 to 37ºC in 384-well plates results in faster enzymatic reaction kinetics for the wells located at the periphery of the microplate, likely due to uneven temperature distribution. This problem introduces a bias in the calculation of the baseline β-galactosidase activity used to discriminate between positive and negative TF-promoter interactions. Likewise, the β-galactosidase assay in agar spotted yeast cells is subject to false positive calls due to color signal diffusion from strong positives into neighboring areas [25]. Finally, quantification of the β-galactosidase activity in a liquid format requires yeast cell permeabilization to allow an efficient enzyme-substrate encounter [24]. Currently used freeze and thaw cycles provide a simple, reproducible and cost-effective method for yeast cell lysis [26], however this is a labor-intensive and rate-limiting step for HT-Y1H screens that is incompatible with automation [16].

Considering all these factors we reasoned that HT-Y1H screen optimization would require of a reporter activity that could be reliably quantified at a fixed time over a wide range of concentrations, and an assay compatible with a fully automated procedure and performed at room temperature. Here, we analyzed the activity of several luciferase reporters in yeast cells and found that cell-surface expressed gLUC (gLUC59) activity can be analyzed directly in a yeast cell culture aliquot at room temperature. We then exhaustively characterized the quantitative capabilities of the gLUC59 assay in yeast cells and determined that has a significantly expanded linear range compared to a fixed-time β-galactosidase assay currently used for HT-Y1H screens. Finally, we used the gLUC59 reporter to establish an optimized Y1H system that is suitable for multiplexed and fully automated gene-centered screens.

Materials and Methods

Plasmid constructs and yeast strains

All primers and the corresponding PCR products are listed in Supplemental Table 4.1.

To build pY1ΔRep (pLacZi vector [Clontech] carrying the *Sna*BI and *Nhe*I restriction sites instead of the *lacZ* gene), the region upstream of the *lacZ* gene in pLacZi was PCR amplified and digested with *Xho*I/*Sna*BI, and the region downstream of the *lacZ* gene in pLacZi was PCR amplified and digested with *Sna*BI/*Ahd*I. These fragments were ligated into the *Xho*I/*Ahd*I sites of pLacZi. To generate pY1-RLUC, pY1-LUC+ and pY1-gLUC, the coding sequence for each luciferase flanked by *Sna*BI and *Nhe*I sites was PCR amplified, and cloned into pY1ΔRep.

Surface reporter vectors for yeast genomic integration were built using the pY1-PGA59emp backbone, which consists of the pLacZi vector (Clontech) carrying the coding and terminator sequences of the *PGA59* gene (from the CIp10::*ACT1p-gLUC59* vector [27]) instead of the *lacZ* reporter gene. To build pY1-PGA59emp (pLacZi vector [Clontech] carrying the coding and terminator sequences of the *PGA59* gene from CIp10::*ACT1p-gLUC59* [27] instead of the *lacZ* gene), the region upstream of the *lacZ* gene in pLacZi followed by the PGA59 signal peptide (+first 2 aa of PGA59) were amplified by PCR. Next, the *PGA59* coding sequence followed by the *PGA59* terminator were cloned upstream of the region containing the origin of replication of pLacZi by using two PCR reactions. The final PCR products were digested using *Sma*I/*Bbu*I and *Bbu*I/*Ahd*I respectively and ligated into the *Sma*I/*Ahd*I of pLacZi. To build pY1-gLUC59, the gLUC59 coding sequence was excised from CIp10::*ACT1p-gLUC59* [27] by digestion with

*Bam*HI/*Pfl*MI and ligated into the corresponding sites of pY1-PGA59emp. To generate pY1-RLUC59 and pY1-LUC+59, each luciferase coding gene (without ATG and stop codons) flanked by *Bbu*I and *Pfl*MI (RLUC) or *Bam*HI and *Pfl*MI (LUC+) sites were PCR amplified, digested with *Bbu*I/*Pfl*MI or *Bam*HI/*Pfl*MI and ligated into the corresponding sites of pY1-PGA59emp.

To generate the Gateway™ cloning (Life Technologies) compatible versions of cytosolic and surface luciferase reporter plasmids, an attR1/attR2 recombination cassette was excised from–pBluescript (Stratagene) [28] using *Eco*RV restriction digestion and blunt end ligated into the *Sma*I site of pY1-RLUC, pY1-LUC+, pY1-gLUC, pY1-RLUC59, pY1-LUC+59, and pY1-gLUC59.

pGLacZi is a Gateway-compatible version of pLacZi (Clontech) [28].

Promoter fragments were PCR amplified from *S. cerevisiae* genomic DNA (*ADH1* and *ADH1*Δ promoters), pBridge plasmid (Clontech) (*MET25* promoter), pCRBII-CCA1prΔ and pCRBII-CCA1prΔ(TBSmut) plasmids [14] (*CCA1 -363/-192* wild-type and TBS-I mutant promoters), and cloned into pENTR/D-TOPO according to the manufacturer's protocol (Life Technologies).

To generate reporter constructs, promoter fragments in pENTR/D were transferred to pGLacZi, pY1-gLUC_GW, pY1-LUC+_GW, pY1-RLUC_GW, pY1-gLUC59_GW, pY1-LUC+59_GW, and/or pY1-RLUC59_GW using LR clonase II according to the manufacturer's protocol (Life Technologies).

YM4271 reporter strains were generated by recombination of reporter plasmids into the *URA3* locus of the yeast genome (Clontech). While single or multiple reporter construct copies may be integrated, stable genomic insertions equalize reporter background levels

for each bait strain [11]. Briefly, reporter plasmids (unable to replicate in yeast) were transformed into YM4271 cells (*ura3-52*). Integration of the reporter plasmid carrying the wild-type *URA3* gene restores the ability of these cells to grow SD medium without uracil. The genomic integration was confirmed by PCR after several passages onto YPD medium as previously described [16]. pDEST22-TCP vectors were obtained from the pDEST22-TF clone library available at the *Arabidopsis* Biological Resource Center (ABRC) (http://abrc.osu.edu) under stock #CD4-89 [8].

Quantification of reporter gene activities in yeast

To quantify the activity of different luciferases in yeast, reporter strains were grown in YPD to saturation overnight at 30°C, then diluted 5 times with fresh YPD medium and grown in the same conditions for 6 additional hours. For PBS washed cells, a 500 µl aliquot of this cell culture was centrifuged 5 min at 1000 x *g*, resuspended in 500 µl of 1xPBS pH 7.4, centrifuged again, and resuspended in 500 µl of 1xPBS pH 7.4. Reporter gene activity was quantified in 100 µl (96-well format) or 25 µl (384-well format) of the cell culture or PBS-washed cells. For all luciferases, flash luminescence emission was determined immediately after addition of 100 µl (96-well format) or 25 µl (384-well format) of the enzyme substrate (detailed below). Glow emission was measured every two minutes thereafter up to 60 min after substrate addition. Integration time for the luminescence detection was 1 sec/well. For LUC+ activity we used: i) two commercial assays, the Dual-Luciferase® Reporter Assay System (using only the Luciferase Assay Reagent II, LAR II) (Promega) and the Bright-Glo™ Luciferase Assay System (Promega), and ii) two lab-made substrate solutions, D-luciferin (A) (25mM Glycylglycine, 15mM

MgSO4, 1mM dithiothreitol, 1mM D-luciferin potassium salt [Gold Biotechnology]) and D-luciferin (B) (0.01% triton X-100, 1mM D-luciferin potassium salt [Gold Biotechnology]). For RLUC activity we used: i) three commercial assays, the *Renilla* Luciferase Assay System (Promega), the *Renilla*-Glo® Luciferase Assay System (Promega) and the BioLux® *Gaussia* Luciferase Assay Kit (New England Biolabs), and ii) two lab-made substrate solutions, coelenterazine native (A) (1xPBS pH 7.4, 5mM NaCl, 20µM coelenterazine [Promega]) and coelenterazine native (B) (1xPBS pH 7.4, 5mM NaCl, 20µM native coelenterazine [Biosynth]). Coelenterazine was dissolved in acidified methanol (10 µl of 1N HCl per ml of solution) at a concentration of 1 mg/ml (100x). For gLUC activity we used: i) two commercial assays, the *Renilla* Luciferase Assay System (Promega) and the BioLux® *Gaussia* Luciferase Assay Kit (New England Biolabs), and ii) the same lab-made substrate solutions used to quantify RLUC activity.

To quantify the β-galactosidase activity, yeast reporter strains were grown in YPD to saturation (overnight at 30ºC), then diluted 5 times with fresh YPD medium and grown in the same conditions for 6 additional hours. A 500 µl aliquot of this cell culture was transferred to an eppendorf tube and centrifuged for 3 min at 1000 x *g*. The supernatant was discarded and the cell pellet was resuspended in 500 µl of Z buffer (60mM Na_2HPO_4, 30mM NaH_2PO_4, 10mM KCl, 1mM $MgSO_4$) (pH 7.0). Tubes were centrifuged, the supernatant discarded, and the cell pellet resuspended in 500 µl of Z buffer. Cells were lysed by performing four freeze/thaw cycles (liquid nitrogen/30ºC water bath) and 100 µl of the lysate were transferred to a 96-deep well plate. The β-galactosidase reaction was started by adding 170 µl of ONPG substrate solution (170 µl Z buffer, 68.8 nl of 2-mercaptoethanol and 28 µg of 2-Nitrophenyl-β-D-galactopyranoside [Sigma]) to each

well. Plates were incubated at 30 ºC between 0.5-24 hours until color development. The enzymatic reaction was stopped by adding 80 µl 1 M Na_2CO_3 per well and cleared by centrifugation for 8 min at 1000 x *g*. OD_{420} was measured in 100 µl of the supernatant using 96-well plates.

All enzymatic activities were normalized to the cultures' OD_{600} and the β-galactosidase activities further normalized by the reaction time. Luminescence and absorbance measurements were performed at room temperature using a Synergy 2 (96-well) or a SynergyH1 (384-well) multi-mode microplate readers (BioTek) equipped with an injector device.

To determine the dynamic range for the quantification of β-galactosidase and gLUC59 activities we used YM4271 cells carrying the *ADH1::lacZ* and *ADH1::gLUC59* reporter constructs. These strains were grown in YPD overnight at 30 ºC, then diluted 5 times with fresh YPD medium and grown in the same conditions for 6 additional hours. After this incubation, OD_{600} was determined, cells were harvested by centrifugation and resuspended to a calculated OD_{600}=5 in YPD. Serial dilutions of this cell suspension were generated using wild-type YM4271 cells grown and treated equally. Aliquots of each dilution (100 µl) were used to determine the β-galactosidase or gLUC (using the lab-made coelenterazine native "B" substrate) activities in a 96-well format as described above. A representative image of gLUC emitted light for each dilution was obtained using a VIM photon counting camera (Hamamatsu Photonics). The linear range of the calibration curve was addressed by means of the Lack-of-Fit test and R^2, using GraphPad Prism version 6.00 (GraphPad Software, www.graphpad.com). Only datapoints statistically

different than background levels were considered (multiple comparisons using one way ANOVA).

Yeast one-hybrid assays

pDEST22-TCP plasmids and the pEXP-AD empty vector control (Life Technologies) were transformed directly into the reporter strains (haploid cell experiments) or into the YU yeast strain [8] (diploid cell experiments) in a 96-well format as described previously [29]. Transformants were selected in SD medium without tryptophan (SD-W).

For experiments using haploid cells, transformed YM4271 strains were resuspended in 70 µl of sterile water (keeping the 96-well format) and 3 µl of this cell suspension were used to inoculate 96-well deep plates containing liquid SD-W medium (100 µl/well). Plates were incubated at 30ºC for 24-36 hours with agitation. Then, 400 µl of YPD were added to each well and incubation continued for 6 additional hours. A 100 µl aliquot of this short-term culture was used to determine the OD_{600}. A second 300 µl aliquot of the short-term culture was transferred to a new deep well plate and centrifuged for 3 min at 1000 x *g*. The supernatant was discarded and the cell pellet was resuspended in 150 µl of Z buffer. Plates were centrifuged for 3 min at 1000 x *g* and the cell pellet was resuspended in 25 µl of Z buffer. Cells were lysed by performing four freeze/thaw cycles (liquid nitrogen/30ºC water bath), and the β-galactosidase reaction was performed as indicated above. The β-galactosidase activity was calculated as [OD_{420} x 1000]/[OD_{600} x time (min) x culture volume (ml)].

For the experiments using diploid cells, YU-TF effector strains (MATα) were mated with YM4271-reporter strains (MATa) as reported previously [8,16]. Briefly, effector strains were resuspended in 70 µl of sterile water (keeping the 96-well format) and 5 µl of this cell suspension were used to inoculate medium lacking tryptophan (600 µl/well). Plates were grown for 24-36 hours at 30ºC with agitation using microplate shakers (700 rpm). Simultaneously, promoter strains were grown in 250 ml flasks containing 50 ml of YPD. After incubation, 10 µl of each culture (promoter and TF strains) were transferred into a new 96-well plate containing 90 µl of YPD per well. Plates were incubated at 30ºC for 24-36 hours without agitation. After mating, cells were washed using SD medium without tryptophan and uracil (SD-WU) (selection medium for diploid yeast cells) and resuspended in 180 µl of SD-WU. A 3 µl aliquot of this cell suspension was transferred to a new 96-deep well plate containing 100 µl of SD-WU and incubated at 30ºC for 24-36 hours with agitation. Then, 400 µl of YPD were added to each well and incubation continued for 6 additional hours. Finally, growth (OD_{600}) and β-galactosidase activity (OD_{420}) were determined as described above for haploid cells.

For gLUC assays in haploid and diploid cells, we followed the same steps described above to determine the OD_{600} of each well. A second 100 µl aliquot of the short-term culture was transferred to a 96-well white plate. Flash and glow luminescence were determined after the addition of 100 µl of the lab-made coelenterazine native “B” substrate (1xPBS pH 7.4, 5mM NaCl, 20 µM native coelenterazine [Biosynth]). The gLUC activity was calculated as Lum/OD_{600}.

β-galactosidase and gLUC activities were then normalized to the average value obtained for control wells (pEXP-AD). Binding cut-off was set at 2-fold over the mean of the control value.

Sequence analyses

Protein sequence alignment and phylogeny trees were generated using the Geneious software version 6.0.6 (http://www.geneious.com) [30].

Results

gLUC59 outperforms other luciferase reporters in *S. cerevisiae*

The activity of most luciferase enzymes can be quantitatively measured over a wide range of concentrations at room temperature. Furthermore, yeast cells are permeable to some luciferase substrates (e.g. coelenterazine) and luciferase enzymes can be expressed in the extracellular compartment (e.g. linked to the cell surface [27]), suggesting that luciferase quantification assays in yeast could be performed without a cell lysis step. Considering that HT-Y1H screen optimization would require a reporter assay with a long linear range, performed at room temperature and amenable for robotic automation, we envisioned that a luciferase reporter could be used to improve the assay. To determine the type of luciferase enzyme and expression format that would provide the best Y1H reporter for high-throughput screens, we generated reporter vectors for either cytosolic or surface expression of the *Photinus pyralis* (firefly) (LUC+), *Renilla reniformis* (RLUC) or *Gaussia princeps* (gLUC) luciferase reporter genes (Figure 4.1). Yeast surface expression was achieved by using a translational fusion between each luciferase reporter

and the GPI-linked cell wall protein (PGA59) of *Candida albicans* [27]. Two versions of each reporter vector were generated to allow the insertion of bait promoter sequences via restriction endonuclease digestion or recombination-based cloning (Figure 4.1). To evaluate the performance of these luciferase reporters, the constitutive *Alcohol Dehydrogenase I* (*ADH1*) gene promoter of *Saccharomyces cerevisiae* was cloned into the cytosolic or surface LUC+, RLUC and gLUC reporter vectors (Figure 4.1).

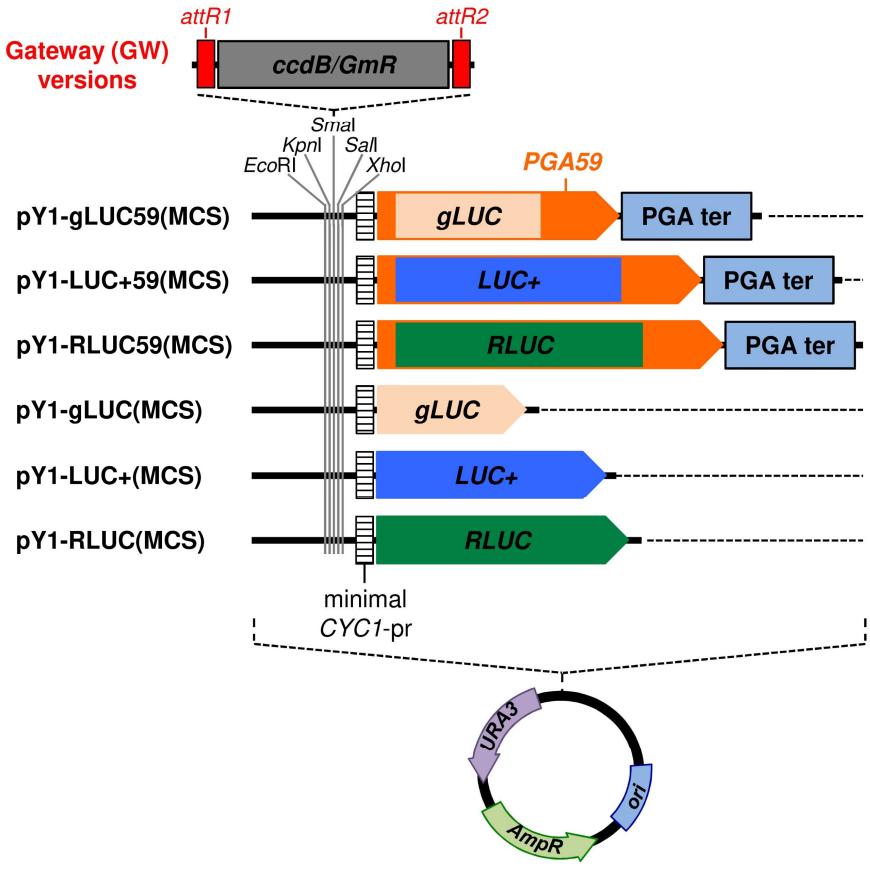

Figure 4.1. Schematic representation of yeast integration vectors for cytosolic and surface-displayed luciferase reporters.
All reporter constructs were built using the pLacZi vector backbone and replacing the *lacZ* gene by each luciferase reporter gene. Surface display vectors also include the *PGA59* gene terminator of *C. albicans* (see materials and methods). For each construct restriction endonuclease-based cloning (MCS) and gateway-based cloning (GW) versions were generated.

These constructs were integrated into the chromosome of YM4271 yeast cells and the luciferase activity of each resulting strain was quantified in 96-well plates using a suite of commercially available and lab-made luciferase assays (Figure 4.2). Both flash and glow luminescence, respectively emitted immediately or between 2-60 minutes after addition of the substrate, were quantified directly from a yeast cell culture aliquot. Results of this experiment indicated that the LUC+ reporter activity was higher in glow than flash bioluminescence assays but exhibited a similar performance when expressed either in the cytosol or the cell surface (Figure 4.2A-B). RLUC activity was also greater in glow than flash bioluminescence assays, however glow light emission was significantly higher when the enzyme was expressed in the cytosol (Figure 4.2A-B). Conversely, the gLUC activity was significantly higher in flash than glow bioluminescence assays, especially when the reporter was expressed in the cell surface (Figure 4.2A-B). Comparing the performance of all reporters, our results indicated that while their activity was similar in glow bioluminescence assays, the activity of cell surface expressed gLUC (gLUC59) was significantly better than the other reporters when flash luminescence was measured. It is important to note that parallel experiments, performed with wild-type YM4271 cells, indicated that these cells did not display an intrinsic bioluminescence activity with any of the enzymatic assays used (Figure 4.2). Since quantification of the luciferase activity was evaluated directly in a cell culture aliquot, we reasoned that growth medium components could affect the activity of some luciferase reporters, especially those expressed at the cell surface. To evaluate this hypothesis, we repeated all luminescence measurements using PBS-washed cells. Interestingly, the luciferase activity for all the reporters tested was significantly lower after the washing step (Figure 4.2C-D), indicating that the

luciferase signal displays higher intensity and better signal to background ratio when measured directly in a yeast cell culture aliquot. Taken together, our initial results indicated that gLUC59 would be a reporter of choice for gene-centered Y1H screens. To determine its performance in a higher throughput format, we ran the gLUC59 assay in 384-well plates measuring both flash and glow luminescence. Importantly, we observed similar luminescence values as those obtained using 96-well plates (Supplemental Figure 4.2), indicating that the gLUC59 reporter was indeed a suitable alternative for automated gene-centered HT-Y1H screens.

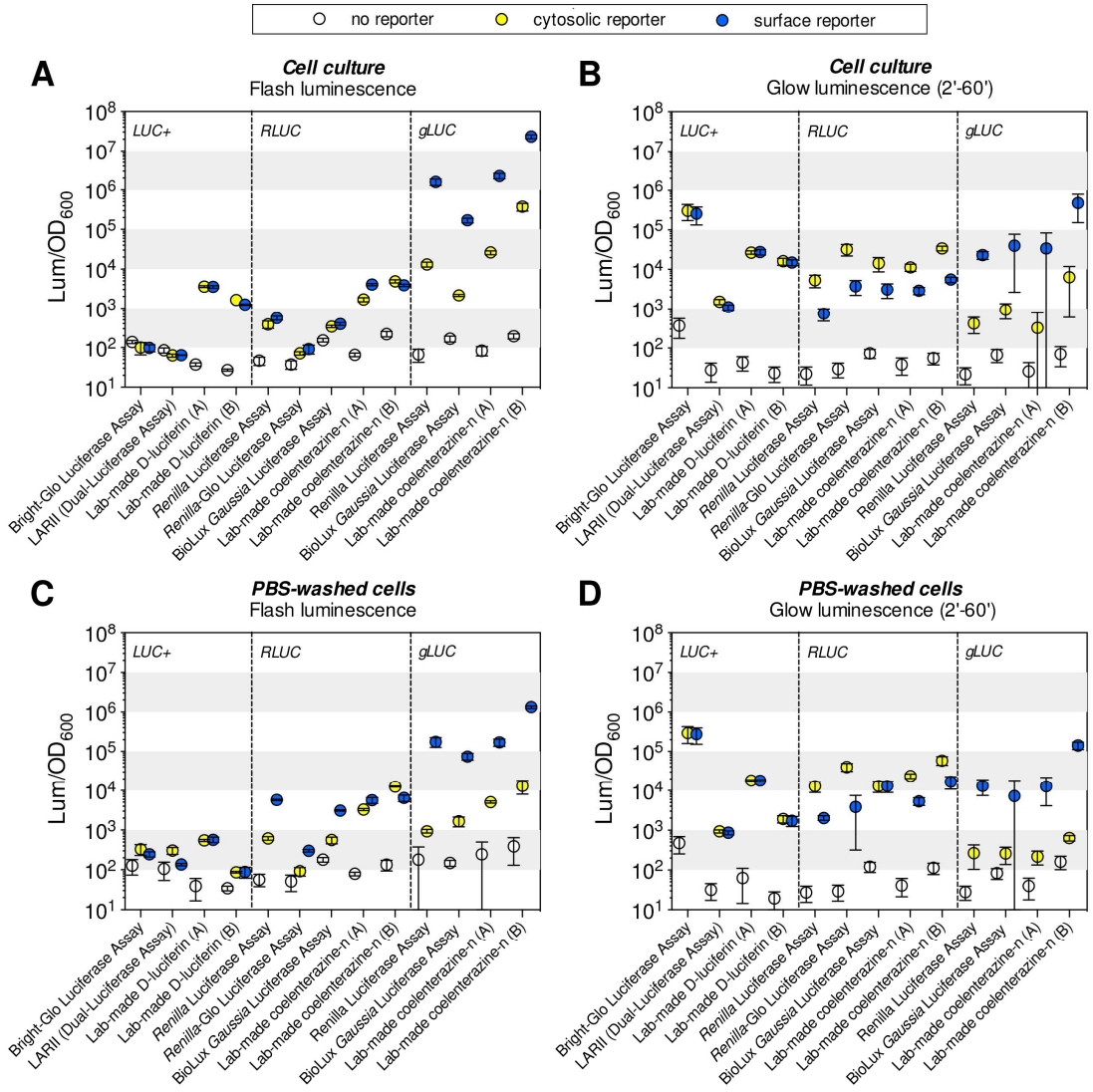

Figure 4.2 Luciferase activity for cytosolic and surface-displayed reporters expressed in *S. cerevisiae* cells.

Luciferase activity from YM4271 strains carrying a chromosomally integrated *ADH1::luciferase* (*LUC+, RLUC and gLUC* as indicated in each panel) reporter construct for either cytosolic (yellow symbols) or cell surface expression (blue symbols). Alternative substrate assay solutions indicated on the x-axis of each graph were tested (see materials and methods). Wild-type YM4271 strains were used as controls (white symbols). (A) Flash luminescence determined directly in a cell culture aliquot immediately after substrate addition (n=3). (B) Glow luminescence determined directly in a cell culture aliquot between 2 and 60 minutes (2'-60') after substrate addition (n=30). (C) Flash luminescence determined using PBS washed cells immediately after substrate addition (n=3). (D) Glow luminescence determined using PBS washed cells between 2 and 60 minutes (2'-60') after substrate addition (n=30). Results were normalized to their respective cell density (OD_{600}) and represent average values ± SD (n=3 independent experiments).

gLUC59 reporter activity correlates with promoter function in intact *S. cerevisiae* cells

To further explore the feasibility of using cell surface expressed gLUC for HT-Y1H screens, we evaluated the linear range of gLUC59 bioluminescence measurements using increasing concentrations of an *ADH1::gLUC59* yeast cell culture. Results of this experiment indicated that the gLUC59 activity linear range extended to four and three orders of magnitude, for flash and glow luminescence measurements respectively (Figure 4.3A-B and Supplemental Figure 4.3A). This represented a significant improvement compared to the quantification range observed for the fixed-time β-galactosidase assay (1-1.5 orders of magnitude) (Supplemental Figure 4.1), suggesting that the *gLUC59* reporter activity could be uniformly and accurately quantified in samples with different reaction kinetics. Having established that luminescence measurements were well correlated with gLUC59 concentrations (provided by different concentrations of *ADH1::gLUC59* cells), we next analyzed the ability of the cell surface reporter to detect different expression levels at constant cell concentrations, the latter being the most likely scenario encountered in Y1H screens. To do this, an additional yeast reporter strain carrying a weaker truncated *ADH1* promoter (*ADH1*Δ) was generated [31]. Reporter cells carrying either the full-length or truncated *ADH1* promoters were grown to the same density and the gLUC59 activity was quantified. Luminescence was about 3-4 times higher in reporter cells carrying the full-length *ADH1* promoter for both flash and glow measurements (Figure 4.3C and Supplemental Figure 4.3B). To test a conditional promoter, we generated a yeast strain carrying the methionine repressed *MET25* promoter [32] driving the expression of the *gLUC59* reporter. In agreement with the results

using the constitutive *ADH1* and *ADH1*Δ promoters, *MET25::gLUC59* cells grown in methionine-depleted medium exhibited higher gLUC59 activity compared to cells grown in methionine-containing medium using both flash and glow luminescence measurements (Figure 4.3D and Supplemental Figure 4.3C). These experiments indicated that the differential expression of *gLUC59* translated into quantitative differences of the emitted bioluminescence. As noted previously, while the fixed-time β-galactosidase assay used in HT-Y1H screens has a limited quantitative capability, a time-optimized assay for each individual sample provides an accurate quantification of the β-galactosidase activity [24]. Since our goal was to implement a reporter system with quantitative capabilities similar to the best performing time-optimized β-galactosidase assay, we decided to use this method as a reference. Therefore, we generated YM4271 strains carrying the *ADH1::lacZ, ADH1*Δ*::lacZ* and *MET25::lacZ* reporter constructs and used them to perform the same experiments described above. Quantification of the β-galactosidase activity using the time-optimized assay (Figure 4.3E-F) showed similar results to those obtained using gLUC59 (Figure 4.3C-D). Importantly, these experiments revealed that the gLUC59 assay measuring luminescence emission for only 1-second displayed similar results as the ONPG-based β-galactosidase assay using an optimal incubation time for each sample.

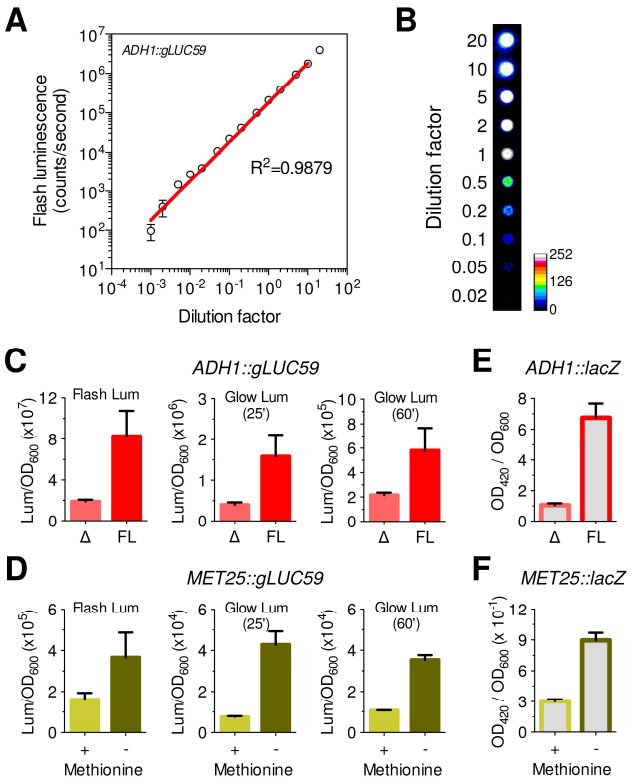

Figure 4.3. Quantitative performance of the gLUC59 reporter in *S. cerevisiae* cells.
(A) Analysis of the linearity for the quantification of gLUC59 activity using increasing *ADH1::gLUC59* reporter cell concentrations. The linear range is indicated by the red line (Lack-of-Fit test, F=0.4047, p=0.9554). Luminescence was measured immediately after addition of the enzyme substrate and the results are average values ± SD (n=5 independent experiments). (B) Representative pseudo-colored image of the dilution series used in C). (C-F) Evaluation of the quantitative capacity of the cell surface *gLUC* reporter system (C & D) in comparison to the *lacZ* reporter system (E & F) using two *ADH1* promoters of different strength (FL= full-length *ADH1* promoter and Δ= truncated *ADH1* promoter) (C & E), or the methionine repressed promoter *MET25* (+ and - indicates the presence or absence of methionine in the culture medium) (D & F). Results were normalized to their respective cell density (OD_{600}) and represent the average values ± SD (n=3 independent experiments).

Given that the gLUC59 reporter had several advantages for HT-Y1H screens when compared to the commonly used *lacZ* reporter, we reasoned that an improved assay for quantitative HT-Y1H screens could be established using either gLUC59 flash or glow luminescence assays. However, quantifying glow luminescence in a large throughput format (i.e. 384-well plates) would require a stable light emission over time as it takes

several minutes for a luminometer to process one microplate. Since in most luciferase assays the luminescence rapidly decays after addition of the enzyme substrate, we evaluated the kinetics of light emission at different gLUC59 concentrations using *ADH1::gLUC59* yeast cells. Our results confirmed a luminescence decrease over time following a two-step exponential decay kinetic for all the gLUC59 concentrations tested. After substrate addition the luminescence first decayed rapidly (half-life ~30 sec) for about 2 minutes and then slowly (half-life ~2 min) for the next 10 minutes, and finally reached plateau levels that were maintained for the following 48 minutes (Figure 4.4A). These results indicated that glow luminescence in gLUC59-based HT-Y1H screens should be measured after the slow decay phase to get comparable quantitative results across multiple wells and plates.

gLUC59 provides an improved reporter system for Y1H screens

We previously established a HT-Y1H screening protocol using a genome-wide clone collection encompassing most *Arabidopsis* TFs [8]. Following this protocol, we set a pilot Y1H experiment using the gLUC59 reporter to investigate the ability of *Arabidopsis* class-I TCP TFs (Supplemental Figure 4.4) to interact with the promoter of the clock gene *CIRCADIAN CLOCK ASSOCIATED1* (*CCA1*). A pioneering gene-centered Y1H screen previously uncovered a class-I TCP (TCP21) named CHE (CCA1 HIKING EXPEDITION), which binds to the *CCA1* promoter region and negatively regulates the *CCA1* promoter activity [14]. Through this regulation, CHE modulates the proper period of clock-controlled rhythms [14]. CHE shares high homology at the DNA binding domain with the other twelve *Arabidopsis* class-I TCPs suggesting that at least some members of the subfamily could

also bind to the *CCA1* promoter [14] (Supplemental Figure 4.4). To evaluate the performance of the luciferase-based assay parallel Y1H experiments were performed using the *lacZ* reporter. Yeast reporter strains carrying a *CCA1* promoter region (-363/-192) that contains a canonical class-I TCP binding site (TBS-I) (GGNCCCAC) were generated. These strains were independently transformed with prey plasmids that drive the constitutive expression of each class-I TCP fused to the Gal4 transcriptional activation domain [8]. Quantification of the gLUC59 or β-galactosidase activity in the transformed yeast reporter cells revealed that in addition to CHE, ten class-I TCPs (TCP7, 8, 9, 14, 15, 16, 19, 20, 22 and 23) were able to interact with the *CCA1* promoter (Supplemental Figure 4.4C). TCP6 and TCP11, did not show interaction with the -363/-192 *CCA1* promoter fragment suggesting that either they were not properly expressed in yeast or that they did not bind to the TBS-I in the promoter bait. In support to the latter, a sequence analysis indicated that indeed the DNA binding domains for both TCP6 and TCP11 are less conserved compared to most other class-I TCPs (Figure 4.4B). To confirm that, as for CHE, the TBS-I mediated the interactions detected for TCP7, 8, 9, 14, 15, 16, 19, 20, 22 and 23, we performed Y1H assays using *gLUC59* and *lacZ* reporter strains carrying a mutated TBS-I (GGTCCCAC to TTGAAACA) within the -363/-192 *CCA1* promoter region [14]. These assays revealed a significant reduction in the reporter activity for TCP7, 8, 9, 14, 15, 19, 20, 21, 22 and 23 transformed cells, indicating that these TFs interacted with the *CCA1* promoter through the TBS-I (Figure 4.4D). TCP16 was the exception showing a reduced but still significant induction of the reporter activity suggesting unique DNA binding abilities for TCP16 among class-I TCPs. Notably, we found a close correlation between the results obtained with the *gLUC59*-based Y1H system, using both flash or

glow bioluminescence measurements, and the *lacZ*-based Y1H system, using the reference time-optimized ONPG-based β-galactosidase assay (Figure 4.4E). This further confirmed our initial observations regarding the quantitative capabilities of the gLUC59 assay and indicated that the gLUC59 reporter outperforms the *lacZ* reporter in gene-centered HT-Y1H screens.

While yeast transformation provides an effective mean to deliver TF prey constructs into reporter cells in a low throughput format, yeast mating provides a more convenient alternative when performing HT-Y1H screens using large TF collections (e.g. 1956 *Arabidopsis* TFs) and multiple yeast reporter strains. For mating-based Y1H screens, TF constructs are first transformed into a MATα yeast strain, then these cells are mated with the Y1H reporter strains (MATa), and finally diploid TF-reporter cells are selected and the reporter activity is quantified [8]. To evaluate if the gLUC59 reporter could be used in a mating-based approach, we transformed class-I TCP constructs into YU yeast cells [8] and mated these cells with the reporter strains carrying the wild-type or TBS-I mutated versions of the -363/-192 *CCA1* promoter region. Quantification of the gLUC59 or β-galactosidase activities in the resulting diploid cells provided similar results, although with lower overall reporter activities (Figure 4.4F-H), as the ones obtained when TF constructs were directly transformed into the reporter cells (Figure 4.4C, D, E and Supplemental Table 4.2). These results further confirmed that the gLUC59 reporter could be effectively used for mating-based HT-Y1H screens.

Figure 4.4. gLUC59-based yeast one-hybrid system.
(A) Bioluminescence kinetics decay after substrate addition at increasing concentrations of YM4271 cells carrying the *ADH1::gLUC59* reporter construct. Results were normalized to their respective cell density (OD_{600}) and represent average values ± SD (n=8 independent experiments). (B) Heat map indicating the number of amino acid differences between the DNA binding domains of class-I TCPs. Rows and columns were sorted based on decreasing sequence identity scores. (C and F) gLUC59- and β-galactosidase-based Y1H screens to evaluate the binding of class-I TCP TFs to the -363/-192 *CCA1* promoter region. Experiments were performed in haploid reporter strains transformed with the effector constructs for each class-I TCP (C) or diploid cells after mating the reporter strain (MATa) with YU cells (MATα) carrying effector constructs for each class-I TCP (F). Results were normalized to the reporter activity obtained with an empty effector construct. Luminescence measurements were performed at 0 (flash) or 25 and 60 minutes (glow) after addition of the gLUC substrate. Each symbol represents the average fold of induction ± SD (n=6 independent experiments). (D and G) gLUC59- and β-galactosidase-based Y1H screens to evaluate the binding of class-I TCPs to the -363/-192 *CCA1* promoter region carrying a mutated class-I TCP binding site (TBS-I mut). Experiment and results were performed as indicated for (C) and (F). (E and H) Comparison of the gLUC59- and β-galactosidase-based Y1H screening results for the experiments shown in (C) and (D) (R^2[flash]=0.9276, R^2[glow-25']=0.9177, and R^2[glow-60']=0.9235), and in (F) and (G) (R^2[flash]= 0.9232, R^2[glow-25']= 0.9327, and R^2[glow-60']= 0.9346).

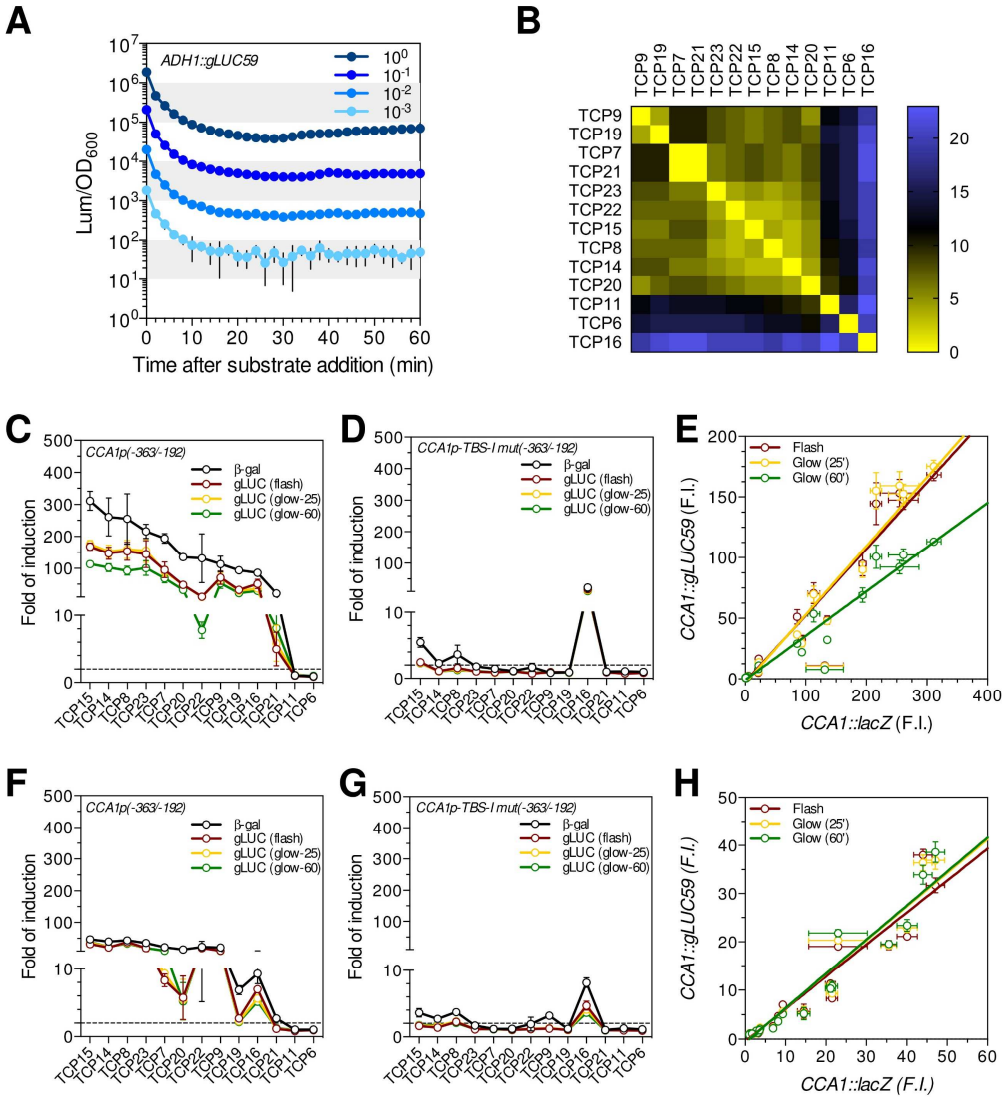
A
ADH1::gLUC59
10^0
10^-1
10^-2
10^-3
Lum/OD600
Time after substrate addition (min)
B
TCP9
TCP19
TCP7
TCP21
TCP23
TCP22
TCP15
TCP8
TCP14
TCP20
TCP11
TCP6
TCP16
C
CCA1p(-363/-192)
β-gal
gLUC (flash)
gLUC (glow-25)
gLUC (glow-60)
Fold of induction
D
CCA1p-TBS-I mut(-363/-192)
E
Flash
Glow (25')
Glow (60')
CCA1::gLUC59 (F.I.)
CCA1::lacZ (F.I.)
F
G
H

Discussion

Gene-centered Y1H screens provide a straightforward, comprehensive and unbiased strategy to unveil the TF-interaction landscape of a single promoter region. By design, the Y1H system is not suited to accurately reveal the strength of TF-DNA interactions and essentially delivers positive or negative results based on the expression level of a reporter gene. Thus, establishing a reliable cut-off value for the reporter activity and confidently determining which are the TF-promoter interactions that result in reporter activities above or below this limit are critical for the interpretation of Y1H screen results. This is especially important for promoter baits that drive high expression of the reporter gene in the absence of effector constructs as high background reporter levels often confound the identification of positive interactions [8]. The improved quantitative capability of the gLUC59 reporter presented here provides a strengthened ability to establish cut-off values and to discern between positive and negative interactions with higher confidence. In addition, the larger linear range of gLUC59 activity quantification allows proper ranking of positive interactions, which (as suggested by our previous work [8]) provides a useful criterion to prioritize TF candidates and guide follow-up studies.

Assays to quantify the commonly used β-galactosidase reporter activity in a high-throughput format exhibit a short linear range and rapidly reach saturation. In addition, the procedures have several technical limitations, such as long and variable incubation times for color development, time-consuming freeze-thaw steps to lyse yeast cells, temperature distribution bias across microplates, or well-to-well color signal diffusion. Here, we describe the characterization of a novel reporter system that improves the quantitative capabilities of gene-centered HT-Y1H screens and that additionally provides

a simplified assay suitable for full automation. We evaluated six different luciferase reporters, including three novel cell surface expressed reporters, and determined that gLUC59 is the most versatile as it displays the best performance for both flash and glow bioluminescence measurements. The gLUC59 assay additionally provides a cost-effective option as the highest luminescence intensities were obtained using a lab-made substrate solution. We also found that, unlike the β-galactosidase activity, the gLUC59 activity can be quantified directly in a yeast cell culture aliquot without additional washing or cell lysis steps. Furthermore, the assay is performed at room temperature and requires minimal incubation time after addition of the enzyme substrate. More importantly, in these conditions the gLUC59 quantification assay displays a linear range that extends for up to 4 orders of magnitude and thus is significantly larger than the one obtained with a fixed-time β-galactosidase assay [16]. This improved quantification capability allows, using a luminescence integration time of only 1 second per well, an accurate quantification of the reporter activity that is comparable to using a β-galactosidase assay where the reaction time is optimized to fit the specific reaction kinetics in each well. Thus, the gLUC59 reporter enables a uniform Y1H screen procedure for the simultaneous quantification of multiple reactions with different enzymatic activities. Furthermore, the increased simplicity of the gLUC59 assay reduces the processing time and enables fully automated gene-centered Y1H screens including experimental procedure and data analyses (Supplemental Figure 4.5 and Supplemental Table 4.3). It should be noted that gLUC59 reporter strains are fully compatible with histidine auxotrophic selection, which could be used in combination with the cell-surface luciferase to call positive interactions [33].

Furthermore, we showed that the gLUC59 reporter could be used for mating-based Y1H assays although with a lower sensitivity compared to experiments where effector plasmids are directly transformed into the reporter strain. This observation is in line with previous reports that compared transformation- and mating-based Y1H screens [34] and suggests that the different sensitivity of the assay in haploid and diploid cells is not dependent on the reporter used but rather an inherent property of diploid cells that affects the overall expression of reporter genes. A transformation-based screen might be considered if a higher sensitivity is needed. In fact, our experiments indicate that the interaction of TCP21/CHE with the *CCA1* promoter is clearly revealed when haploid cells were used, which is consistent with TCP21/CHE being initially discovered in a small-scale gene-centered Y1H screen using haploid cells [14]. However, transformation of a genome-wide clone collection (e.g. ~2000 *Arabidopsis* TF clones) into reporter strains is time-consuming and thus a mating-based approach would be of choice for gene-centered HT-Y1H screens. Given the increased quantitative power of the gLUC59 assay we anticipate that by analyzing HT-Y1H screen results, where thousands of interactions are evaluated simultaneously, it will be possible to establish more accurate baseline and cut-off values, thereby improving our ability to define positive interactions and ultimately the sensitivity of mating-based Y1H screens. In support to this notion the Y1H experiment using diploid cells also revealed the TCP21/CHE-*CCA1* promoter interaction as indicated by the higher gLUC59 reporter activity compared to the background control (Supplemental Table 4.2).

Results of pilot experiments using the gLUC59-based Y1H assay confirmed its improved performance. In particular, these experiments indicate that TCP7, 8, 9, 14, 15,

16, 19, 20, 22 and 23 interact with the *CCA1* promoter suggesting that several class-I TCPs regulate the *Arabidopsis* clock function through *CCA1*. These results are in part validated by a recent report showing that TCP20 and TCP22 bind to the *CCA1* promoter and regulate *CCA1* expression *in planta*, and that *tcp20/22* loss-of function shortens the period of clock-controlled rhythms [35]. We found that two class-I TCPs, TCP6 and TCP11, do not interact with the -363/-192 *CCA1* promoter region. In support to this finding, an amino acid sequence comparison of all class-I TCPs indicates that the DNA binding domain of TCP6 and TCP11 is significantly different compared to the other subfamily members (Figure 4.4B and Supplemental Figure 4.4). Furthermore, it was recently reported that TCP11 shows a different DNA-binding specificity, with preference for the GTGGGCCNNN sequence, due to a threonine residue at position 15 of the TCP domain [36] (Supplemental Figure 4.4C). The binding of TCP7, 8, 9, 14, 15, 19, 20, 22 and 23 was mediated by the TBS-I in the *CCA1* promoter (Figure 4.4 D and G). However, this was not the case for TCP16 suggesting that this TF binds to the mutated TBS or to another element within the -363/-192 region of the *CCA1* promoter. In support to the latter, it is important to note that TCP16 is phylogenetically distant from all other class-I TCPs, has a DNA binding domain significantly different to most of them (~50% identity) (Figure 4.4 B and Supplemental Figure 4.4), and was shown to preferentially interact with the consensus binding site for class-II TCP proteins (GTGGNCCCNN) [37]. Taken together, our results indicate that most class-I TCPs bind to the *CCA1* promoter and thus likely regulate the clock function, and that TCP16 function is possibly associated to responses of both TCP classes. Given that class-I TCPs regulate plant responses to several signals such as light, and biotic and abiotic stress [38], our findings suggest that these TFs

represent a regulatory hub that controls the *Arabidopsis* clock function by multiple environmental cues.

Here, we established a novel luciferase-based Y1H system that is faster, simpler and more powerful than the current methods used for gene-centered screens (Supplemental Figure 4.5 and Supplemental Table 4.3). Importantly, the enhanced quantitative capabilities of the gLUC59 reporter assay improves the detection of positive interactions and allows a uniform procedure and data analysis regardless of each promoter bait background activity. In addition, gLUC59-based Y1H screens have minimal pre-assay requirements, and demand less and shorter steps that are fully compatible with automation. Notably, these improvements did not create any concomitant disadvantage when compared to existing methods (Supplemental Table 4.3). Furthermore, the gLUC59 reporter could further contribute to develop future approaches that may require the isolation of yeast cells carrying positive interactions (i.e. Y1H coupled to next generation sequencing technologies) [33], as yeast expressing the cell-surface reporter could be immuno-labeled and purified by cell sorting or other cell isolation methods. Given the success of gene-centered Y1H screens to unveil TF-promoter interactions and the continuous development of genome-wide TF clone collections, we anticipate that the upgraded approach presented here will be widely adopted and further contribute to the longstanding efforts towards disentangling the intricate mechanisms that regulate gene expression across species.

ACCESSION NUMBERS

Sequences for the pY1-gLUC59(MCS) and pY1-gLUC59(GW) plasmids are available on GenBank under accession numbers KY581738 and KY581739 respectively.

FUNDING

This work was supported by the National Institutes of Health [R01GM056006 to J.L.P-P (co-investigator)], the National Science foundation [1158254 to J.L.P-P. (co-investigator)] and the Hellman Foundation [to J.L.P-P].

CONFLICT OF INTEREST

The authors declare no competing conflicts of interest.

Supplementary Information

Supplementary figures

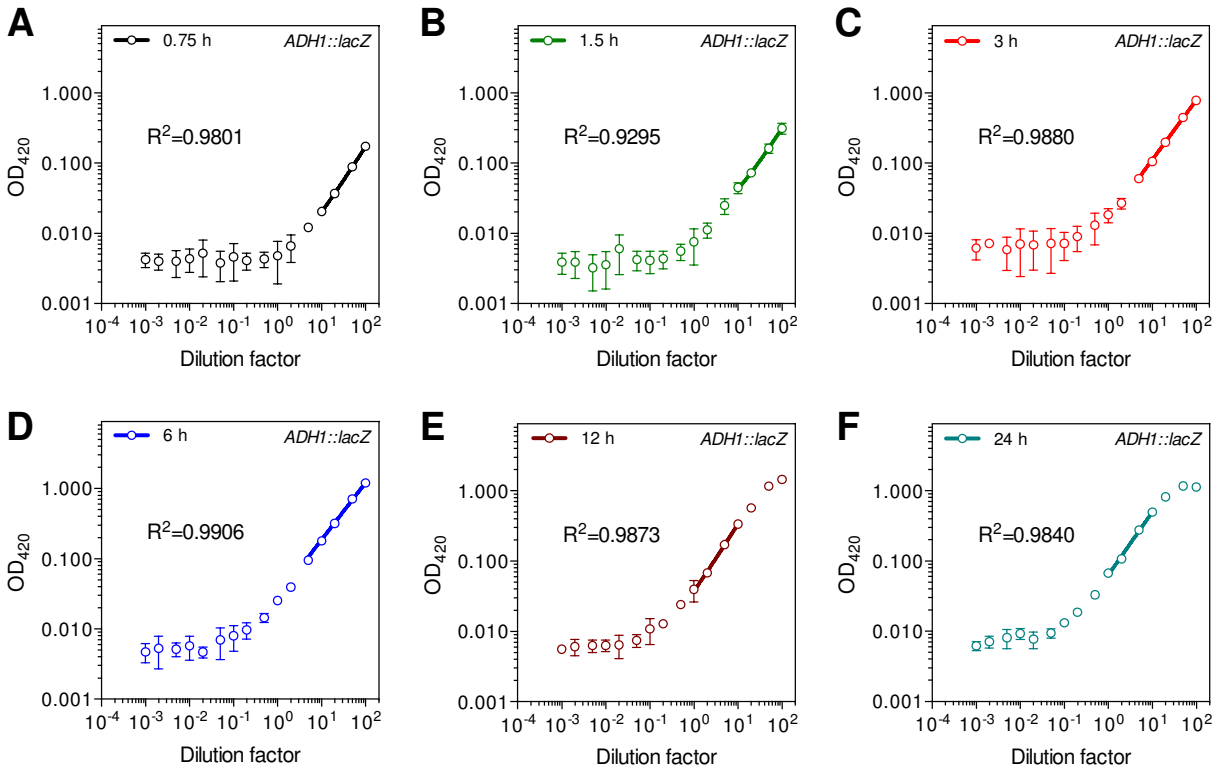

Supplemental Figure 4.1 Analysis of the linear range for the quantification of β-galactosidase activity in a high-throughput format.
The β-galactosidase activity determined in a dilution series of increasing *ADH1::lacZ* reporter cell concentrations. Enzyme reaction product was determined at alternative end-points using the OD_{420nm} (A-F) in 96-well plates. For each incubation time, the linear range for all datapoints statistically different than background levels (multiple comparisons using one way ANOVA) is indicated by the solid line. Each point represents average values ± SD (n=9 independent experiments).

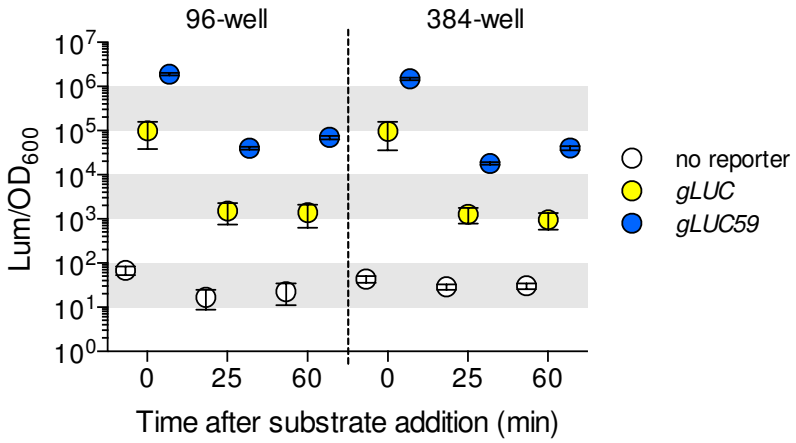

Supplemental Figure 4.2. Luciferase activity for cytosolic and surface-displayed gLUC reporters measured in 96- and 384-well plates.
Flash (0') and glow (25' & 60') gLUC activity obtained from YM4271 strains carrying a genome integrated *ADH1::gLUC* (cytosolic) (yellow symbols) or *ADH1::gLUC59* (cell surface) (blue symbols) reporter constructs. Wild-type YM4271 cells were used as controls (white symbols). gLUC activity was determined in 96- and 384-well plates directly in a cell culture aliquot. Results represent average values ± SD (n=8 independent experiments).

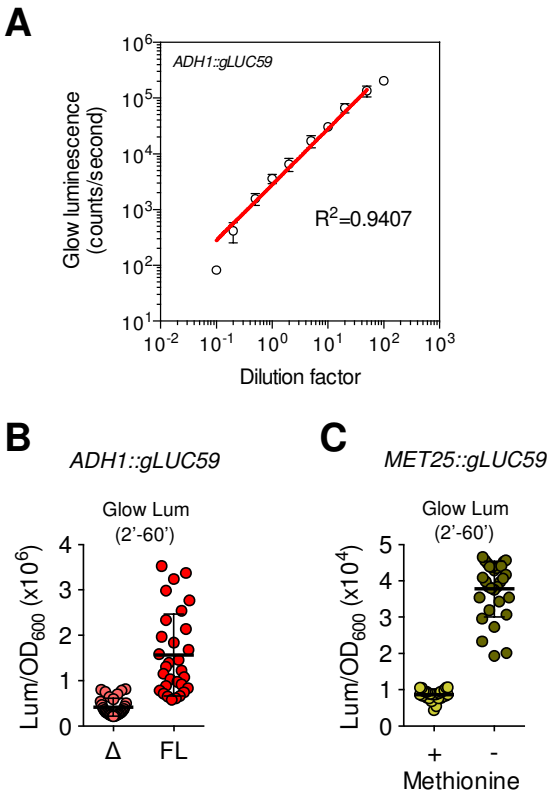

Supplemental Figure 4.3. Evaluation of the quantitative capacity of the *gLUC* reporter system (glow light emission).
(A) Analysis of the linearity for the quantification of gLUC59 activity using increasing *ADH1::gLUC59* reporter cell concentrations. The linear range is indicated by the red line (Lack-of-Fit test, F=0.7876, p=0.6167). Luminescence was meassured 25 minutes after addition of the enzyme substrate and the results are average values ± SD (n=5 independent experiments). (B and C) Individual glow luminescence measured at 2 minute intervals between 2-60 minutes after addition of the gLUC enzyme substrate, from YM4271 cells carrying two *ADH1* promoters of different strength (FL= full-length *ADH1* promoter and Δ= truncated *ADH1* promoter) (B), or the methionine repressed promoter *MET25* (+ and - indicates the presence or absence of methionine in the culture medium) (C). Results were normalized to their respective cell density (OD_{600}). Each symbol represents the average value ± SD at each time and the line represents the overall average value ± SD considering all times (n=3 independent experiments).

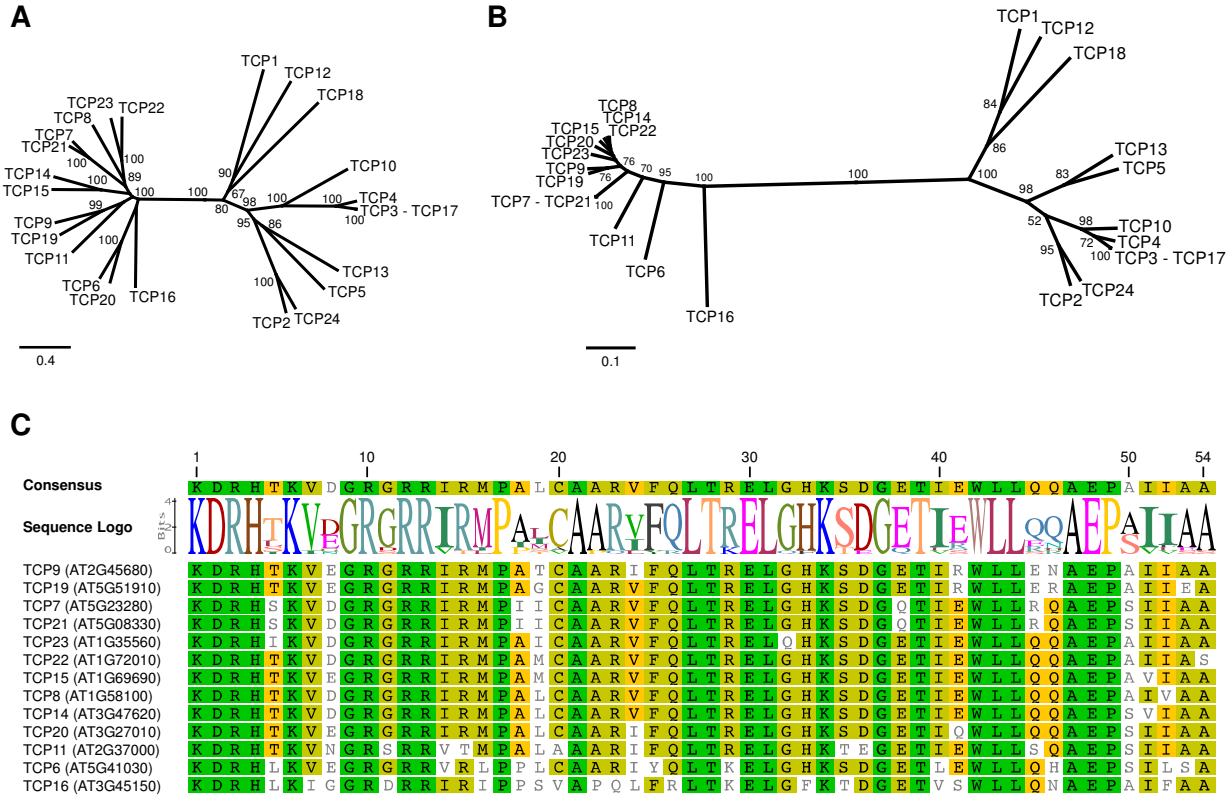

Supplemental Figure 4.4. Amino acid sequence comparisons for *Arabidopsis* TCP transcription factors.

(A and B) Phylogenetic analysis of the full-length protein sequences (A) and the DNA binding domain protein sequences (B) of *Arabidopsis* TCP transcription factors. Analysis was performed with the Geneious software using the UPGMA tree building method. The percentage of replicate trees in which the associated sequences clustered together in the bootstrap test (1000 replicates) are shown next to the branches. (C) Multiple sequence alignment for the predicted DNA binding domain of class-I TCPs. Amino acid sequences were aligned with ClustalW using the Geneious software. For each position, the percentage of identity is indicated by amino acids in green boxes (identical in all sequences), amino acids in brown boxes (identical in at least 80% of the sequences), and amino acids yellow boxes (identical in at least 60% of the sequences). Consensus sequence and sequence logo are indicated above the aligned sequences.

The following AGI numbers correspond to the TCP transcription factors shown in (a) and (b). Class-I: TCP6 (At5g41030), TCP7 (At5g23280), TCP8 (At1g58100), TCP9 (At2g45680), TCP11 (At2g37000), TCP14 (At3g47620), TCP15 (At1g69690), TCP16 (At3g45150), TCP19 (At5g51910), TCP20 (At3g27010), TCP21 (CHE; At5g08330), TCP22 (At1g72010), TCP23 (At1g35560); and class-II: TCP1 (At1g68800), TCP2 (At4g18390), TCP3 (At1g53230), TCP4 (At3g15030), TCP5 (At5g60970), TCP10 (At2g31070), TCP12 (At1g67260), TCP13 (At3g02150), TCP17 (At5g08070), TCP18 (TBL1; At3g18550), TCP24 (At1g30210).

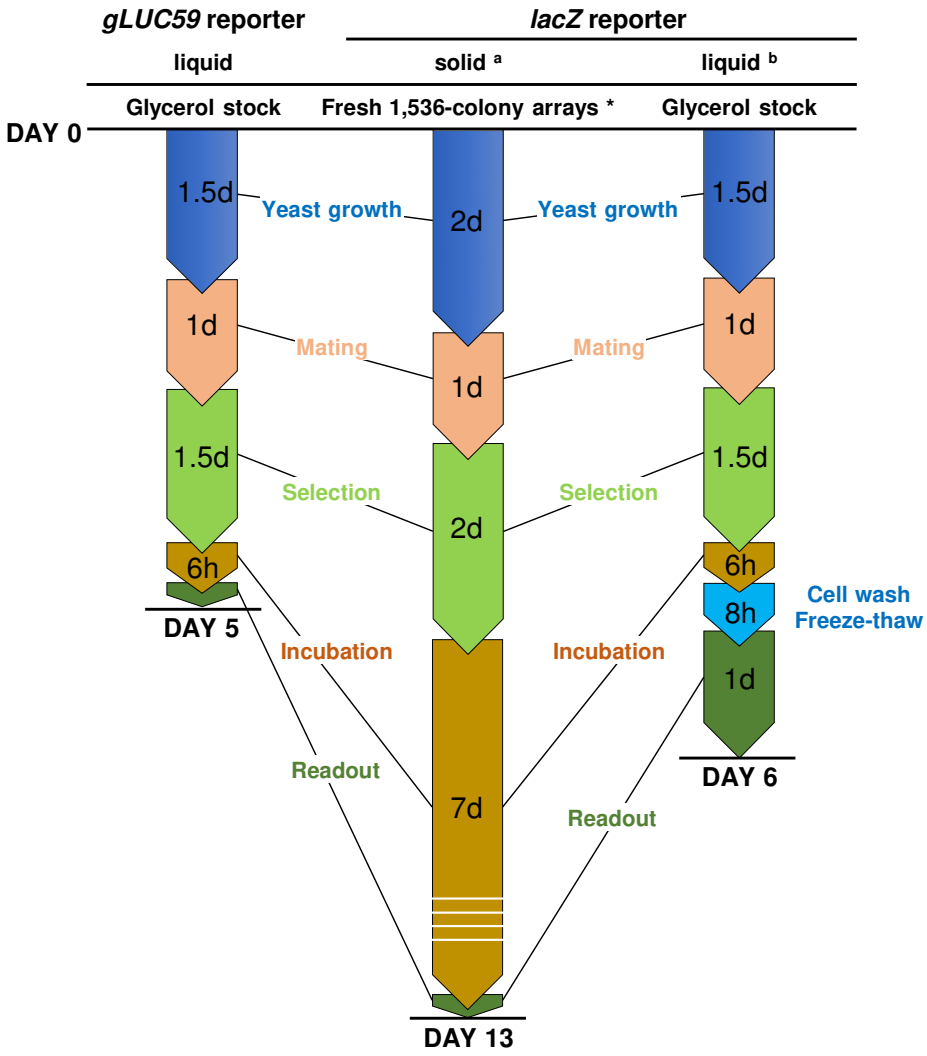

Supplemental Figure 4.5. The gLUC59 reporter enables faster and fully automated HT-Y1H screens.
Timeline and workflow for *gLUC59*-based HT-Y1H screens performed entirely in liquid format compared to *lacZ*-based HT-Y1H screens performed in liquid or solid (agar plates) formats. *additional days required to prepare fresh 1536-colony arrays; [a]Reece-Hoyes et al. (25); [b]Pruneda-Paz et al. (8).

Supplementary tables

Supplemental Table 4.1 PCR primers used in this study

Plasmid	Primer name	Primer sequence (5' to 3')	product
pY1ΔRep	**pLacZi_Xho(Fw)**	GACCTCGAGGCATGTGCTCTGTATG	Region upstream of the lacZ gene in pLacZi flanked by XhoI and AfhI-SnaBI restriction sites.
	pLacZi-lacZ5'_AdhI-SnaBI(Rv)	GACGGGGAGTCTACGTATATTAATTTA GTGTGTGTATTTGTG	
	pLacZi-lacZ3'_SnaBI-NheI(Fw)	ATTTACGTAGCTAGCGGAAATCCATTA TGTACTATTTAAA	Region downstream of the lacZ gene in pLacZi flanked by SnaBI-NheI and AdhI restriction sites.
	pLacZi-AmpR_AdhI(Rv)	ACACGACGGGGAGTCAGGCAACTATG	
pY1-LUC+	**LUC+_SnaBI(Fw)**	ATTTACGTAATGGAAGACGCCAAAAAC ATAAAGAAAG	LUC+ protein coding region flanked by SnaBI and NheI restriction sites.
	LUC+_NheI(Rv)	AATGCTAGCTTACACGGCGATCTTTCC GCCCTTCTTG	
pY1-RLUC	**RLUC_SnaBI(Fw)**	ATTTACGTAATGACTTCGAAAGTTTAT GATCCAG	RLUC protein coding region flanked by SnaBI and NheI restriction sites.
	RLUC_NheI(Rv)	AATGCTAGCTTATTGTTCATTTTTGAGA ACTC	
pY1-gLUC	**gLUC_SnaBI(Fw)**	ATTTACGTAATGGGTGTTAAAGTTTTG TTCGCTTTG	gLUC protein coding region flanked by SnaBI and NheI restriction sites.
	gLUC_NheI(Rv)	AATGCTAGCTTAGTCACCACCAGCAC CTTTATTTTT	
pY1-PGA59emp	**pLacZi_HindIII(Fw)**	GAAAAGCTTGAATTCGAGCTCGG	Region upstream of the lacZ gene in pLacZi followed by the PGA59 signal peptide + first 2 aa of PGA59, flanked by SmaI-BbuI restriction sites.
	pLacZi-PGA59sig-BamHI-BbuI(Rv)	GCATGCGGATCCGTAAGTGGCTAAAG CGGAACCAGCAACAGCAGATAAGATA ATAGCGGATGAGAATTGCATTATTAAT TTAGTGTGTGTAT	
	BbuI-PGA59(Fw)	ATTGCATGCCCATGGTATGGATGAATT GTACAAAG	PGA59 protein coding region followed by the PGA59 terminator (from CIp10::ACT1p-gLUC59) and the region downstream of the lacZ gene in pLacZi .
	pLacZi-PGA59(Rv)	AAATAGTACATAATGGATTTCCTCAGG AGAAACAAAGATGTATAAG	
	pLacZi-AmpR_AdhI(Rv)	ACACGACGGGGAGTCAGGCAAC	

To be continued

Supplementary Table 4.1 PCR primers used in this study (continued)

Plasmid	Primer name	Primer sequence (5' to 3')	product
pY1-LUC+59	**LUC+_BamHI(Fw)**	ATTGGATCCGAAGACGCCAAAAACATAAAGAAAG	LUC+ protein coding region without ATG and stop codons and flanked by BamHI and PflMI restriction sites.
	LUC+_PflMI(Rv)	TTCATCCATACCATGGGTCACGGCGATCTTTCCGCCCTTCTTG	
pY1-RLUC59	**RLUC_BbuI(Fw)**	ATTGCATGCACTTCGAAAGTTTATGATCCAG	RLUC protein coding region without ATG and stop codons and flanked by BbuI and PflMI restriction sites.
	RLUC_PflMI(Rv)	TTCATCCATACCATGGGTTTGTTCATTTTTGAGAACTCGC	
pENTR/D-ADH1pr	**ADH1pr(Fw)**	CACCAAGAAATGATGGTAAATGAAATAGG	Full length and truncated ADH1 promoter region.
pENTR/D-ADH1prΔ	**ADH1prΔ(Fw)**	CACCGTTGTCTCACCATATCCGC	
	ADH1pr(Rv)	TATTGTGCAGAAAAAGAAACAAGGA	
pENTR/D-MET25pr	**MET25pr(Fw)**	CACCGGATGCAAGGGTTCGAATC	MET25 promoter region.
	MET25pr(Rv)	ATTGTATCTATGTATCTGACGA	
pENTR/D-CCA1pr(-363/-192)	**CCA1pr(-363)(Fw)**	CACCCACGAGAATGCGCGTTC	Wild-type and TBS-I mutant CCA1 promoter (-363/-192) region.
	CCA1pr(-192)(Rv)	CCTGAAAGGTTAAAAAG	

Supplemental Table 4.2 Statistical analysis of mean LUM/OD600 ratios for each prey construct compared to the mean ratio for the empty vector control[a].

HAPLOID CELLS

Prey construct	FLASH LUMINESCENCE				GLOW LUMINESCENCE (25 min)				GLOW LUMINESCENCE (60 min)			
	LUM/OD600		p value [b] (vs control)	Fold of induction	LUM/OD600		p value [b] (vs control)	Fold of induction	LUM/OD600		p value [b] (vs control)	Fold of induction
	Mean	SD			Mean	SD			Mean	SD		
Empty vector	110844	22179	-	1.0	3144	408	-	1.0	2571	278	-	1.0
TCP15	18648930	1302747	<0.0001	168.2	513782	58695	<0.0001	163.4	383493	53792	<0.0001	149.2
TCP14	16868298	1850386	<0.0001	152.2	433053	38768	<0.0001	137.8	315763	30402	<0.0001	122.8
TCP8	17408518	3379419	<0.0001	157.1	420807	48600	<0.0001	133.9	272396	37668	<0.0001	106.0
TCP23	15043319	2061385	<0.0001	135.7	384738	62839	<0.0001	122.4	311142	57381	<0.0001	121.0
TCP7	9962878	1562038	<0.0001	89.9	253254	45441	<0.0001	80.6	202583	40647	<0.0001	78.8
TCP20	5127075	284508	<0.0001	46.3	122912	12143	<0.0001	39.1	82856	9616	<0.0001	32.2
TCP22	1053523	13420	<0.0001	9.5	28172	1369	<0.0001	9.0	20775	834	<0.0001	8.1
TCP9	7407305	1576969	<0.0001	66.8	190768	42856	<0.0001	60.7	140096	35925	<0.0001	54.5
TCP19	3477112	1078643	<0.0001	31.4	75881	22297	<0.0001	24.1	44554	4872	<0.0001	17.3
TCP16	5356112	812387	<0.0001	48.3	107150	10318	<0.0001	34.1	70921	5106	<0.0001	27.6
TCP21	505099	187278	<0.0001	4.6	13801	4975	<0.0001	4.4	13920	3930	0.0352	5.4
TCP11	103371	17465	0.4832	0.9	3014	428	0.5395	1.0	2434	258	0.0000	0.9
TCP6	92571	15155	0.0899	0.8	2710	295	0.0348	0.9	2264	391	0.0710	0.9

To be continued

Supplementary Table 4.2 Statistical analysis of mean LUM/OD600 ratios for each prey construct compared to the mean ratio for the empty vector control a (continued)

	DIPLOID CELLS											
	FLASH LUMINESCENCE				GLOW LUMINESCENCE (25 min)				GLOW LUMINESCENCE (60 min)			
Prey construct	LUM/OD600		p value [b] (vs control)	Fold of induction	LUM/OD600		p value [b] (vs control)	Fold of induction	LUM/OD600		p value [b] (vs control)	Fold of induction
	Mean	SD			Mean	SD			Mean	SD		
Empty vector	737059	102621	-	1.0	17076	2514	-	1.0	10776	1605	-	1.0
TCP15	23350025	2553991	<0.0001	31.7	630313	33316	<0.0001	36.9	413901	20178	<0.0001	38.4
TCP14	15159279	932588	<0.0001	20.6	392311	35265	<0.0001	23.0	252296	23653	<0.0001	23.4
TCP8	27986125	2041533	<0.0001	38.0	624424	63931	<0.0001	36.6	365149	33505	<0.0001	33.9
TCP23	13907166	2021116	<0.0001	18.9	332933	64533	<0.0001	19.5	213330	42037	<0.0001	19.8
TCP7	6182577	957073	<0.0001	8.4	160769	29344	<0.0001	9.4	116727	22814	<0.0001	10.8
TCP20	4300996	2425699	0.0002	5.8	95522	54116	0.0002	5.6	57590	31786	0.0002	5.3
TCP22	13872816	1263691	<0.0001	18.8	328546	31927	<0.0001	19.2	218514	23262	<0.0001	20.3
TCP9	8388710	835495	<0.0001	11.4	188215	23608	<0.0001	11.0	110861	15781	<0.0001	10.3
TCP19	1863516	338029	<0.0001	2.5	39318	5431	<0.0001	2.3	23573	3463	<0.0001	2.2
TCP16	5211747	296157	<0.0001	7.1	96801	11707	<0.0001	5.7	55349	6457	<0.0001	5.1
TCP21	879786	105508	0.0228	1.2	20780	2216	0.0135	1.2	13633	1201	0.0033	1.3
TCP11	630556	79060	0.0599	0.9	15798	1210	0.3042	0.9	10247	1318	0.5314	1.0
TCP6	708568	74402	0.5886	1.0	16320	2109	0.5693	1.0	10575	1617	0.8199	1.0

[a] Grey cells: mean baseline values, Green cells: mean values above the baseline, Red cells: mean values equal to or below the baseline

[b] two-tailed Student's t-test

Supplemental Table 4.3 Summary of gLUC59-based Y1H assay advantages

Current limitations (*lacZ*-based Y1H assays) (a) Pruneda-Paz et al., 2014 (ref. #8); (b) Reece-Hoyes et al., 2011 (ref. #25)	Improvements (*gLUC59*-based Y1H assay)	Advantage for gene-centered screens
Rapid signal saturation[a, b] Limits detection of positive interactions for high background promoter baits	**Larger signal linear range** Extended linear range (3 orders of magnitude larger) enhances differences between positive and background signal levels	**Improves result analysis**
High reporter activity signal bleeding[b] Signal from strong positives diffuses into neighboring areas, manual checking recommended	**Low well-to-well signal crosstalk** Minimal luminescence signal diffusion using opaque plates and top-reading instrument	**Improves throughput and automation**
Extended incubation time[a, b] 1 to 7 days incubation after substrate addition, incubation at 30°C required	**No incubation required** Readout performed immediately after substrate addition, at room temperature	**Improves throughput and automation**
Reaction time adjustment depending on bait background activity[a, b] Required to minimize the negative effects of rapid signal saturation	**Equal reaction time for all promoter baits** Extended linear range allows uniform processing regardless of background reporter activity	**Improves throughput and automation**
Freeze/thaw cell lysis cycles[a] Incompatible with automation, time consuming	**Reporter assay performed with intact cells** gLUC59 activity measured directly in a liquid cell culture aliquot	**Improves throughput and automation**
Pre-assay agar plate preparation[b] Requires careful handling to obtain flat surface and overnight drying, time consuming	**Minimal pre-assay preparation** Liquid yeast growth medium and enzyme substrate solution	**Improves throughput and automation**
High TF expression required for proper assay sensitivity[b] Significant yeast growth inhibition observed using a high copy number (2u ori) Arabidopsis TF library	**Increased signal sensitivity and assay linearity** Assay suitable for TF libraries in low copy number vectors (CEN ori)	**Improves coverage and widespread usage**

Acknowledgment

This chapter, in full, is a reprint of the material as: Katia Bonaldi, Zheng Li, S. Earl Kang, Ghislain Breton, Jose L. Pruneda-Paz. Novel cell surface luciferase reporter for high-throughput yeast one-hybrid screens. Nucleic Acids Res. 2017 Oct 13;45(18):e157. The dissertation author was the co-first investigator and co-first author of this paper.

We thank Dr. Christophe D'Enfert for providing the CIp10::*ACT1p-gLUC59* vector.

Author contributions: J.L.P-P. conceived the project and designed the experiments. J.L.P-P., K.B. & Z.L. performed the experiments. S.E.K. contributed to execute some experiments. J.L.P-P. & G.B. analyzed results for all experiments. J.L.P-P., K.B. & Z.L. wrote the manuscript. All authors contributed to discussions and edited the manuscript.

References

1. Vaquerizas, J.M., Kummerfeld, S.K., Teichmann, S.A. and Luscombe, N.M. (2009) A census of human transcription factors: function, expression and evolution. Nature reviews. Genetics, **10**, 252-263.

2. Holland, M.J. (2002) Transcript abundance in yeast varies over six orders of magnitude. The Journal of biological chemistry, **277**, 14363-14366.

3. Czechowski, T., Bari, R.P., Stitt, M., Scheible, W.R. and Udvardi, M.K. (2004) Real-time RT-PCR profiling of over 1400 *Arabidopsis* transcription factors: unprecedented sensitivity reveals novel root- and shoot-specific genes. The Plant journal : for cell and molecular biology, **38**, 366-379.

4. Burdo, B., Gray, J., Goetting-Minesky, M.P., Wittler, B., Hunt, M., Li, T., Velliquette, D., Thomas, J., Gentzel, I., dos Santos Brito, M. Mejia-Guerra, M.K., Connolly, L.N., Qaisi, D., Li, W., Casas, M.I., Doseff, A.I., and Grotewold, E. (2014) The

Maize TFome--development of a transcription factor open reading frame collection for functional genomics. The Plant journal : for cell and molecular biology, **80**, 356-366.

5. Gaudinier, A., Zhang, L., Reece-Hoyes, J.S., Taylor-Teeples, M., Pu, L., Liu, Z., Breton, G., Pruneda-Paz, J.L., Kim, D., Kay, S.A. Walhout, A.J. Ware, D., and Brady, S.M. (2011) Enhanced Y1H assays for *Arabidopsis*. Nature methods, **8**, 1053-1055.

6. Gubelmann, C., Waszak, S.M., Isakova, A., Holcombe, W., Hens, K., Iagovitina, A., Feuz, J.D., Raghav, S.K., Simicevic, J. and Deplancke, B. (2013) A yeast one-hybrid and microfluidics-based pipeline to map mammalian gene regulatory networks. Molecular systems biology, **9**, 682.

7. Hens, K., Feuz, J.D., Isakova, A., Iagovitina, A., Massouras, A., Bryois, J., Callaerts, P., Celniker, S.E. and Deplancke, B. (2011) Automated protein-DNA interaction screening of Drosophila regulatory elements. Nature methods, **8**, 1065-1070.

8. Pruneda-Paz, J.L., Breton, G., Nagel, D.H., Kang, S.E., Bonaldi, K., Doherty, C.J., Ravelo, S., Galli, M., Ecker, J.R. and Kay, S.A. (2014) A genome-scale resource for the functional characterization of *Arabidopsis* transcription factors. Cell reports, **8**, 622-632.

9. Reboul, J., Vaglio, P., Rual, J.F., Lamesch, P., Martinez, M., Armstrong, C.M., Li, S., Jacotot, L., Bertin, N., Janky, R. Moore, T., Judson, J.R., Hartley, J.L., Brasch, M.A., Vandenhuate, J., Boulton, S., Endress, G.A., Jenna, S., Chevet, E., Papasotiropoulos, V., Tolias, P.P., Ptacek, J., Snyder, M., Huang, R., Chance, M.R., Lee, H., Doucette-Stamm, L., Hill, D.E., and Vidal, M. (2003) C. elegans ORFeome version 1.1: experimental verification of the genome annotation and resource for proteome-scale protein expression. Nature genetics, **34**, 35-41.

10. Reece-Hoyes, J.S., Barutcu, A.R., McCord, R.P., Jeong, J.S., Jiang, L., MacWilliams, A., Yang, X., Salehi-Ashtiani, K., Hill, D.E., Blackshaw, S. (2011) Yeast one-hybrid assays for gene-centered human gene regulatory network mapping. Nature methods, **8**, 1050-1052.

11. Deplancke, B., Dupuy, D., Vidal, M. and Walhout, A.J. (2004) A gateway-compatible yeast one-hybrid system. Genome research, **14**, 2093-2101.

12. Deplancke, B., Mukhopadhyay, A., Ao, W., Elewa, A.M., Grove, C.A., Martinez, N.J., Sequerra, R., Doucette-Stamm, L., Reece-Hoyes, J.S., Hope, I.A. Zhu, H., Dekker, J., and Walhout, A.J. (2006) A gene-centered C. elegans protein-DNA interaction network. Cell, **125**, 1193-1205.

13. Fuxman Bass, J.I., Sahni, N., Shrestha, S., Garcia-Gonzalez, A., Mori, A., Bhat, N., Yi, S., Hill, D.E., Vidal, M. and Walhout, A.J. (2015) Human gene-centered

transcription factor networks for enhancers and disease variants. Cell, **161**, 661-673.

14. Pruneda-Paz, J.L., Breton, G., Para, A. and Kay, S.A. (2009) A functional genomics approach reveals CHE as a component of the *Arabidopsis* circadian clock. Science, **323**, 1481-1485.

15. Taylor-Teeples, M., Lin, L., de Lucas, M., Turco, G., Toal, T.W., Gaudinier, A., Young, N.F., Trabucco, G.M., Veling, M.T., Lamothe, R. Handakumbura, P.P., Xiong, G., Wang, C., Corwin, J., Tsoukalas, A., Zhang, L., Ware, D., Pauly, M., Kliebenstein, D.J., Dehesh, K., Tagkopoulos, I., Breton, G., Pruneda-Paz, J.L, Ahnert, S.E., Kay, S.A., Hazen, S.P., and Brady, S.M. (2015) An *Arabidopsis* gene regulatory network for secondary cell wall synthesis. Nature, **517**, 571-575.

16. Breton, G., Kay, S.A. and Pruneda-Paz, J.L. (2016) Identification of *Arabidopsis* Transcriptional Regulators by Yeast One-Hybrid Screens Using a Transcription Factor ORFeome. Methods in molecular biology, **1398**, 107-118.

17. Chow, B.Y., Sanchez, S.E., Breton, G., Pruneda-Paz, J.L., Krogan, N.T. and Kay, S.A. (2014) Transcriptional regulation of LUX by CBF1 mediates cold input to the circadian clock in *Arabidopsis*. Current biology : *CB*, **24**, 1518-1524.

18. Guan, P., Wang, R., Nacry, P., Breton, G., Kay, S.A., Pruneda-Paz, J.L., Davani, A. and Crawford, N.M. (2014) Nitrate foraging by *Arabidopsis* roots is mediated by the transcription factor TCP20 through the systemic signaling pathway. Proceedings of the National Academy of Sciences of the United States of America, **111**, 15267-15272.

19. Ito, S., Song, Y.H., Josephson-Day, A.R., Miller, R.J., Breton, G., Olmstead, R.G. and Imaizumi, T. (2012) FLOWERING BHLH transcriptional activators control expression of the photoperiodic flowering regulator CONSTANS in *Arabidopsis*. Proceedings of the National Academy of Sciences of the United States of America, **109**, 3582-3587.

20. Kolmos, E., Chow, B.Y., Pruneda-Paz, J.L. and Kay, S.A. (2014) HsfB2b-mediated repression of PRR7 directs abiotic stress responses of the circadian clock. Proceedings of the National Academy of Sciences of the United States of America, **111**, 16172-16177.

21. Li, L., Ljung, K., Breton, G., Schmitz, R.J., Pruneda-Paz, J., Cowing-Zitron, C., Cole, B.J., Ivans, L.J., Pedmale, U.V., Jung, H.S., Ecker, J.R., Kay, S.A., and Chory, J. (2012) Linking photoreceptor excitation to changes in plant architecture. Genes & development, **26**, 785-790.

22. Zheng, X.Y., Zhou, M., Yoo, H., Pruneda-Paz, J.L., Spivey, N.W., Kay, S.A. and Dong, X. (2015) Spatial and temporal regulation of biosynthesis of the plant

immune signal salicylic acid. Proceedings of the National Academy of Sciences of the United States of America, **112**, 9166-9173.

23. Miller, J.H. (1972) *Experiments in Molecular Genetics*. Cold Spring Harbor Laboratory, Cold Spring Harbor, N.Y.

24. Serebriiskii, I.G. and Golemis, E.A. (2000) Uses of lacZ to study gene function: evaluation of beta-galactosidase assays employed in the yeast two-hybrid system. Analytical biochemistry, **285**, 1-15.

25. Reece-Hoyes, J.S., Diallo, A., Lajoie, B., Kent, A., Shrestha, S., Kadreppa, S., Pesyna, C., Dekker, J., Myers, C.L. and Walhout, A.J. (2011) Enhanced yeast one-hybrid assays for high-throughput gene-centered regulatory network mapping. Nature methods, **8**, 1059-1064.

26. Schneider, S., Buchert, M. and Hovens, C.M. (1996) An in vitro assay of beta-galactosidase from yeast. BioTechniques, **20**, 960-962.

27. Enjalbert, B., Rachini, A., Vediyappan, G., Pietrella, D., Spaccapelo, R., Vecchiarelli, A., Brown, A.J. and d'Enfert, C. (2009) A multifunctional, synthetic Gaussia princeps luciferase reporter for live imaging of Candida albicans infections. Infection and immunity, **77**, 4847-4858.

28. Helfer, A., Nusinow, D.A., Chow, B.Y., Gehrke, A.R., Bulyk, M.L. and Kay, S.A. (2011) LUX ARRHYTHMO encodes a nighttime repressor of circadian gene expression in the *Arabidopsis* core clock. Current biology : CB, **21**, 126-133.

29. Walhout, A.J. and Vidal, M. (2001) High-throughput yeast two-hybrid assays for large-scale protein interaction mapping. Methods, **24**, 297-306.

30. Kearse, M., Moir, R., Wilson, A., Stones-Havas, S., Cheung, M., Sturrock, S., Buxton, S., Cooper, A., Markowitz, S., Duran, C., Thierer, T., Ashton, B., Meintjes, P., and Drummond, A. (2012) Geneious Basic: an integrated and extendable desktop software platform for the organization and analysis of sequence data. Bioinformatics, **28**, 1647-1649.

31. Tornow, J. and Santangelo, G.M. (1990) Efficient expression of the Saccharomyces cerevisiae glycolytic gene ADH1 is dependent upon a cis-acting regulatory element (UASRPG) found initially in genes encoding ribosomal proteins. Gene, **90**, 79-85.

32. Ronicke, V., Graulich, W., Mumberg, D., Muller, R. and Funk, M. (1997) Use of conditional promoters for expression of heterologous proteins in Saccharomyces cerevisiae. Methods in enzymology, **283**, 313-322.

33. Reece-Hoyes, J.S. and Marian Walhout, A.J. (2012) Yeast one-hybrid assays: a historical and technical perspective. Methods, **57**, 441-447.

34. Vermeirssen, V., Deplancke, B., Barrasa, M.I., Reece-Hoyes, J.S., Arda, H.E., Grove, C.A., Martinez, N.J., Sequerra, R., Doucette-Stamm, L., Brent, M.R., and Walhout, A.J. (2007) Matrix and Steiner-triple-system smart pooling assays for high-performance transcription regulatory network mapping. Nature methods, **4**, 659-664.

35. Wu, J.F., Tsai, H.L., Joanito, I., Wu, Y.C., Chang, C.W., Li, Y.H., Wang, Y., Hong, J.C., Chu, J.W., Hsu, C.P. and Wu, S.H. (2016) LWD-TCP complex activates the morning gene CCA1 in *Arabidopsis*. Nature communications, **7**, 13181.

36. Viola, I.L., Uberti Manassero, N.G., Ripoll, R. and Gonzalez, D.H. (2011) The *Arabidopsis* class I TCP transcription factor AtTCP11 is a developmental regulator with distinct DNA-binding properties due to the presence of a threonine residue at position 15 of the TCP domain. The Biochemical journal, **435**, 143-155.

37. Viola, I.L., Reinheimer, R., Ripoll, R., Manassero, N.G. and Gonzalez, D.H. (2012) Determinants of the DNA binding specificity of class I and class II TCP transcription factors. The Journal of biological chemistry, **287**, 347-356.

38. Danisman, S. (2016) TCP Transcription Factors at the Interface between Environmental Challenges and the Plant's Growth Responses. *Frontiers in plant* science, **7**, 1930.

Chapter 5 Identification of TCP21 interacting transcription factors with novel high throughput yeast two hybrid screen system

Introduction

Yeast two hybrid screen, as a powerful tool to discover novel protein-protein interactions, has been heavily exploited in almost all fields of biological study [1,2]. Traditional yeast two hybrid screen strategy involves a bait protein which is fused with Gal4 DNA binding domain, and prey protein library which is fused with GAL4 activation domain. If the bait protein interacts with a prey protein, the GAL4 activation domain will be brought to the promoter of reporter gene which contains the binding site for GAL4 DNA binding domain [1,2]. Then the reporter gene is expressed and reporter activity is scored. The most commonly used reporters are auxotrophic reporters such as HIS3 reporter and the β-galactosidase reporter which is encoded from the *lacZ* gene [3]. In recent years, with the integration of high-throughput sequencing techniques, yeast two hybrid screen method also evolved with faster screening process and the ability to obtain larger amount of protein-protein interaction information [4–6]. However, these techniques either starts with cDNA library which is biased towards highly expressed genes or grow yeast cells as mixtures rendering proteins that affect yeast fitness less likely to be selected. With the novel cell surface luciferase reporter which allows for high throughput yeast screens [7] and the availability of more genome scale individually cloned protein collections [8–11], development of a gene-centered high throughput yeast two hybrid screening system is both highly useful and achievable. By integrating the reporter cassette of the MEL1 promoter with multiple GAL4 binding sites driving the expression of the gLUC59 reporter

into the AH109 yeast genome, we established a stable yeast two hybrid reporter strain which is fully compatible with the current *Arabidopsis* transcription factor library [8] and the screening process can be fully automated. We screened for TCP21(CHE) interacting proteins with this new system and discovered 68 interactors and discovered that class I TCPs are significantly enriched.

Results

AH109-gLUC59 reporter strain was constructed for high throughput yeast two hybrid screens

Since the *Arabidopsis* transcription factor library was already cloned in the pDEST22 vector (expressed together with GAL4 activation domain) and transformed in the YU strain for yeast one hybrid screens [8], we wanted to construct a reporter stain which is compatible with the existing TF library and suitable for high throughput screens. Considering that the YU strain originates from Y187 [8], and that Y187 and AH109 strains are frequently used mating pair for yeast two hybrid assay, we started to create a yeast two hybrid strain with the cell surface luciferase reporter gLUC59 based on the AH109 strain [3]. The PCRBII vector backbone was used to construct the yeast integration vector PCRBII-gLUC59: The upstream and downstream sequences of the AH109 MEL1 gene were cloned to flank the reporter cassette for integration into the AH109 MEL1 locus through double homologous recombination (Figure 5.1). MEL1 promoter was used to drive the expression of gLUC59 reporter and triplicate GAL4 binding sites (UAS) were cloned into the MEL1 promoter to increase the sensitivity of the assay. A geneticin resistance gene *KanMX* was also cloned into the cassette for selection of successfully integrated yeast (Figure 5.1).

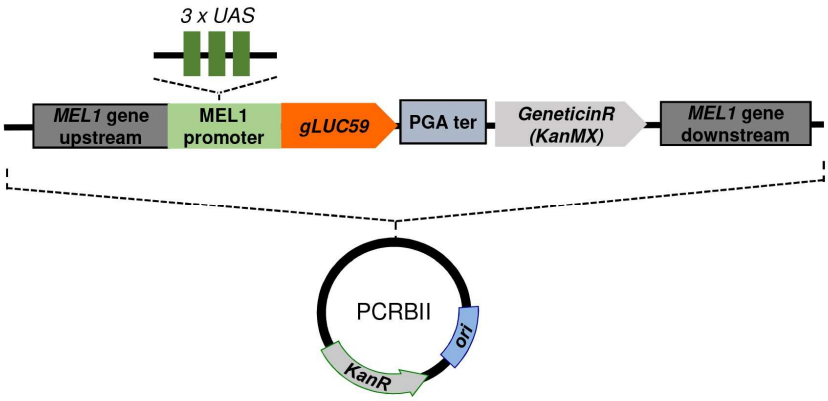

Figure 5.1 Schematic representation of yeast integration vector to create yeast two hybrid strain with gLUC59 reporter.
The yeast integration vector was constructed with the PCR Blunt II backbone. The upstream and down sequences of AH109 MEL1 gene were cloned to flank the cassette to be integrated into the AH109 genome. The replicate origin of PCRBII vector does not funciton in yeast, thus the reporter cassette could only be preserved by the yeast through integration into the genome.

After obtaining the yeast with reporter cassette integrated into the genome (named as AH109-gLUC59 strain), we tested if the expression of the luciferase reporter could be induced. By transforming the AH109-gLUC strain with pDEST32 TCP21-VP64, a fusion protein of GAL4 DNA binding domain, TCP21and the VP64 which is a tetrameric repeat of VP16 minimal activation domain [12], was expressed in the yeast. Light signal was detected from the AH109-gLUC59 yeast carrying pDEST32 TCP21-VP64 after spraying transformed yeast with gLUC substrate coelenterazine, indicating that the expression of gLUC reporter was induced by the fusion protein and the expressed luciferase existed on the cell surface as expected (Figure 5.2). No light was detected in the AH109-gLUC yeast transformed with pDEST32 MCS (multiple cloning site) where only the GAL4 DNA binding domain was expressed (Figure 5.2).

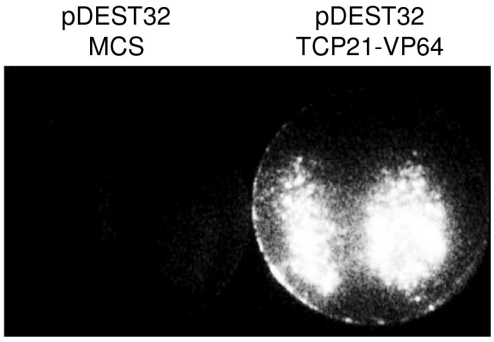

Figure 5.2 Induction of gLUC59 reporter expression by GAL4 DBD-TCP21-VP64 in the AH109-gLUC59 strain.
AH109-gLUC59 strain was transformed with pDEST32 MCS (multiple cloning site) and pDEST32 TCP21-VP64 respectively. Resulting yeast was sprayed with coelenterazine and imaged in dark under CCD camera.

Novel TCP21 interactors were identified through yeast two hybrid screen with AH109-gLUC reporter strain

TCP21 (CHE), as a class I TCP transcription factor, is involved in the regulation of circadian clock function and defense responses [13,14]. As TCP transcription factors tend to form dimers to bind DNA [15-17], we screened for transcription factors that can interact with TCP21. We transformed pDEST32 TCP21 vector into the AH109-gLUC reporter strain and then mated the resulting yeast with the YU strain carrying the *Arabidopsis* TF library (in pDEST22 vector). Diploid cells were selected and cultured for the reading of gLUC enzymatic activity. A brief illustration of the yeast two hybrid screen process with the new reporter strain is indicated in Figure 5.3.

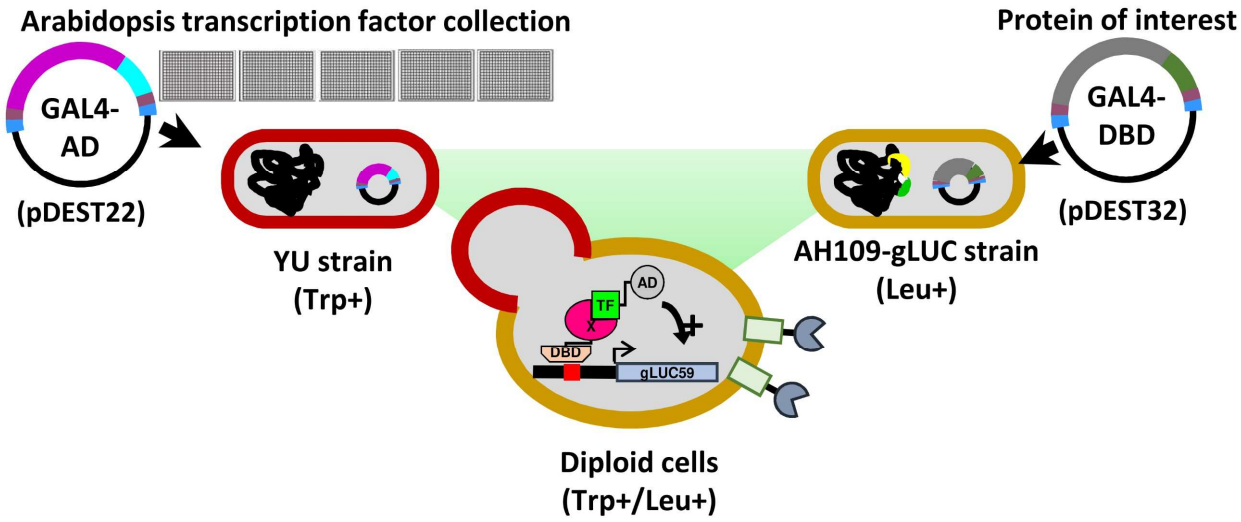

Figure 5.3 High throughput yeast two hybrid screen procedure.
Coding sequence of protein of interest was cloned in pDEST32 vector and transformed into the AH109-gLUC strain. Then the homogeneous culture from one colony of the resulting yeast was mated with YU stain carrying the *Arabidopsis* TF library individually. Diploid cells were selected and assayed for gLUC reporter activity.

We identified 68 transcription factors that interacted with TCP21 from two replicates of screen (Figure 5.4A and Supplemental Table 5.2), they were from 20 different transcription factor families (Supplemental Table 5.3). Duplicates of screens with the pDEST32-MCS were done as control for self-activation of transcription factors (data not shown). Among the transcription factor families, bHLH, TCP, SRS, VOZ and WRKY transcription factor families were enriched for TCP21 binding proteins (Supplemental Table 5.3). In the TCP family, class I TCPs were more enriched for the binding of TCP21 compared to class II TCPs (Supplemental Table 5.3 and Figure 5.4B) revealing the complex cooperation between class I TCP transcription factors.

Interaction between TCP19 and TCP21 was confirmed with BiFC assay in planta

TCP19 (AT5G51910) from the class I TCP subfamily was ranked as the top interactor of TCP21 according to the gLUC activity in the yeast two hybrid screen. We

tested the interaction between TCP21 and TCP19 with BiFC system in *Nicotiana benthamiana*. The YFP fluorescent signal was detected only when TCP19 and TCP21 were co-infiltrated compared to the controls and the fluorescent signal existed in the nucleus (Figure 5.4C). This result indicates that TCP19 and TCP21 interaction also happened in planta.

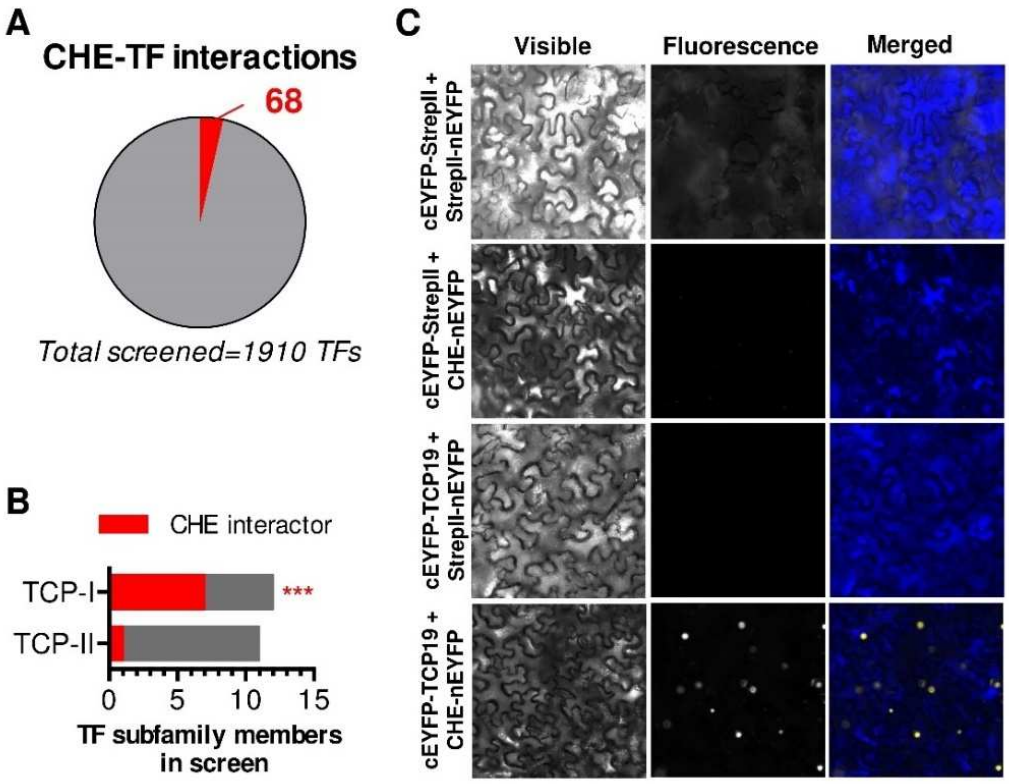

Figure 5.4 Class I TCPs were enriched for TCP21 interactors.
(A) 68 out of total 1910 TFs were identified as TCP21 interactors in yeast two hybrid screen. (B) Class I TCPs were enriched for TCP21 interactors (red). Total number of subfamily members in the screen is indicated as gray. (C) BiFC results in *Nicotiana benthamiana* systems. strepII tag was cloned in corresponding vector for control purposes.

Discussion

After the labor-intensive cloning of the *Arabidopsis* transcription factor library [8], researchers have gain a lot of information about transcriptional regulation by performing

yeast one hybrid (Y1H) screens with this TF collection. The early Y1H screens were performed using β-galactosidase as reporter which has several limitations [7,8]. Then, with the development of the cell surface luciferase reporter gLUC59, the Y1H screen process was much more standardized and automated. Taking advantage of the TF library and the gLUC59 reporter, we established the AH109-gLUC strain for yeast two hybrid (Y2H) screens. Traditionally, the compatible vectors to perform Y2H screens with AH109 and Y187 partner strains are usually the vector systems that have 2-micron replicate origin such as pACT and pAS vectors [3]. These vectors replicate to high numbers in yeast cells [18] and correspondingly produce higher levels of protein product [19]. However, this is problematic to the *Arabidopsis* TF collection as expressing many *Arabidopsis* TFs to high level in yeast has adverse effect on yeast growth which renders the screen to be low on coverage (data not shown). With the large dynamic range of gLUC59 reporter and the fact that we increased the number of GAL4 DNA binding site in the reporter cassette, the AH109-gLUC59 and YU partner strains are working well with the low copy number pDEST22 and pDEST32 vector system (Invitrogen) which allows much better coverage of the *Arabidopsis* TF collection. The procedure of Y2H screen with AH109-gLUC59 against the TF collection is very similar to the Y1H screen procedure, being beneficial to the standardization of the protocol and fully automation of the process. This Y2H system is not only applicable to the *Arabidopsis* TF collection. It could be applied to potentially any protein collection from any organism.

The interaction between TCP21 and other TCP transcription factors revealed the complexity of transcriptional regulation by TCPs. The dimerization not only happens between TCP21 and other TCPs, it also occurs between other TCPs [16,17]. On top of

this complexity, while TCP21 was reported as a transcriptional repressor, TCP20 and TCP22 were activators of CCA1 transcription indicating differential activities of transcriptional regulation among the TCPs [13,20]. Thus, different homo- and hetero-dimers between TCP transcription factors and even between TCPs and transcription factors of other families could be co-existing in the plant working cooperatively or competitively. More works need to be done to dissect this complicated network, for example, determining the spatial and temporal pattern of TCPs could reduce the possible combination of dimers and narrow down to the real functioning ones under certain conditions.

Materials and Methods

Construction of PCRBII-gLUC59 vector:

Fragments of the following DNA (1) PCRBII backbone, (2) AH109 MEL1 locus upstream, (3) MEL1 promoter, (4) gLUC59 CDS-PGA terminator cassette, (5) TEF promoter-KanMX CDS-TEF terminator cassette and (6) MEL1 locus downstream were amplified with corresponding template and primers as indicated in Supplemental Table 5.1. Note that the amplified DNA fragments all have a piece of overlapping for Gibson cloning. The fragments of DNA were cloned into one vector PCRBII-gLUC59 (1xUAS) by Gibson cloning. To generate PCRBII-gLUC59 with 3 times MEL1 UAS, oligo19 and oligo20 were annealed to have the 3XUAS fragment and the PCRBII-gLUC59 (1xUAS) vector were digested with NdeI. Then they were cloned together with Gibson cloning.

Integration of reporter cassette into AH109 genome

PCRBII-gLUC59 plasmid was transformed into AH109 and the resulting yeast population was plated on YPD plates containing 200mg/L G418 (geneticin). Then single

colony was streaked on YPD plates with G418 twice and followed by single colony streaking on YPD without G418 twice to remove selection pressure for any unstable insertion and possible residue of PCRBII-gLUC59 plasmid in the yeast. After that, reporter yeast was confirmed by streaking single colony again on YPD with G418 twice and after the final streak, cells from the plate was scraped and glycerol stocked to be saved as AH109-gLUC59.

Testing gLUC59 induction in AH109-gLUC59 yeast

pDEST32 TCP21-VP64 and pDEST32 MCS (multiple cloning site) were transformed into AH109-gLUC59 and plated on SD-L (SD media lacking Leucine) plates respectively. After positive colonies arose, coelenterazine (20uM coelenterazine native, 1xPBS pH 7.4, 5mM NaCl) was sprayed to the plates. Images were taken in dark with Wasabi imaging system.

TCP21 yeast two hybrid screen with AH109-gLUC59

pDEST32-TCP21 was transformed into AH109-gLUC59 and selected on SD-L medium. Single colony was streaked on SD-L again. 50ml of SD-L liquid culture of AH109-gLUC59 carrying pDEST32-TCP21 was started from single colony and cultured in 250ml flask for 24-36 hours at 30°C (180rpm shaking). At the same time, SD-T (SD media lacking tryptophan) liquid medium was added to glycerol stocked YU-TF library (120ul SD-T medium per well) and cultured at 30 °C (600rpm shaking) for 24-36 hours. After this culture, transfer 3.5ul of each well of YU-TF library culture (mix each well by pipetting first) to new plates (the mating microplates) with 40ul YPD medium. Then we added 50ml of YPD to the overnight AH109-gLUC culture carrying pDEST32-TCP21, mixed well and transferred 10-20ul of this cell suspension into each well of the mating microplates. The

mating microplates were sealed (breathable seal), votexed for 10sec at 1000 rpm and incubated at 30 °C for 12-48 hours without shaking in a humid environment. Mated cells were collected by centrifuging at 1000g for 3min and supernatant was removed. After that, cells were resuspended in 40ul of SD media lacking Leucine and Tryptophan (SD-TL) by votexing for 15sec at 1000 rpm and then cells were centrifuged at 1000g for 3min again. Supernatant was then removed to get rid of any residue YPD. And cells were resuspended in 65ul of SD-TL medium. 10ul of these mated cells were transferred to new deep 384 well plates containing 45ul of liquid SD-TL medium each well. These plates were incubated at 30°C (600rpm shaking) for 24-36 hours. Then 120ul YPD was added to each well and continue to be cultured at the same condition for 5-6 hours. After this culture process, we mixed the culture well by pipetting and 25ul of this culture was transferred to clear 384 well plates (absorbance microplate). The absorbance microplates with culture were first vortexed for 20 sec at 1000rpm and put into plate reader to determine the OD600 of each well. Another 25ul of the YPD culture was transferred to 384-well white plate and 25ul of native coelenterazine substrate (1xPBS pH7.4, 5mM NaCl, 24uM native coelenterazine [Biosynth]) was added to each well. The plates were votexed for 20sec at 1000 rpm and luminescence was read 8-10min later by plate reader with integration time as 1 sec/well. To calculate the normalized gLUC activity of each well, means of readings from empty control wells were first subtracted from luminescence readings and OD600 readings, then Lum/OD600 was calculated as the gLUC activity.

TCP21-TCP19 interaction detection in *Nicotiana benthamiana* systems

TCP21 and TCP19 was cloned into corresponding BIFC destination vectors by gateway cloning, and StrepII tag was used as empty control. Agrobacterium strain

GV3101 carrying BIFC vectors and agrobacterium carrying HA-P19 were cultured overnight at 28°C. In the second morning, agrobacterium cells were harvested by centrifugation (4000 rpm, 10min-12min) and resuspended in infiltration buffer (10mM $MgCl_2$, 10mM MES PH5.7, 150uM acetosyringone) to OD600 as 0.5. Equal volume of each of the combination of desired test pairs and the HA-P10 were mixed and slowly shaken at room temperature for 3 hours. The cell mixtures were injected into expanded leaves of young *Nicotiana benthamiana* plants with 1ml syringe without needle and fluorescence signal was scored 2-3 days later.

Supplementary Information

Supplemental Table 5.1 Oligonucleotide sequences

primer name	primer sequence (5' to 3')	purpose
primer 241	AAGGGCGAATTCCAGCACACT	to amplify PCRBII backbone from pCR Blunt II vector
primer 246	TGCAGATATCCATCACACTGG	
primer 244	GCTGGAATTCGCCCTTGGATCAAAGGAAAAATATTTCT	to amplify AH109 MEL1 locus upstream sequence from AH109 genomic DNA
primer 288	GAAGTCGACTTCGGTAGGGTGCTATCCT	
primer 289	CTACCGAAGTCGACTTCTAAGTAAACACCA	to amplify MEL1 promoter from AH109 genome
primer 24	GATAATAGCGGATGAGAATTGCATCGTCGTTGCTTTTATTACCGTTGC	
primer 21	ATGCAATTCTCATCCGCTATTATC	to amplify gLUC59 CDS-PGA terminator cassette from the PY1-gLUC59 (MCS version)
primer 256	TCAGGAGAAACAAAGATGTATAAGGAACA	
primer 258	TCTTTGTTTCTCCTGAAGCTTGCCTCGTCCCCGCCGGGT	to amplify TEF promoter-KanMX CD-TEF teminator cassette from pKT140 vector
primer 257	CAACAATAAGCTCAAGATGGATGGCGGCGTTAGTATCGA	
primer 232	TCTTGAGCTTATTGTTGAGCAAAGC	to amplify AH109 MEL1 locus downstream sequence from AH109 genomic DNA
primer 247	GTGATGGATATCTGCAGGATCCCGAGTTTCTCAGA	
oligo19	TTGGCTTTCATTCGGCCATATGTCTTCCGAAAGAATTTCATTCGGCCATATGTCTTCCGAAAGAATTTCATTCGGCCATATGTCTTCCGA	to anneal to form the DNA fragment with 3x MEL1 UAS
oligo20	TCGGAAGACATATGGCCGAATGAAATTCTTTCGGAAGACATATGGCCGAATGAAATTCTTTCGGAAGACATATGGCCGAATGAAAGCCAA	

Supplemental Table 5.2 TCP21 (CHE)-TF interactions (Yeast two-hybrid)

Gene identifier (AGI)	TF family	gLUC activity (cut off normalized)			Interaction rank (based on gLUC activity)		
		Rep 1	Rep 2	Average	Rep 1	Rep 2	Average
AT5G51910	TCP [a,b,c]	83.6	84.7	84.2	1	1	1.0
AT1G28520	VOZ [a,b]	49.5	42.6	46.0	2	3	2.5
AT3G50510	LOB [a] / AS2 [b]	32.4	50.7	41.5	3	2	2.5
AT3G57800	bHLH [a,b]	11.2	33.5	22.3	5	5	5.0
AT2G40470	LOB [a] / AS2 [b]	12.7	22.4	17.6	4	6	5.0
AT5G50915	bHLH [a,b]	8.2	40.8	24.5	8	4	6.0
AT2G37000	TCP [a,b,c]	10.6	21.9	16.2	7	7	7.0
AT3G21330	bHLH [a,b]	10.7	16.3	13.5	6	10	8.0
AT2G31280	bHLH [e]	8.1	10.3	9.2	10	12	11.0
AT4G04885	C2H2 [e]	5.4	17.7	11.6	14	9	11.5
AT1G32640	bHLH [a,b]	5.7	9.2	7.5	12	14	13.0
AT3G59060	bHLH [a,b]	8.1	7.8	8.0	9	19	14.0
AT2G45680	TCP [a,b,c]	4.2	11.6	7.9	17	11	14.0
AT2G31210	bHLH [a,b]	5.6	8.7	7.2	13	16	14.5
AT1G72010	TCP [a,b,c]	3.5	18.6	11.0	24	8	16.0
AT1G09530	bHLH [a,b]	6.3	7.5	6.9	11	21	16.0
AT5G12330	SRS [a,b]	3.5	9.8	6.6	25	13	19.0
AT1G27660	ND	3.5	9.1	6.3	26	15	20.5
AT1G21700	MYB-related [a]	4.6	6.5	5.6	16	25	20.5
AT3G17860	ZIM [b,c]	3.9	7.5	5.7	21	22	21.5
AT1G69690	TCP [a,b,c]	3.1	7.9	5.5	29	18	23.5
AT2G20880	AP2-EREBP [a,b,c]	3.9	6.1	5.0	20	27	23.5
AT5G45980	HB [a,b,c]	3.1	7.6	5.3	31	20	25.5
AT1G48150	MADS [a,b]	3.6	4.6	4.1	23	32	27.5
AT1G06170	bHLH [a,b]	3.5	5.1	4.3	27	29	28.0
AT2G47700	ND	3.7	3.9	3.8	22	36	29.0
AT4G23810	WRKY [a,b,c]	2.8	6.5	4.7	34	26	30.0
AT1G51140	bHLH [a,b]	3.1	5.0	4.1	30	30	30.0
AT3G24140	bHLH [a,b]	3.9	3.1	3.5	19	43	31.0
AT3G47620	TCP [a,b,c]	2.2	6.6	4.4	40	24	32.0
AT5G46880	HB [a,b]	1.8	8.6	5.2	48	17	32.5

To be continued

Supplemental Table 5.2 TCP21 (CHE)-TF interactions (Yeast two-hybrid) (continued)

Gene identifier (AGI)	TF family	gLUC activity (cut off normalized)			Interaction rank (based on gLUC activity)		
		Rep 1	Rep 2	Average	Rep 1	Rep 2	Average
AT1G68810	bHLH [a,b]	2.9	4.6	3.7	33	33	33.0
AT2G18300	bHLH [a,b]	2.0	5.6	3.8	44	28	36.0
AT5G27130	MADS [a,b]	3.4	3.1	3.2	28	44	36.0
AT3G30530	bZIP [a,b,c]	2.1	4.8	3.5	42	31	36.5
AT3G15030	TCP [a,b,c]	3.0	3.2	3.1	32	41	36.5
AT1G55650	ARID [a,b]	2.1	3.5	2.8	41	38	39.5
AT4G01720	WRKY [a,b,c]	2.1	3.7	2.9	43	37	40.0
AT2G22760	bHLH [a,b]	1.4	6.7	4.0	58	23	40.5
AT3G27010	TCP [a,b,c]	5.3	NG	5.3	15	68	41.5
AT4G02590	bHLH [a,b]	1.8	4.2	3.0	49	34	41.5
AT4G11070	WRKY [a,b,c]	2.3	2.9	2.6	38	45	41.5
AT1G60250	Orphans [a]	4.0	NG	4.0	18	66	42.0
AT4G00730	HB [a,b]	2.0	3.2	2.6	46	42	44.0
AT2G23760	HB [a,b]	1.5	4.2	2.8	55	35	45.0
AT4G04450	WRKY [a,b,c]	2.3	2.4	2.3	39	51	45.0
AT1G68920	bHLH [a,b]	2.4	2.2	2.3	37	55	46.0
AT3G01220	HB [a,b]	1.6	3.3	2.4	54	40	47.0
AT5G41315	bHLH [a,b]	2.0	2.3	2.1	45	52	48.5
AT1G32240	G2-like [a,b]	1.9	2.3	2.1	47	53	50.0
AT4G35270	RWP-RK [a] / NIN-like [b]	2.5	1.5	2.0	36	65	50.5
AT1G66600	WRKY [a,b,c]	2.6	NG	2.6	35	67	51.0
AT3G54390	TRIHELIX [a,b]	1.5	2.7	2.1	56	47	51.5
AT1G24590	AP2-EREBP [a,b,c]	NG	3.5	3.5	67	39	53.0
AT4G35040	bZIP [a,b,c]	1.2	2.8	2.0	62	46	54.0
AT5G16560	G2-like [a,b]	1.4	2.6	2.0	59	49	54.0
AT1G19790	SRS [a,b]	1.7	2.2	1.9	51	57	54.0
AT4G22070	WRKY [a,b,c]	1.7	2.2	1.9	52	56	54.0
AT1G34180	NAC [a,b]	1.2	2.6	1.9	61	48	54.5
AT2G24430	NAC [a,b]	1.8	2.0	1.9	50	64	57.0
AT4G33880	bHLH [a,b]	1.1	2.5	1.8	64	50	57.0
AT5G14010	C2H2 [a,b,c]	1.6	2.0	1.8	53	63	58.0
AT1G68240	bHLH [a,b]	1.5	2.1	1.8	57	59	58.0

To be continued

Supplemental Table 5.2 TCP21 (CHE)-TF interactions (Yeast two-hybrid) (continued)

Gene identifier (AGI)	TF family	gLUC activity (cut off normalized)			Interaction rank (based on gLUC activity)		
		Rep 1	Rep 2	Average	Rep 1	Rep 2	Average
AT1G64625	bHLH [e]	1.0	2.2	1.6	65	54	59.5
AT4G37940	MADS [a,b]	1.4	2.1	1.7	60	61	60.5
AT2G31220	bHLH [a,b]	1.1	2.2	1.6	63	58	60.5
AT4G13640	G2-like [a,b]	1.0	2.1	1.6	66	60	63.0
AT1G72210	bHLH [a,b]	NG	2.1	2.1	68	62	65.0

[a] Source: http://plntfdb.bio.uni-potsdam.de
[b] Source: http://datf.cbi.pku.edu.cn
[c] Source: http://www.transcriptionfactor.org
NG: no growth of yeast

Supplemental Table 5.3 TF-family analysis for TCP21 (CHE)-TF interactions

TF family	TF-family members screened (out of 1910 TFs)	Number of TCP21-TF interactions	TF-family enrichment	
			p-value [a]	significance
AP2-EREBP	135	2	9.6E-01	n.s.
ARID	10	1	3.0E-01	n.s.
bHLH	118	22	1.4E-11	****
bZIP	63	2	6.7E-01	n.s.
C2H2	119	2	9.3E-01	n.s.
G2-like	37	3	1.4E-01	n.s.
HB	60	5	5.9E-02	n.s.
LOB / AS2	35	2	3.6E-01	n.s.
MADS	81	3	5.6E-01	n.s.
MYB-related	58	1	8.8E-01	n.s.
NAC	88	2	8.3E-01	n.s.
ND	83	2	8.1E-01	n.s.
Orphans	38	1	7.5E-01	n.s.
RWP-RK / NIN-like	5	1	1.7E-01	n.s.
SRS	5	2	1.2E-02	*
TCP	23	8	5.5E-07	****
TRIHELIX	22	1	5.5E-01	n.s.
VOZ	1	1	3.6E-02	*
WRKY	60	6	1.8E-02	*
ZIM	14	1	4.0E-01	n.s.
TCP subfamily analysis				
TCP-classI	12	7	3.7E-08	****
TCP-classII	11	1	3.3E-01	n.s.

[a] p-value of enrichment calculated by hypergeometric probability calculator from Geneprof.

Acknowledgement

I would also like to acknowledge Eleni Tente who made great effort to validate protein interaction with tobacco BIFC system.

References

1. Bruckner, A., Polge, C., Lentze, N., Auerbach, D., and Schlattner, U. (2009). Yeast two-hybrid, a powerful tool for systems biology. Int. J. Mol. Sci. *10*, 2763–2788.

2. Fields, S., and Song, O. (1989). A novel genetic system to detect protein-protein interactions. Nature *340*, 245–246.

3. Yeast protocols handbook. Clontech.

4. Trigg, S.A., Garza, R.M., MacWilliams, A., Nery, J.R., Bartlett, A., Castanon, R., Goubil, A., Feeney, J., O'Malley, R., Huang, S.-S.C., Zhang, Z.Z., Galli, M., and Ecker, J.R. (2017). CrY2H-seq: a massively multiplexed assay for deep-coverage interactome mapping. Nat. Methods *14*, 819–825.

5. Yu, H., Tardivo, L., Tam, S., Weiner, E., Gebreab, F., Fan, C., Svrzikapa, N., Hirozane-Kishikawa, T., Rietman, E., Yang, X., Sahalie, J., Salehi-Ashtiani, K., Hao, T., Cusick, M.E., Hill, D.E., Roth, F.P., Braun, P., and Vidal, M. (2011). Next-generation sequencing to generate interactome datasets. Nat. Methods *8*, 478–480.

6. Suter, B., Zhang, X., Pesce, C.G., Mendelsohn, A.R., Dinesh-Kumar, S.P., and Mao, J.-H. (2015). Next-Generation Sequencing for Binary Protein-Protein Interactions. Front. Genet. *6*, 346.

7. Bonaldi, K., Li, Z., Kang, S.E., Breton, G., and Pruneda-Paz, J.L. (2017). Novel cell surface luciferase reporter for high-throughput yeast one-hybrid screens. Nucleic Acids Res. *45*, e157–e157.

8. Pruneda-Paz, J.L., Breton, G., Nagel, D.H., Kang, S.E., Bonaldi, K., Doherty, C.J., Ravelo, S., Galli, M., Ecker, J.R., and Kay, S.A. (2014). A genome-scale resource for the functional characterization of *Arabidopsis* transcription factors. Cell Rep. *8*, 622–632.

9. Walhout, A.J., Temple, G.F., Brasch, M.A., Hartley, J.L., Lorson, M.A., van den Heuvel, S., and Vidal, M. (2000). GATEWAY recombinational cloning: application to the cloning of large numbers of open reading frames or ORFeomes. Methods Enzymol. *328*, 575–592.

10. Lamesch, P., Li, N., Milstein, S., Fan, C., Hao, T., Szabo, G., Hu, Z., Venkatesan, K., Bethel, G., Martin, P., Rogers, J., Lawlor, S., McLaren, S., Dricot, A., Borick, H., Cusick, M.E., Vandenhaute, J., Dunhan, I., Hill, D.E., Vidal, M. (2007). hORFeome v3.1: a resource of human open reading frames representing over 10,000 human genes. Genomics *89*, 307–315.

11. Bischof, J., Sheils, E.M., Bjorklund, M., and Basler, K. (2014). Generation of a transgenic ORFeome library in Drosophila. Nat. Protoc. *9*, 1607–1620.

12. Beerli, R.R., Segal, D.J., Dreier, B., and Barbas, C.F. 3rd (1998). Toward controlling gene expression at will: specific regulation of the erbB-2/HER-2 promoter by using polydactyl zinc finger proteins constructed from modular building blocks. Proc. Natl. Acad. Sci. U. S. A. *95*, 14628–14633.

13. Pruneda-Paz, J.L., Breton, G., Para, A., and Kay, S.A. (2009). A Functional Genomics Approach Reveals CHE as a Component of the *Arabidopsis* Circadian Clock. Science. *323*, 1481–1485.

14. Zheng, X.-Y., Zhou, M., Yoo, H., Pruneda-Paz, J.L., Spivey, N.W., Kay, S.A., and Dong, X. (2015). Spatial and temporal regulation of biosynthesis of the plant immune signal salicylic acid. Proc. Natl. Acad. Sci. U. S. A. *112*, 9166–9173.

15. Aggarwal, P., Das Gupta, M., Joseph, A.P., Chatterjee, N., Srinivasan, N., and Nath, U. (2010). Identification of specific DNA binding residues in the TCP family of transcription factors in *Arabidopsis*. Plant Cell *22*, 1174–1189.

16. Kosugi, S., and Ohashi, Y. (2002). DNA binding and dimerization specificity and potential targets for the TCP protein family. Plant J. *30*, 337–348.

17. Viola, I.L., Uberti Manassero, N.G., Ripoll, R., and Gonzalez, D.H. (2011). The *Arabidopsis* class I TCP transcription factor AtTCP11 is a developmental regulator with distinct DNA-binding properties due to the presence of a threonine residue at position 15 of the TCP domain. Biochem. J. *435*, 143–155.

18. Zakian, V.A., Brewer, B.J., and Fangman, W.L. (1979). Replication of each copy of the yeast 2 micron DNA plasmid occurs during the S phase. Cell *17*, 923–934.

19. Rajagopala, S.V., Hughes, K.T., and Uetz, P. (2009). Benchmarking yeast two-hybrid systems using the interactions of bacterial motility proteins. Proteomics *9*, 5296–5302.

20. Wu, J.-F., Tsai, H.-L., Joanito, I., Wu, Y.-C., Chang, C.-W., Li, Y.-H., Wang, Y., Hong, J.C., Chu, J.-W., Hsu, C.-P., and Wu, S.-H. (2016). LWD-TCP complex activates the morning gene CCA1 in *Arabidopsis*. Nat. Commun. *7*, 13181.

Chapter 6 Conclusions

We exploited a leaf localized *Pseudomonas syringae* infection approach to assess the response of circadian clock function to biotic stress and we discovered that localized *Pst* DC3000 infection systemically lengthened the period and reduced the amplitude of circadian rhythms in distal uninfected tissues. Upon *Pseudomonas syringae* infection, the production of defense related hormone salicylic acid (SA) is transiently induced. We found that transient SA treatment to the plant also reduced the amplitude of clock-controlled rhythms and induced a phase delay. The master regulator of SA signaling, NPR1, antagonized the clock responses triggered by *Pst* DC3000 infection or SA transient treatment indicating a protective role of NPR1. At the same time, the NADPH oxidase RBOHD which produces apoplastic ROS, partially mediated the observed clock responses. We also discovered that the observed clock responses triggered by localized *Pst* DC3000 infection were more drastic in the shoot apex than the peripheral tissues and the development of the plant upon localized *Pst* DC3000 infection was delayed.

Since several TCP transcription factors have been shown to be involved in circadian regulation and TCP DNA binding activity are regulated by the redox state, to find the possible link from the ROS production triggered by defense responses to the regulation of the clock function, we started to explore TCP transcription factors. We established a novel cell surface reporter gLUC59 for yeast one hybrid assays and with this system, we discovered that most class I TCP transcription factors were able to bind CCA1 promoter through TBS. Then we developed a new yeast two hybrid system which uses the gLUC59 as reporter. With this yeast two hybrid system, we identified 68 TCP21

interactors and discovered that class I TCPs were especially enriched for TCP21 interactors.

Since these results of TCP transcription factors are just providing a starting point, more future work need to be done to finally test if TCPs are the link to regulate clock function by defense signals. Since our results suggest that exceptionally complicated cooperation exists among TCPs, in the future, spatial and temporal studies need to be done to narrow down the list of TCPs to be tested.

Another future work to be done is to study the relationship between the modulation of the clock in the shoot apex and the development delay in the SAM upon localized *Pseudomonas* syringae infection. Due to the complicated nature of circadian clock research itself, little work has been done to study circadian rhythms at different developmental stage of the plant and research about clock function in different tissues of the plant has just began. Whether an alteration in the development would have an impact on the clock or the alteration in circadian rhythms upon infection is driving the observed development delay at least partially or they are just two unlinked responses upon infection is an interesting and important question to be answered.